A study of Dirac sea effects on the integer quantum Hall states of graphene.

By

Vinu Lukose

PHYS10200604001

The Institute of Mathematical Sciences, Chennai

A thesis submitted to the

Board of Studies in Physical Sciences

In partial fulfillment of requirements

For the Degree of

DOCTOR OF PHILOSOPHY

of

HOMI BHABHA NATIONAL INSTITUTE

September, 2014

Homi Bhabha National Institute

Recommendations of the Viva Voce Board

As members of the Viva Voce Board, we certify that we have read the dissertation prepared by Vinu Lukose entitled "A study of Dirac sea effects on the integer quantum Hall states in graphene" and recommend that it maybe accepted as fulfilling the dissertation requirement for the Degree of Doctor of Philosophy.

_____ Date:

Chair - Gautam I. Menon

_____ Date:

Guide/Convener - R. Shankar

_____ Date:

Member 1 - A. K. Mishra

_____ Date:

Member 2 - Rahul Siddarthan

_____ Date:

Member 3 - G. Baskaran

_____ Date:

External Examiner

Final approval and acceptance of this dissertation is contingent upon the candidate's submission of the final copies of the dissertation to HBNI.

I hereby certify that I have read this dissertation prepared under my direction and recommend that it may be accepted as fulfilling the dissertation requirement.

Date:

Place: Chennai R. Shankar

STATEMENT BY AUTHOR

This dissertation has been submitted in partial fulfillment of requirements for an advanced degree at Homi Bhabha National Institute (HBNI) and is deposited in the Library to be made available to borrowers under rules of the HBNI.

Brief quotations from this dissertation are allowable without special permisiion, provided that accurate acknowledgement of source is made. Requests for permisiion for extended quotation from or reproduction of this manuscriptin whole or in part may be granted by the Competent Authority of HBNI when in his or her judgement the proposed use of the material is in the interests of scholarship. In all other instances, however, permission must be obtained from the author.

Vinu Lukose

DECLARATION

I, hereby declare that the investigtion presented in the thesis has been carried out by me. The work is original and has not been submitted earlier as a whole or in part for a degree / diploma at this or any other Institution / University.

Vinu Lukose

List of Publications arising from the thesis

Journal

1. "Novel Electric Field Effects on Landau Levels in Graphene.", Vinu Lukose, R. Shankar and G. Baskaran, Phys. Rev. Lett. **98**, 116802 (2007).

Vinu Lukose

ACKNOWLEDGEMENTS

I cannot properly express my gratitude to all the people who supported me during this lengthy and sometimes difficult process, but I do have to at least try. I want to thank Gautam first because he was my supervisor in the beginning. Thank you for pushing me to succeed and ultimately letting me find my own way. I want to thank Date for his constant administrative support through all obstacles and delays. I want to thank Hassan, Rajesh, Anu, and Naveen for walking the line between friend and coach. Your support, motivation, gyan and occasional pastries helped me keep going. I also want to thank Niruj, Durba and Khusro for forgetting that line and just pushing me when I faltered.

To Naru, one-time officemate and roommate, thank you for your support and companionship and for taking me in without a second thought. To Mrs. Sharada Ramachandran, thank you for granting me refuge in your home. The Shangrila apartment was a haven for me. To my committee members, I have not been the most orthodox of PhD candidates, and I am very grateful for your faith in me. To Aruna, thank you for housing me, feeding me, and pushing me to be positive and to keep moving forward. On so many levels, this would not have happened without you. And finally, I want to thank Shankar. But I honestly do not know how. How can I sum up over a decade of guidance and support and friendship? I can only really say thank you, thank you for more than I can express.

Contents

List of Figures

Chapter 1

Introduction.

Graphene is a planar hexagonal structure formed by carbon atoms. The sp^2 hybridized orbitals of the carbon atoms forms the covalent bonds between the carbon and its three nearest neighbors. Graphene can visualized as the building block of some the carbon allotropes, for example, $3d$ structures like graphite, quasi $1d$ structures carbon nanotubes and quasi $0d$ structures fullerenes. Until recently, isolating the graphene has eluded the scientific community.

One of the methods for isolating graphene for experiments is done by exfoliation [15]. Highly oriented pyrolytic graphite platelets pressed against glass substrate which has freshly layered μm thick photoresist and baked so that mesas get attached to the photoresist layer. The rest of the sample cleaved off and then repeatedly use scotch tape to peel off the flakes of graphite. Thin flakes that are left on the photoresist and released in acetone. A Si wafer is dipped in the solution and washed with water and propanol. This captures some flakes on the wafer surface and the single graphene is selected from the resulting films by using a combination of optical, electron beam and atomic force microscopy. Graphene samples have been prepared on various substrates. The samples prepared on boron nitride [17] and suspended graphene samples [4] have higher electron mobilities than on SiO_2.

1.1 Lattice and band structure

A triangular lattice with each site decorated with two carbon atoms gives the honeycomb structure of graphene. The lattice spacing for the triangular lattice, $a = 2.46$ Å for graphene and the two carbon atoms separated by a distance $a/\sqrt{3}$. The lattice sites points are defined by ordered pair of integers, $\boldsymbol{n} \equiv (n_1, n_2)$ where $n_1, n_2 \in \mathbb{Z}$,

$$\boldsymbol{n} = n_1 \boldsymbol{e}_1 + n_2 \boldsymbol{e}_2 \tag{1.1}$$

$\boldsymbol{e}_1$ and $\boldsymbol{e}_2$ are the linearly independent vectors for the primitive translation vectors for the triangular lattice. In Cartesian coordinates, with $\hat{\mathbf{x}}$ and $\hat{\mathbf{y}}$ as unit vectors along the axes, the primitive vectors described as following,

$$\begin{aligned} \boldsymbol{e}_1 &= a\,\hat{\mathbf{x}} \\ \boldsymbol{e}_2 &= -\frac{1}{2}a\,\hat{\mathbf{x}} + \frac{\sqrt{3}}{2}a\,\hat{\mathbf{y}} \end{aligned} \tag{1.2}$$

There are number of operations that leaves the graphene lattice invariant. This includes

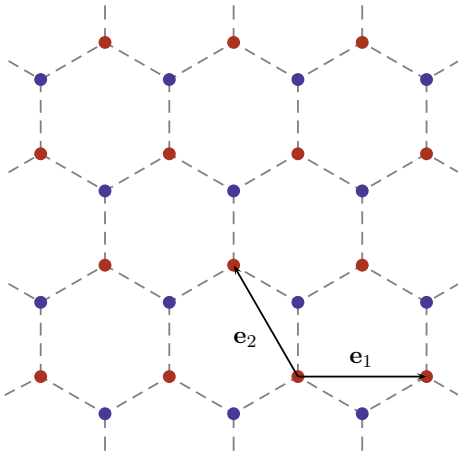

Figure 1.1: The figure shows a honeycomb lattice structure. Triangular lattice with basis vectors $\boldsymbol{e}_1$ and $\boldsymbol{e}_2$ with each site decorated with two geometrically nonequivalent carbon atoms, shown here with blue and red circles

translations, rotations, mirror reflection and glide reflection. The space group assigned

for graphene is $P6/mmm$.

The electronic properties are obtained by studying the tight binding model for the π-electrons of graphene,

$$\mathcal{H} = -t \sum_{\boldsymbol{n}\,\sigma} c^{\dagger}_{\boldsymbol{n},\,1,\,\sigma}(c_{\boldsymbol{n},\,2,\,\sigma} + c_{\boldsymbol{n}+\boldsymbol{e}_2,\,2,\,\sigma} + c_{\boldsymbol{n}+\boldsymbol{e}_1+\boldsymbol{e}_2,\,2,\,\sigma}) + \text{h.c.} \tag{1.3}$$

$c_{\boldsymbol{n},\,r,\,\sigma}$ are the lattice fermion operators for the π-electron at triangular lattice point $\boldsymbol{n}$, r is the sublattice index and σ specifies the spin of the electron. $t \approx 3.03$ eV is value of the overlap integral, which is the measure of energy cost for the electron hopping from one site to another.

The spectrum for the tight binding model is obtained by taking Fourier transformation of lattice fermion operators,

$$c_{\boldsymbol{n},\,r,\,\sigma} = \sum_{\boldsymbol{k}} \mathrm{e}^{\mathrm{i}\,\boldsymbol{k}\cdot\boldsymbol{n}}\, c_{\boldsymbol{k},\,r,\,\sigma} \tag{1.4}$$

Here $\boldsymbol{k} \equiv (k_1, k_2)$, reciprocal lattice vector

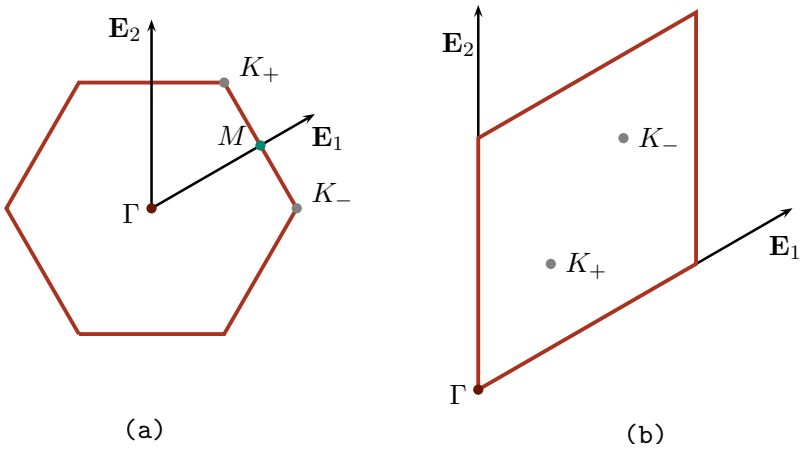

Figure 1.2: The two figures show the same Brillouin zone. In (a) the high symmetry points, Γ, K, M, of the Brillouin zone. The two K points in each is Brillouin zone is more transparent in (b).

$$\boldsymbol{k} = k_1\mathbf{E}_1 + k_2\mathbf{E}_2 \tag{1.5}$$

with $\mathbf{E}_1$, $\mathbf{E}_2$ primitive vectors in the reciprocal space is given by,

$$\begin{aligned} \mathbf{E}_1 &= \frac{4\pi}{\sqrt{3}}\left(\frac{\sqrt{3}}{2}\hat{\mathbf{x}} + \frac{1}{2}\hat{\mathbf{y}}\right) \\ \mathbf{E}_2 &= \frac{4\pi}{\sqrt{3}}\hat{\mathbf{y}} \end{aligned} \tag{1.6}$$

and satisfy the condition, $\boldsymbol{e}_j \cdot \mathbf{E}_k = 2\pi\,\delta_{j,k}$. The invariance of scalar product of $\boldsymbol{k}\cdot\boldsymbol{n}$ under point group symmetry operations results in three points of high symmetry in the Brillouin zone. Γ point has a six-fold rotation symmetry, K point and three-fold symmetry and M has a two-fold symmetry as shown in Fig 1.2.

The eigenvalues are given by,

$$\epsilon_{\boldsymbol{k}} = \pm\, t\big(1 + \mathrm{e}^{\mathrm{i}\,k_2} + \mathrm{e}^{\mathrm{i}\,(k_1+k_2)}\big)^{\frac{1}{2}} \tag{1.7}$$

The Fermi surface are two points in the Brillouin zone. These points are given by the roots of the $1 + \mathrm{e}^{\mathrm{i}\,k_2} + \mathrm{e}^{\mathrm{i}\,(k_1+k_2)} = 0$, i.e. $\boldsymbol{K}_\pm = (\pm 2\pi/3, \pm 2\pi/3)$ and are called Dirac points. The interesting feature of the band structure that in the proximity of the Dirac points, $\boldsymbol{k} = \boldsymbol{K}_\pm + \boldsymbol{q}$ in Eq.(1.7), the energy has a linear dependence on the wavevector.

$$\epsilon_{\boldsymbol{q}} = \pm\hbar\, v_F |\boldsymbol{q}| \tag{1.8}$$

$v_F = (\sqrt{3}\,a\,t)/(2\,\hbar) \approx 10^6\, m\, sec^{-1}$ is the Fermi velocity.

1.2 Quantum Hall measurements

Graphene placed on the silicon [16, 23] or boron nitride substrate or suspended graphene is almost an ideal realization of a two dimensional system and ideal for quantum Hall measurement. It is very different from the physical realization of two dimensional systems in the semiconductors which relies on the creation of inversion layers. Inversion layers are

formed at the interface between a semiconductor (Si) and an insulator(SiO_2) or between two semiconductors (GaAs-$Al_{0.8}Ga_{0.2}As$) where latter plays the role of the insulator. An electric field perpendicular to the interface confines the electrons from the semiconductor in a quantum well created by the electric field and the interface. The motion perpendicular to interface is quantized and the orbital degrees of freedom are frozen to a single level by conducting the experiments at very low temperatures. The wavelengths of these confined electrons are long, so an effective mass approximation with parabolic bands is a good theory to describe their behaviour. A metallic electrode is plated on one side of insulator which is charged by application of external 'gate voltage' to control the density of the electrons in the inversion layer.

In the case of graphene, there is no need for creation of inversion layer because of two dimensional structure of the material. The device comprises of graphene placed on thermally grown $300\ nm$ thick SiO_2 insulator over Si substrate. Si serves as gate electrode and SiO_2 acts as gate dielectric to control the carrier density in graphene. The graphene samples are 3-10 μm in lateral size, multiple electrode arranged for the conductivity measurements. The charge density induced on graphene is by tuning the gate voltage V_g and this gives a way to control the desired fermi level.

Quantum Hall effect

The quantum Hall effect manifests in graphene in transport measurements of transverse and longitudinal currents in samples with high mobilities as a function of magnetic field at fixed gate voltage. At large magnetic fields, the transverse resistance exhibits plateaus and the longitudinal resistance vanishes, which are signature of the quantum Hall effect. The plateaus are observed at transverse conductivity equals to [16, 23]

$$\sigma_H = \text{sgn}(n)\ 4\Big(|n| + \frac{1}{2}\Big)\frac{e^2}{h}$$

Here n is an integer which is the index of highest completely occupied Landau level. The factor of 4 corresponds to the degeneracy of each Landau level due to two spin and two valley quantum number. The factor of $1/2$ is related to the Berry's phase in graphene.

A simple minded picture to understand the quantization of Hall conductivity is from the one-particle picture. The energy eigenvalues for the Dirac particle in magnetic field is given by

$$\epsilon_{n,l} = \text{sgn}(n)\sqrt{2|n|}\frac{\hbar v_F}{\ell_c}$$

Each Dirac particle comes in four flavors, two valley and two spin. Each Landau level with positive index corresponds to electron states and the one with negative index corresponds to hole states. The $n = 0$ level is shared by both electron and hole states, i.e. two electron states and two hole states.

The samples with higher electron mobilities and high magnetic field, $B \sim 45$ additional plateaus were observed [22, 12, 21, 2]. In the first experiments [22, 12, 2], the degeneracy of $n = 0$ Landau level was fully lifted with Hall plateaus at $\sigma_H = 0, \pm 1$ were reported. Only partial degeneracy was lifted for $n = 1$ Landau level with the occurrence of Hall plateaus at $\sigma_H = \pm 4$. Quantum Hall measurements with tilted magnetic field, i.e. the graphene plane makes an angle with the applied magnetic field, is an important tool to understand the lifting of spin degeneracy. The Zeeman energy depends on the total applied magnetic field, (B_T), whereas the orbital motion of electron only feels the magnetic field perpendicular, ($B_\perp$), to the planar motion. The measurements of activation gaps in tilted magnetic field, where the $B_\perp$ is kept constant to ensure magnetic field is the range for quantum Hall plateaus and vary the B_T by tilting the plane. The dependence of this gap with B_T enables helps to conclude if the lifting of degeneracy caused by Zeeman splitting. It was concluded [22] that $\sigma_H = \pm 4$ was caused by lifting of the spin degeneracy from the tilted magnetic field experiments. The gaps for quantum Hall states at $\sigma_H = \pm 1$ showed $\sqrt{B}$ dependence [12], ruled out lifting of spin degeneracy. By excluding spin, it was conclude that lifting of the valley degeneracy resulted in Hall plateaus at $\sigma_H = \pm 1$.

The quantum Hall state for $\sigma_H = 0$ received more attention because of it unusual nature. A quantum Hall plateau for the transverse conductivity is accompanied with a vanishing longitudinal conductivity. The first few quantum Hall plateau at $\sigma_H = 0$ [22, 2] were reported with finite large longitudinal resistivity. The experiments reported a diverging longitudinal resistance [5, 6, 21], hence ruling out the counter propagating edge modes for $\sigma_H = 0$ state. The state for quantum Hall plateau $\sigma_H = 0$ is a quantum Hall insulator, i.e. vanishing transverse and diverging longitudinal resistivity, unlike the other plateaus in graphene.

In this thesis, we investigate the nature of quantum Hall states for $\sigma_H = 0, \pm 1$, hence the review of the reported experimental works is centered around these states. The quantum Hall experiments for graphene on boron nitride substrate [21] and suspended graphene [1] are most relevant to us. The graphene on boron nitride [17] provided high quality samples with mobilities three times larger than seen with graphene on silicon di-oxide. For magnetic field $B_\perp \sim 14\,T$ in [21], quantum Hall plateaus were observed at all integer values and an insulating state for $\sigma_H = 0$. A detailed report on the tilted field measurements have been presented and these measurements were used to extract information about the spin of the charged excitation for the states for all quantum Hall plateaus. The gaps for quantum Hall state at $\sigma_H = 0$ was reported to have a linear $B_\perp$ dependence in the range of $10\,T$ to $30\,T$. The decrease in the activation gaps with B_T for fixed $B_\perp$ lead them to conclude that state for $\sigma_H = 0$ is spin-unpolarized. The tilted field measurement for the quantum Hall state at $\sigma_H = -1$ was reported to show increase in activation gaps with B_T suggesting that excitations are from a spin-polarized state. In reference [12], the activation gaps for quantum Hall state at $\sigma_H = 1$ was shown fitted with a $\sqrt{B_\perp}$ dependence for the range, $10 < B_\perp < 45$. It was also noted that activation gaps for $\sigma_H = \pm 1$ were approximately half of that seen for $\sigma_H = 0$.

In the reference [1], local compressibility measurements using scanning single-electron transistor technique was used to extract energy gaps for quantum Hall states at $\sigma_H =$

$0, -1$. The gap measurements were reported for a range of magnetic fields, $\sim 1\,T$ to $12\,T$. Gaps for both these states were shown to have $\sqrt{B}$ dependence and the magnitude of gaps for $\sigma_H = -1$ was half when compared to gaps for $\sigma_H = 0$.

We now review theory paper that addressed $SU(4)$ symmetry breaking phenomenon for integer quantum Hall states in graphene.

Nomura and MacDonald [14] used the phenomenon of electron-electron interaction induced gaps and symmetry breaking at integer filling factors, known as quantum Hall ferromagnetism, to explain the quantum Hall plateaus at integer values for high magnetic field in graphene. Their model had kinetic and long ranged Coulomb interaction terms. They neglected the Zeeman coupling and treating the Coulomb interaction in Hartree-Fock approximation and the disorder in the self-consistent Born approximation (SBCA). This leads to a criterion where the exchange integral is competing with the Landau level spectral function within SCBA, called it Stoner criterion for quantum Hall ferromagnetism. The disorder potential was related to zero magnetic field mobility taken from the experiments. The phase diagram obtained from the Stoner criterion is a figure with filling fraction versus a quantity that is inversely proportional to sample mobility and magnetic field strength. The results from the Stoner criterion are in agreement with the observed quantum Hall plateaus. Quantum Hall ferromagnetism predicts plateaus should be observed at all integer filling.

Alicea and Fisher [3] have considered two possible mechanism for additional plateaus. First, quantum Hall ferromagnetism where screened Coulomb interaction modify the single particle picture. Second, quantum Hall paramagnetism where explicit symmetry breaking terms stabilize the states for additional quantum Hall plateaus. In the case of quantum Hall ferromagnetism, the model adopted has kinetic term, long ranged Coulomb and Hubbard terms at the lattice level and they obtain a continuum version by considering the long wavelength modes around the Dirac points. To compute the mean field energies they have projected out the states away from $n = 0$ Landau level and non-interacting wave

functions reside on one of the sub-lattice points. The long ranged Coulomb interaction provided the spontaneous symmetry breaking and anisotropic terms decide the nature of the ground state. For $\sigma_H = 1$, the ground state is a spin polarized charge density wave and the excitation favor a valley flip. For $\sigma_H = 0$, they have considered two competing ground states, first is spin-polarized valley singlet and second valley polarized spin singlet which also exhibits charge ordering. The nature of the ground state will be decided by the strength of Zeeman coupling and Hubbard repulsion relative to sub-lattice repulsion. The second case considered the quantum Hall paramagnetism, they considered model which comprises of kinetic and explicitly symmetry breaking terms. This also resulted in similar ground states as seen in quantum ferromagnetism case, the only difference in the two cases was that quantum ferromagnetism predicts Hall plateaus for all integer values, where are paramagnetism case shows additional plateaus at $\sigma_H = 0, \pm 1, \pm 4, \pm 10 \ldots$

Goerbig et. al. in the reference [9] considered the lattice model with interaction and computed the effective model for electrons restricted to single Landau level. They found the leading symmetry breaking terms were proportional to small parameter, ratio of lattice constant and magnetic length. They showed that for when one of the quartet for a Landau level is occupied, then $n \neq 0$ Landau levels will have easy-plane anisotropy order parameter. The difference is most prominent between $n = 0$ and $n = \pm 1$.

Fuchs and Lederer in reference [7] consider the possibility of a spontaneous out-of-plane lattice distortion breaks the inversion symmetry of graphene lattice in presence on magnetic field. This magnetic field dependent Peierls distortion breaks the valley symmetry and the order parameter gives mass to Dirac particle. This order parameter is proportional to difference in on-site energies of sub-lattice point resulting from electron phonon interaction. This theory like the quantum Hall paramagnetism case [3] shows additional plateaus at $\sigma_H = 0, \pm 1, \pm 4, \pm 10 \ldots$ after Zeeman splitting is also taken into account.

Herbut in reference [11] considered the extended Hubbard model for graphene in weak coupling limit and in presence of magnetic field. They solved the model by allowing an

anti-ferromagnetic state with staggered magnetization parallel to magnetic field. In this theory quantum Hall plateaus were predicted for all even integer values and also zero and ± 1. The ground state for $\sigma_H = 0$ was shown to have charged ordering, anti-ferromagnetic or ferromagnetic ordering depending on the strength of coupling parameters. And at $\sigma_H = \pm 1$ it was reported that system is always in translation symmetry breaking phase with finite magnetization.

Tőke et. al. in reference [19] presented gaps for pseudoskyrmion-antiskyrmion pair for $\sigma_H = 1$ state. Yang et. al. [20] presented the gapless collective modes in absence of symmetry breaking perturbations and discussed properties of skyrmions of graphene. They both considered only the long ranged Coulomb interaction.

Kharitonov [13] considered the contact interaction terms took into account the valley and sub-lattice asymmetric short ranged electron-electron interactions and electron-phonon interactions. A renomalization analysis showed that some of the key anisotropic terms exceeded the Zeeman coupling parameter and signs of anisotropic energies could also change. The phase diagram showed four phases which had order parameters corresponding to spin-polarized ferromagnetic, canted anti-ferromagnetic, charge density and Kekulé distortion. Kekulé distortion order is characterized by unit vector for valley is on the equator of the Bloch sphere. In the absence of Zeeman coupling the canted anti-ferromagnetic ordered state was replaced by anti-ferromagnetic ordered state.

We end this review section with a brief outline of the variational mean field presented in this thesis to highlight its salient features when compared with works described above. We start with interacting lattice model for graphene and present a systematic long wavelength continuum approximation. We show that the short ranged interaction can be modeled by considering nearest neighbour and Hubbard and treat their interaction strengths are parameters. Our variational calculations also takes into account the filled Dirac sea of Landau levels for Hall conductivities considered in this thesis. For this we have formulated a new technique with heat kernel method for Dirac particle in graphene. We are

the first to take into account the filled Dirac sea and long ranged Coulomb interaction at mean field level. Moreover we explore a through search in $SU(4)$ space for all possible symmetry breaking with our model. We are also first to present the qualitative effects on titled field measurements on particle-hole gaps for the ground states at $\sigma_H = 0, \pm 1$.

1.3 Outline of the thesis

In this section we present the outline for subsequent chapters in this thesis.

In Chapter 2, we provide analytical and numerical solutions to the problem of electrons in graphene subjected to cross electric and magnetic field. Within the continuum model, we obtain the spectrum for graphene subjected to cross electric and magnetic field. We utilize the relativistic structure of continuum theory and trick of Lorentz boost to obtain exact analytical solutions. These solutions reveal collapse of Landau level spectrum for a critical electric field. We also present numerical calculations for the same problem on lattice to show that the electric field effects on the Landau levels are not artifacts of continuum theory.

In Chapter 3 we show a systematic continuum approximation for the interacting lattice model for graphene and provide motivation for the choice of continuum interacting model studied in this thesis.

Chapter 4 presents a discussion on the choice of Landau levels for massive Dirac to construct the variational wavefunctions. We describe the parameterization for the variational wave functions for ground states for Hall conductivity at $\sigma_H = 0$ and $\sigma_H = -1$. Using the heat kernel method we develop a suitable expression for two point correlator for massive Dirac particle in magnetic field. The two point correlator are used to evaluate the mean field energies and particle-hole excitation gaps.

In Chapter 5 we present the results of mean field calculation for the $SU(4)$ symmetric

model, which only takes into account the kinetic and long ranged Coulomb interaction. We show that Coulomb interactions spontaneous break the $SU(4)$ symmetry. We also present results of particle-hole excitation within symmetric model.

In Chapter 6 we present the effects of symmetry breaking terms on the nature of ground states and excitation for the ground states. We illustrate the role of various symmetry breaking terms in obtaining the $SU(4)$ polarization for the ground states. We also show the effects of tilted magnetic field effects on the gaps and connect our results with those reported in experiments.

Chapter 7 present summary of findings of this thesis.

Chapter 2

Electric field effects on Landau levels in graphene.

Graphene is an excellent system to study $(2+1)\,d$ Dirac particles. Even before the experimental first quantum Hall effects were reported, Gusynin and Sharapov [10] had predicted the novel nature of quantum Hall plateaus for Dirac particles in graphene. This can be understood by solving the single particle problem of Dirac particle in two spatial dimensions subjected to magnetic field perpendicular to the plane. The eigenvalues have an square root dependence on the Landau level index and the applied magnetic field.

$$\epsilon_{n,l} = \sqrt{2|n|}\frac{\hbar\, v_F}{\ell_c} \tag{2.1}$$

here , n is the Landau level index which takes all integer values, v_F the fermi velocity and $\ell_c = \sqrt{\hbar/e\,B}$ is the magnetic length and B is applied magnetic field. All these feature make the Landau levels for a two dimension Dirac particles distinct from a non-relativistic particle seen in semiconductor hetrostructure.

In this chapter we solve analytically the problem of Dirac particle in two dimension subjected to magnetic field perpendicular to the plane and an electric field applied parallel

to the plane. This problem of Dirac particle subjected to cross electric and magnetic field is solved using by making use of Lorentz transformation. We highlight the new features of inferred from the solutions which are different from that of similar problem for non-relativistic particle. We solve the cross electric and magnetic field problem for graphene electron on lattice and hence show that effects seen from the solutions of continuum model are not artifacts of continuum approximation used for graphene electrons. We show a simple analysis from these solutions to arrive conclusion on the phenomena of dielectric breakdown and the discuss the experimental realization of our predictions in quantum Hall experiments conducted by Singh and Deshmukh [18].

2.1 Cross electric and magnetic field

In this section we present analytical results of the electric field effects on the Landau levels in graphene. We have considered graphene placed in x-y plane with constant magnetic field pointing along z-axis, $\boldsymbol{B} = B\hat{\boldsymbol{z}}$, and for simplicity we take constant electric field along the x-axis, $\boldsymbol{E} = E\hat{\boldsymbol{x}}$. Here B and E are constants for magnitude of magnetic and electric fields. The continuum hamiltonian derivation from the lattice model is handled as described in section 3.1, with additional assumptions that the magnetic flux passing through each honeycomb plaquette is small compared to the area of plaquette and the variation of scalar potential corresponding to electric field is small on the length scale of lattice spacing. The long wavelength approximation results in non-interacting hamiltonian,

$$\mathcal{H} = \int \mathrm{d}^2x\ \Psi^\dagger(\boldsymbol{x})\Big(\big(v_F\,\boldsymbol{\alpha}\cdot\boldsymbol{\pi} + e\,E\,x\,\mathbb{1}_2\big)\otimes\mathbb{1}_4\Big)\Psi(\boldsymbol{x}) \tag{2.2}$$

Here, $\Psi(\boldsymbol{x})$ are the fermion field operators, $\boldsymbol{\pi} = \boldsymbol{p} + e\boldsymbol{A}$, is covariant derivative, $\boldsymbol{A}$ is vector potential, α_x, α_y are Pauli matrices and $\mathbb{1}_2$ is 2×2 identity matrix and v_F is the fermi velocity. The identity matrix $\mathbb{1}_4$ is 4×4 matrix with corresponds to $SU(4)$ symmetry which results from degeneracy of valley and spin quantum numbers. This implies that we

have four decoupled copies of the 2×2 one particle hamiltonian, hence we restrict to only one. We start with the one particle hamiltonian from the Eq.(2.2) to explore the effects of electric field on the Landau levels.

$$h = v_F \, \boldsymbol{\alpha} \cdot \boldsymbol{\pi} + eE \, x \, \mathbb{1}_2 \tag{2.3}$$

Eq.(2.3), has the Lorentz covariant form for a massless particle with Fermi velocity, v_F, playing the role of the speed of light. It is well known fact from special relativity, when the electric and magnetic fields are perpendicular ($\boldsymbol{E} \cdot \boldsymbol{B} = 0$), it is possible to find a Lorentz frame where electric field vanishes, $\boldsymbol{E} = 0$ if $|\boldsymbol{E}|/v_F|\boldsymbol{B}| < 1$ or a frame where magnetic field vanishes $\boldsymbol{B} = 0$ provided that $v_F|\boldsymbol{B}|/|\boldsymbol{E}| < 1$. And it is not possible to make a Lorentz transformation that will take frame with pure magnetic field to another one with only electric field. Making use of this fact and Lorentz transformation we transform the problem of cross magnetic and electric field to pure magnetic field one with restriction that $|\boldsymbol{E}|/v_F|\boldsymbol{B}| < 1$.

Lorentz transformation on the space-time coordinate system for us is a mathematical convenience to find the exact solutions. The specific choice of the rapidity of the Lorentz transformation enables to take the problem of cross magnetic and electric field to a pure magnetic field case with reduced magnitude. The knowledge of exact spectrum of Landau level problem, and inverse Lorentz transformation enables us to obtain the exact analytical solutions for the hamiltonian in Eq.(2.3). To implement the above procedure, we start with time dependent Schrodinger equation for hamiltonian in Eq.(2.3),

$$\mathrm{i}\,\hbar \frac{\partial}{\partial t} \Psi(\boldsymbol{x}, t) = \Big(v_F \, \boldsymbol{\alpha} \cdot \boldsymbol{\pi} + eE \, x \, \mathbb{1}_2 \Big) \Psi(\boldsymbol{x}, t) \tag{2.4}$$

Here Ψ is two component object. We rewrite Eq.(2.4) in manifestly covariant time dependent Dirac equation in $(2+1)d$ for a massless Dirac particle subjected to electromagnetic

fields,

$$\mathrm{i}\,\hbar\gamma^{\mu}(\partial_{\mu} - \mathrm{i}\,\frac{e}{\hbar}A_{\mu})\Psi(x^{\mu}) = 0 \tag{2.5}$$

Here coordinates, $x^0 = v_F t$, $x^1 = x$, $x^2 = y$ are the contravariant components of the *three-vector*, $\partial_\mu = \partial/\partial x^\mu$ is corresponding partial derivative. $A^0 = \phi$, the scalar potential, $A^1 = A_x$, $A^2 = A_y$ are the components of three-vector potential. The 2×2 Dirac matrices are defined in terms of Pauli matrices,

$$\gamma^0 = \alpha^z, \qquad \gamma^1 = \mathrm{i}\,\alpha^y, \qquad \gamma^2 = -\mathrm{i}\,\alpha^x$$

These choices for the Dirac matrices are not unique, other choices are also possible and they are related to each other by similarity transformation.

We choose to work with Landau gauge as it is the natural choice for our problem as this keeps the analysis simple. We now apply a Lorentz boost along the y-direction. The coordinates transformation is given by,

$$\begin{pmatrix} \tilde{x}^0 \\ \tilde{x}^1 \\ \tilde{x}^2 \end{pmatrix} = \begin{pmatrix} \cosh(\theta) & 0 & \sinh(\theta) \\ 0 & 1 & 0 \\ \sinh(\theta) & 0 & \cosh(\theta) \end{pmatrix} \begin{pmatrix} x^0 \\ x^1 \\ x^2 \end{pmatrix} \tag{2.6}$$

Here θ is the rapidity of the Lorentz transformation. The Lorentz transformation of the coordinates in Eq.(2.6) results in spinor wave function to transform in the following way,

$$\tilde{\Psi}(\tilde{x}^{\mu}) = \mathrm{e}^{\frac{\theta}{2}\alpha_y}\Psi(x^{\mu}) \tag{2.7}$$

We verify that Lorentz transformation leaves $\bar{\Psi}(x^\mu)\Psi(x^\mu)$ invariant, where $\bar{\Psi}(x^\mu) = \Psi^\dagger(x^\mu)\gamma^0$. The mathematical convenience to obtain the spectrum of cross electric and magnetic field problem lies in the specific choice of the rapidity of the transformation. The specific choice of $\tanh(\theta)$ can either reduce the cross electric and magnetic field problem to either pure electric or magnetic field problem. Since our interest is to see

the effect of electric fields on Landau levels, hence we restrict to the case, $E/v_F B < 1$. We make the choice $\tanh(\theta) = E/(v_F B) = \beta$ for the rapidity of the transformation in Eq.(2.6) to transform the problem of cross magnetic and electric fields to pure magnetic field problem in boosted coordinates. This specific choice of transformation is applied to Eq.(2.5), the transformed Dirac equation,

$$\Big(\gamma^0\tilde{\partial}_0 + \gamma^1\tilde{\partial}_1 + \gamma^2\big(\tilde{\partial}_2 + \frac{\mathrm{i}}{\ell_c^2}\sqrt{1-\beta^2}\,\tilde{x}^1\big)\Big)\tilde{\Psi}(\tilde{x}^\mu) = 0 \tag{2.8}$$

In the transformed coordinates, Eq. (2.8), the massless Dirac electron in a cross magnetic and electric problem is reduced to a problem of massless Dirac particle subjected to pure (reduced) magnetic field, $\tilde{B} = B\sqrt{1-\beta^2}$, with $\beta < 1$. The eigenvalue for the Landau level problem is used to obtain the eigenvalues for the pure (reduced) magnetic field.

$$\tilde{\epsilon}_{n,\tilde{k}_y} = \mathrm{sgn}(n)\sqrt{2|n|}\frac{\hbar v_F}{\ell_c}(1-\beta^2)^{\frac{1}{4}} \tag{2.9}$$

The magnetic length $\tilde{\ell_c} = \ell_c/(1-\beta^2)^{\frac{1}{4}}$ increases in the boosted frame. Since energy is time component of 3-momentum, is not an invariant quantity under Lorentz transformation. This implies that eigenvalues of boosted coordinates system, $\tilde{\epsilon}_{n,\tilde{k}_y}$ in Eq.(2.9) are not the physical energy eigenvalues of our problem. We have to apply the inverse Lorentz transformation with the same value for rapidity, β, to obtain the eigen solutions to the original problem of massless Dirac particle subjected to cross magnetic and electric field. After performing the inverse Lorentz transformation on 3-momentum, the eigenvalues are

$$\epsilon_{n\,k_y} = \mathrm{sgn}(n)\sqrt{2|n|}\,\frac{\hbar v_F}{\ell_c}(1-\beta^2)^{\frac{3}{4}} - \hbar v_F\beta\,k_y \tag{2.10}$$

Here we made use of the fact that the scalar product of two 3-vectors is invariant under

Lorentz transformation. The corresponding eigen states,

$$\Psi_{n,k_y}(x,y) = \frac{\mathrm{e}^{\mathrm{i}\,k_y\,y}}{\sqrt{L_y}} \frac{\mathrm{e}^{-\frac{\theta}{2}\alpha_y}}{\sqrt{2\cosh(\theta)}} \begin{pmatrix} \varphi_{|n|-1,k_y}(\xi') \\ \mathrm{i}\,\mathrm{sgn}(n)\,\varphi_{|n|,k_y}(\xi') \end{pmatrix} \tag{2.11}$$

Here $\varphi(\xi^{'})$ are the orthonormal wave functions for non-relativistic electron gas in two dimensions and the dimensionless $\xi^{'}$ gives information about the center of gaussian peaks.

$$\xi' \equiv \frac{(1-\beta^2)^{\frac{1}{4}}}{\ell_c} \left(x + k_y \ell_c^2 + \mathrm{sgn}(n) \frac{\sqrt{2|n|}\,\ell_c \beta}{(1-\beta^2)^{\frac{1}{4}}} \right) \tag{2.12}$$

The eigenstates in Eq.(2.11) were verified to be orthonormal. The details of the derivation of the exact analytic solutions are provided in Appendix B.

The eigenstates for the case of non-relativistic electron is given by eigen solutions of harmonic oscillator times plane waves , $\mathrm{e}^{\mathrm{i}\,k_y\,y}\varphi_n(\bar{\xi})$ and the dimensionless $\bar{\xi}$

$$\bar{\xi} = \frac{1}{\ell_c}\Big(x + k_y \ell_c^2 + \frac{m\ell_c^2}{\hbar} \left(\frac{E}{B} \right) \Big) \tag{2.13}$$

Comparing the equations (2.12), (2.13) we can easily read off a non-trivial dependence for the center of gaussian peaks on the Landau level index, n, in the case of graphene, unlike the standard $2d$ electron gas where the center of cyclotron motion is independent of Landau level index. The effect of the electric field is to (un)squeeze the oscillator states as well as to mix the particle and hole wave-functions. Squeezing corresponds to the change in magnetic length, ℓ_c and the eigenstates in Eq.(2.11) can be expanded as superposition of Landau levels for massless Dirac particle.

$$\Psi_{n\,k_y}(x,y) = \sum_q f_q \Phi_{q\,k_y}(x,y) \tag{2.14}$$

This is possible because of non-vanishing overlap of the integral of the oscillator states

whose gaussian spread are different,

$$\int \mathrm{d}x\, \varphi^*_{n,k_y}(\xi)\varphi_{\tilde{n},k_y}(\xi') \tag{2.15}$$

here $\xi' \equiv \xi(1-\beta^2)^{\frac{1}{4}} + \mathrm{sgn}(n)\sqrt{2|n|}\beta$. Thus, unlike in the usual semiconductor samples, here in graphene the electric field causes Landau level mixing.

The eigenvalues Eq. (2.10) and the eigen states Eq. (2.11), in the limit $E \to 0$ reduces to the eigenvalues for pure magnetic field case. As the electric is tuned the effective magnetic length increases $\ell_c \to \ell_c(1-\beta^2)^{-\frac{3}{4}}$. This implies that for massless Dirac electron in two dimensions, effect of magnetic field decreases as the strength of the electric field is increased. This is in contrast to the case of two dimensional non-relativistic electron gas where the magnetic length is unaffected on applying an electric field. This can be readily observed from the eigenvalues for the non-relativistic electron gas in two dimensions in presence of cross magnetic and electric field,

$$\bar{\epsilon}_{n,k_y} = \left(n+\frac{1}{2}\right)\hbar\omega_c - \hbar k_y \frac{E}{B} - \frac{m}{2}\left(\frac{E}{B}\right)^2 \tag{2.16}$$

In both the cases, for non-relativistic electron gas and massless Dirac electron, the degeneracy of the Landau levels is lifted by the linear dependence on quantum number k_y. The main difference between the two cases, besides the $\sqrt{n}$ and $\sqrt{B}$, is that *the low lying graphene Landau levels spacing scales as* $(1-\beta^2)^{\frac{3}{4}}$, for a given value of k_y, Eq.(2.10), whereas the spacing is independent of the electric field in the non-relativistic case Eq.(2.16). Another interpretation is, for a fixed magnetic field as the electric field is increased the effect of magnetic field on the graphene electron reduces. There is a critical electrical field corresponding to $\beta = 1$, which results in collapse of Landau levels.

As $\beta \to 1$, from Eq.(2.12) we infer that, to keep the gaussian shifts within the linear extent of the system

$$k_y\ell_c^2 + \mathrm{sgn}\sqrt{2|n|}\,\ell_c\frac{\beta}{(1-\beta^2)^{\frac{1}{4}}} \leq L_x \tag{2.17}$$

Thus it requires larger values of k_y. But our results are strictly valid for the long wavelength approximation, which is valid for small values of wave vectors. As $\beta \to 1$, the results from the continuum approximation are not reliable because one of the condition in continuum approximation requires scalar potential should be slowing varying over lattice spacing is violated. Moreover, Eq.(2.10) hands a collapse of the Landau level spectrum at $\beta = 1$. The obvious questions that arise from this is to what extent the continuum approximation results are reliable and is the collapse of Landau levels in graphene an artifact of the low energy approximation? To answer these questions, we performed numerical diagonalization of full tight binding hamiltonian and discussed in the following sections. As expected, we find that the eigenvalues from the continuum theory holds well for small values of β. And the collapse of Landau levels persists, and in fact it occurs for a value of β even smaller than unity as continuum theory suggests.

2.2 Numerical diagonalization of lattice model

In this section, we diagonalize the tight binding hamiltonian on honeycomb lattice. This numerical computation is part of built up to solve the desired problem of cross electric and magnetic field problem for graphene.

The tight binding model for graphene is a non-interacting one. This enables us to reduce the many particle problem to solving a one particle problem on honeycomb lattice. Lattice models with periodic boundary condition are well understood analytically after taking the Fourier transform. It is desirable to find the spectrum of the tight binding model with various boundary conditions and understand its effects. A finite size lattice can have a variety of boundary conditions. We study the lattice model by solving the hamiltonian numerically with a zig-zag boundary. To keep things simple, we consider a finite lattice with periodic boundary condition along one axis of the unit cell of triangular lattice and open boundary condition along the other axis. This boundary results in zig-zag boundary

, well known boundary in carbon nanotube literature. There are other choices for the boundary, but we will restrict our study to zig-zag boundary. The lattice sizes can be decided based upon the computational power of the machines. In this section we present the discussion of results from the tight binding model on finite size lattice varying from 60×60 to 600×600 lattice points. In order to formulate in matrix form, we start with the tight binding model and the Schrödinger equation reads

$$\begin{aligned} \epsilon\, c_{\boldsymbol{n},1,\sigma} &= -\,t\big(c_{\boldsymbol{n},2,\sigma} + c_{\boldsymbol{n}+\boldsymbol{e}_2,2,\sigma} + c_{\boldsymbol{n}+\boldsymbol{e}_1+\boldsymbol{e}_2,2,\sigma}\big) \\ \epsilon\, c_{\boldsymbol{n},2,\sigma} &= -\,t\big(c_{\boldsymbol{n},1,\sigma} + c_{\boldsymbol{n}-\boldsymbol{e}_2,1,\sigma} + c_{\boldsymbol{n}-\boldsymbol{e}_1-\boldsymbol{e}_2,1,\sigma}\big) \end{aligned} \tag{2.18}$$

There are two scales in the given problem - one is the length scale, the lattice spacing 'a' and second is the energy scale governed by the hopping parameter 't'. Since the inputs in the numerical program are numbers we express all the lengths in the units of lattice spacing and all the energies in the units of hopping parameter. For convenience, we put both lattice spacing and hopping parameter to unity and expand the fermion operators in terms of wave functions

$$c_{\boldsymbol{n},r,\sigma} = \sum_{p,\boldsymbol{k}} \phi^{\boldsymbol{k},p}_{\boldsymbol{n},r} c_{\boldsymbol{k},p,\sigma} \tag{2.19}$$

Here $\boldsymbol{k}$ is the wave vector and p is the band index. The eigenvalue equations in terms of wave functions are

$$-\epsilon\, \phi^{\boldsymbol{k},p}_{\boldsymbol{n},1} = \phi^{\boldsymbol{k},p}_{\boldsymbol{n},2} + \phi^{\boldsymbol{k},p}_{\boldsymbol{n}+\boldsymbol{e}_2,2} + \phi^{\boldsymbol{k},p}_{\boldsymbol{n}+\boldsymbol{e}_1+\boldsymbol{e}_2,2} \tag{2.20}$$

$$-\epsilon\, \phi^{\boldsymbol{k},p}_{\boldsymbol{n},2} = \phi^{\boldsymbol{k},p}_{\boldsymbol{n},1} + \phi^{\boldsymbol{k},p}_{\boldsymbol{n}-\boldsymbol{e}_2,1} + \phi^{\boldsymbol{k},p}_{\boldsymbol{n}-\boldsymbol{e}_1-\boldsymbol{e}_2,1} \tag{2.21}$$

We can solve equations (2.20),(2.21) written in plane wave function basis. This amounts to diagonalizing a matrix of size $2N^2 \times 2N^2$ for a triangular lattice of size $N \times N$. We reduce the problem of diagonalizing one very large matrix of size $\mathcal{O}(N^2)$ to solving N matrices of size $\mathcal{O}(N)$ by taking periodic boundary condition along the $\boldsymbol{e}_2$-axis and open

boundary along $\boldsymbol{e}_1$-axis, i.e. $\phi^{\boldsymbol{k},p}_{\boldsymbol{n},1} \to \mathrm{e}^{\mathrm{i}\,k_2 n_2}\phi^{\boldsymbol{k}\,p}_{n_1,1}$.

$$-\epsilon\ \phi^{\boldsymbol{k},p}_{n_1,1} = (1+\mathrm{e}^{\mathrm{i}\,k_2})\phi^{\boldsymbol{k},p}_{n_1,2} + \mathrm{e}^{\mathrm{i}\,k_2}\phi^{\boldsymbol{k},p}_{n_1+1,2} \tag{2.22}$$

$$-\epsilon\ \phi^{\boldsymbol{k},p}_{n_1,2} = (1+\mathrm{e}^{-\mathrm{i}\,k_2})\phi^{\boldsymbol{k},p}_{n_1,1} + \mathrm{e}^{-\mathrm{i}\,k_2}\phi^{\boldsymbol{k},p}_{n_1-1,1} \tag{2.23}$$

After applying the periodic boundary condition along $\boldsymbol{e}_2$, equations (2.22) and (2.23), we have reduced the problem of diagonalizing a matrix of size $2N^2 \times 2N^2$ to diagonalizing N complex valued matrices of $2N \times 2N$ size. Hence the periodic boundary condition along one direction has reduced the problem of diagonalizing a very large matrix to diagonalizing a large number of smaller sized matrices and this increases the efficiency of required computation time. To further increase efficiency of numerical computation, it is desirable to transform the complex matrix to real matrix, i.e. getting rid of complex coefficients with appropriate real coefficients with some suitable transformation. This is amounts to finding a unitary transformation matrix that reduces the complex matrix to real matrix. In the present case we can achieve this by pulling out a phase factor out of the wave functions in equations (2.22) and (2.23),

$$\phi^{\boldsymbol{k},p}_{n_1,r} \to \mathrm{e}^{\mathrm{i}\,\theta_{n_1,r}(k_2)}\ \phi^{\boldsymbol{k},p}_{n_1,r} \tag{2.24}$$

And then choosing phase appropriately, reduce the complex coefficients to real. With the following choice of the phase factors,

$$\begin{aligned}\theta_{n_1,1}(k_2) &= -(n_1-1)\frac{k_2}{2}\\ \theta_{n_1,2}(k_2) &= -n_1\frac{k_2}{2}\end{aligned} \tag{2.25}$$

The complex hermitian matrix is reduced to real symmetric.

$$-\epsilon\ \phi^{\mathbf{k},p}_{n_1,1} = 2\cos\left(\frac{k_2}{2}\right)\ \phi^{\mathbf{k},p}_{n_1,2} + \phi^{\mathbf{k},p}_{n_1+1,2} \tag{2.26}$$

$$-\epsilon\ \phi^{\mathbf{k},p}_{n_1,2} = 2\cos\left(\frac{k_2}{2}\right)\ \phi^{\mathbf{k}\,p}_{n_1,1} + \phi^{\mathbf{k},p}_{n_1-1,1} \tag{2.27}$$

Equations (2.26), (2.27) are used to construct the real matrix of size $2N \times 2N$ for each

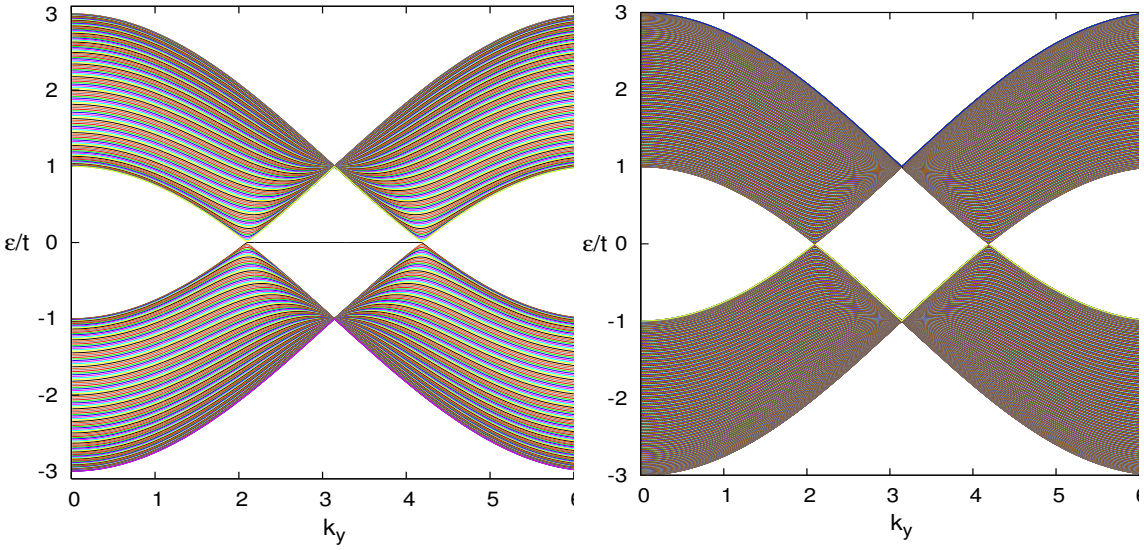

Figure 2.1: Eigenvalues for 600×600 lattice points for graphene with zig-zag boundary (a) along $\boldsymbol{e}_2$ and (b) with periodic boundary condition along both axes. Both spectrum show the two Dirac point at $k_y = 2\pi/3$ and $k_y = 4\pi/3$ as expected from the continuum model. For the zig-zag boundary there are a string of zero eigenvalue states for each value of k_y between the two Dirac points. The zero eigenvalue states are localized along the two open boundaries

value of k_2, which are N in number. We used Householder algorithm to diagonalize the matrix and obtained the eigenvalues and eigenvectors for the tight binding model for the graphene with zig-zag boundary. Fig.(2.1) shows the full spectrum obtained from numerical diagonalization. Fig.(2.1b) is the spectrum with periodic boundary conditions applied along both $\boldsymbol{e}_1$ and $\boldsymbol{e}_2$ axes of the $N \times N$ lattice and the Fig.(2.1a) is for the case when the periodic boundary condition is applied only in the $\boldsymbol{e}_2$ direction. One consequence of the zig-zag boundary is the presence of the string of zero eigenvalues for k_2 between two Dirac points. These zero eigenvalues are well known in literature as the edge states that are localized at the boundary. These zero energy edge states are the consequence of the open boundary condition can be confirmed by plotting the density of states. These zero eigenvalue states give a finite density of states at zero energy and as the system size is increases the contribution to density of states from these states decreases. These edge states are unique to the zig-zag boundary of the graphene. In the zig-zag boundary for

graphene, there are carbon atoms with one dangling bond, i.e. one of the covalent bond is not attached to any other atom. This results in states that are localized at the boundary and decay exponentially as we go into the sample.

These localized eigen-functions for edge states can be obtained by solving equations (2.26), (2.27) for zero eigenvalue.

$$\phi^{\mathbf{k},p}_{n_1,1} = \left(2\cos\left(\frac{k_2}{2}\right)\right)^{-n} \phi^{\boldsymbol{k},p}_{0,1} \tag{2.28}$$

$$\phi^{\boldsymbol{k},p}_{n_1,2} = \left(2\cos\left(\frac{k_2}{2}\right)\right)^{n} \phi^{\boldsymbol{k},p}_{0,2} \tag{2.29}$$

For simplicity we consider the semi-infinite case, i.e., we have zig-zag boundary along the $\boldsymbol{e}_2$-axis and the system extends to infinity along the positive $\boldsymbol{e}_1$ axis. For the given boundary condition, the sub-lattice '2' has one dangling bond, i.e., $\phi^{\boldsymbol{k},p}_{0,2}$ can take any value. To obtain normalized wave function, the condition on the wave-vector k_2 is

$$\left|2\cos\left(\frac{k_2}{2}\right)\right| < 1 \qquad \Rightarrow \qquad \frac{2\pi}{3} < k_2 < \frac{4\pi}{3}$$

For the zero eigenvalues for a semi-infinite system, the wave functions reside on one of the sub-lattice for a range of values of k_2 and they localized near boundary. This is consistent with our numerically obtained wave functions for a finite system. These edge states are a peculiar feature of the boundary condition on honeycomb lattice. The choice of armchair boundary condition does not have these zero eigenvalue edge states.

2.3 Numerical solution for graphene lattice in magnetic field

In this section we discuss the spectrum obtained from numerically solving the tight binding problem of graphene in magnetic field. We discuss the chiral edge states that are

responsible for the Hall conductivity. The difference between wave functions of the degenerate states at zero energy eigenvalue, i.e. chiral edge states and $n = 0$ Dirac-Landau levels.

For purpose of numerical diagonalization, we choose the vector potential $\boldsymbol{A}$ in such a way that only one of the hopping term in tight binding hamiltonian acquires phase due to magnetic field and ensure that magnetic flux through each plaquette corresponds to the applied magnetic field. The resulting hamiltonian is (here we have suppressed the display of spin index),

$$\mathcal{H} = -t \sum_{\boldsymbol{n}} c^{\dagger}_{\boldsymbol{n},1}(c_{\boldsymbol{n},2} + \mathrm{e}^{\mathrm{i}\, n_1 \varphi} c_{\boldsymbol{n}+\boldsymbol{e}_2,2} + c_{\boldsymbol{n}+\boldsymbol{e}_1+\boldsymbol{e}_2}) + \text{h.c.} \tag{2.30}$$

$$\varphi \equiv 2\pi \frac{\frac{\sqrt{3}}{2} B a^2}{\frac{h}{e}}$$

φ is the magnetic flux passing through each plaquette. The eigenvalue equations in terms of wave functions is

$$-\frac{\epsilon}{t}\, \phi^{\boldsymbol{k}}_{\boldsymbol{n},1} = \phi^{\boldsymbol{k}}_{\boldsymbol{n},2} + \mathrm{e}^{\mathrm{i}\, n_1 \varphi} \phi^{\boldsymbol{k}}_{\boldsymbol{n}+\boldsymbol{e}_2,2} + \phi^{\boldsymbol{k}}_{\boldsymbol{n}+\boldsymbol{e}_1+\boldsymbol{e}_2,2} \tag{2.31}$$

$$-\frac{\epsilon}{t}\, \phi^{\boldsymbol{k}}_{\boldsymbol{n},2} = \phi^{\boldsymbol{k}}_{\boldsymbol{n},1} + \mathrm{e}^{-\mathrm{i}\, n_1 \varphi} \phi^{\boldsymbol{k}}_{\boldsymbol{n}-\boldsymbol{e}_2,1} + \phi^{\boldsymbol{k}}_{\boldsymbol{n}-\boldsymbol{e}_1-\boldsymbol{e}_2,1} \tag{2.32}$$

The translation symmetry along the $\boldsymbol{e}_2$ axis of the lattice is preserved. We choose periodic boundary condition along the $\boldsymbol{e}_2$ and apply the same method to reduce the complex matrix eigenvalue problem to real matrix eigenvalue problem as we did for the case of zero magnetic field problem, i.e. finding a unitary transformation. The choice of θ_1 and θ_2 are

$$\theta_1 = -(n_1 - 1)\frac{k_2 a}{2} + \frac{n_1(n_1+1)}{4}\varphi \tag{2.33}$$

$$\theta_2 = -n_1 \frac{k_2 a}{2} + \frac{n_1(n_1-1)}{4}\varphi \tag{2.34}$$

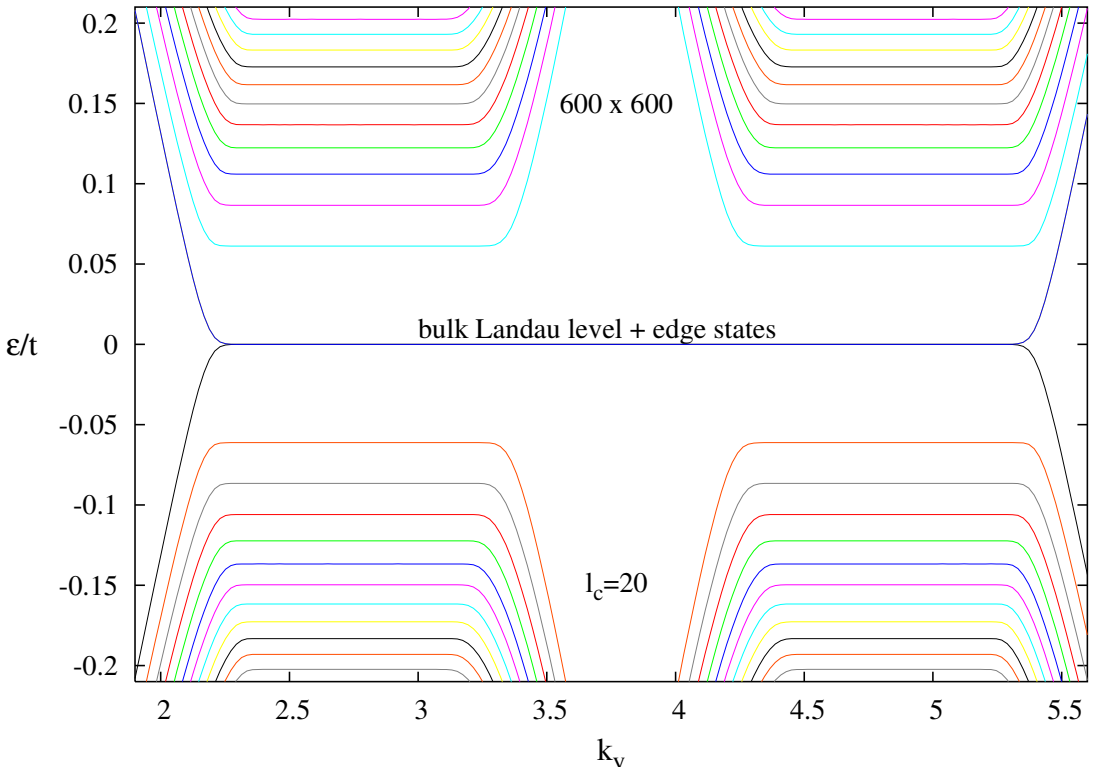

Figure 2.2: Eigenvalues of tight binding model for honeycomb lattice in presence of magnetic field near the two Dirac points. Here the system size is 600×600 and the magnetic field applied $B \approx 27.12\,T$, which corresponds to magnetic length $\ell_c = 20a$. The zero eigenvalues that do not vary with k_y are the $n = 0$ Landau levels and the edge states that are localized at the sample edge (consequence of zig-zag edge). The non-zero eigenvalues that do not vary with k_y are Landau levels with index $n > 0$, the index increases with energy (Landau level index decreases with the decrease in the value of eigenvalue for negative energies). Energy eigenvalues are measured in units of 't'.

The Harper equations that are solved numerically are

$$-\frac{\epsilon}{t}\,\phi^{\boldsymbol{k}}_{n_1,1} = 2\cos\left(\frac{k_2+n_1\varphi}{2}\right)\phi^{\boldsymbol{k}}_{n_1,2} + \phi^{\boldsymbol{k}}_{n_1+1,2} \tag{2.35}$$

$$-\frac{\epsilon}{t}\,\phi^{\boldsymbol{k}}_{n_1,2} = 2\cos\left(\frac{k_2+n_1\varphi}{2}\right)\phi^{\boldsymbol{k}}_{n_1,1} + \phi^{\boldsymbol{k}}_{n_1-1,1} \tag{2.36}$$

For numerical diagonalization, we choose the value of the magnetic field such that $L \gg \ell_c \gg a$, where L is the linear extent of the system. The condition $\ell_c \gg a$, assures that a very small magnetic flux passes through each plaquette. This ensures that we stay away from the Hofstadter butterfly kind of commensurability effects on the spectrum. The other condition that the system size is much larger than the magnetic length, $L \gg \ell_c$, ensures that a large number of cyclotron orbits fit in the sample. For the purpose of numerical computations, we once again expressed all energies in units of t and all lengths in units of a.

The resulting spectrum from the numerical diagonalization is shown in the Fig.(2.2). The set of eigenvalues that have no variation with respect to k_2 are the Landau levels. The corresponding lattice wave functions have a prominent Gaussian peak and these Gaussian peaks shifts across the length of system with k_2. The low energy levels i.e. the eigenvalues near the two Dirac points are in excellent agreement with continuum results. Comparison between the exact results from the continuum model and the exact diagonalization are shown in Fig.(2.3). The $\sqrt{n}$ dependence of Landau level index of the eigenvalues is in good agreement with the continuum model result.

The zero eigenvalue is doubly degenerate. There are two kinds of eigenstates corresponding to the zero eigenvalue. They are identified by examining the corresponding wave function. These are the Landau levels with index $n = 0$, identified due to the Gaussian peaks and the second class of states are the wave functions that are localized at the two boundaries for the zig-zag boundary conditions applied to Harper equations. The distinction between the $n = 0$ Landau levels and the localized edge states will become clear

when we discuss the spectrum for cross electric and magnetic field.

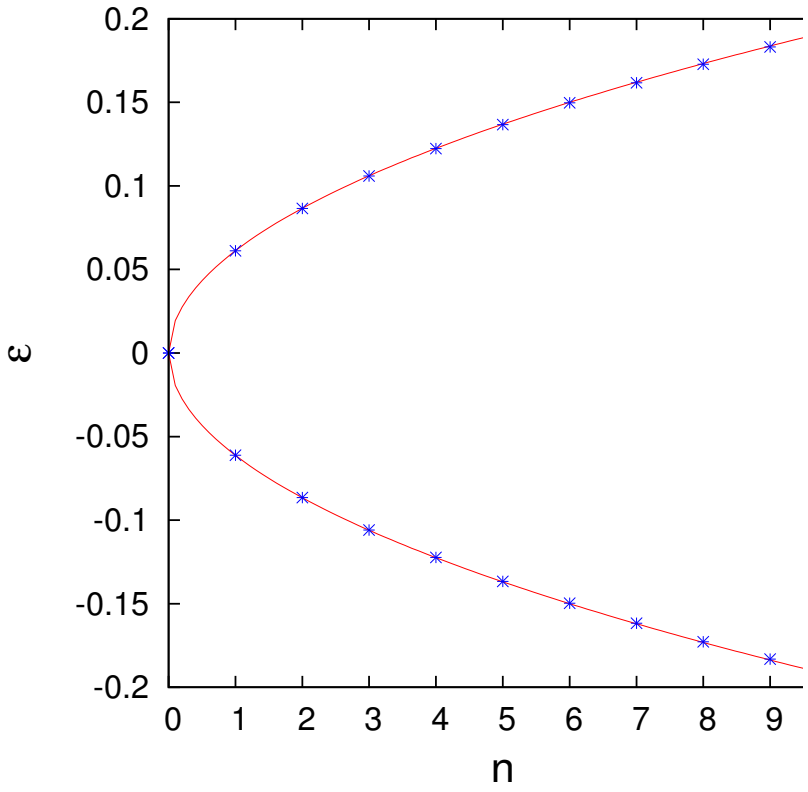

Figure 2.3: The blue asterisk points shows the eigenvalues computed from the numerical exact diagonalization of honeycomb lattice (blue points) and the eigenvalues from the continuum approximation (red line). The size of the lattice is 600×600 and magnetic field $B = 27.12\,T$ or $\ell_c = 20a$. The red line corresponds to eigenvalues obtained from continuum theory, $\sqrt{2|n|}\hbar v_F/\ell_c$. The blue points are the eigenvalues from exact diagonalization for a fixed value of k_y. There is excellent agreement between results continuum theory and the lattice theory.

The edge states, localized at the boundary, are reminiscent of the edge states that were observed from the zero magnetic field case. As in the case of zero magnetic field, the edge states continue to be localized at the boundary and have an exponential decay as we move into the system.

2.4 Numerical solution for graphene lattice in cross electric and magnetic field

The numerical diagonalization of the cross magnetic and electric problem for electrons in graphene is simple extension of the magnetic problem done in section 2.3. The tight binding hamiltonian for graphene subjected to constant magnetic field perpendicular to plane of the graphene plane is incorporated by a phase term to the hopping terms and the electric field along the $\boldsymbol{e}_1$-axis of the lattice is

$$\mathcal{H} = -t \sum_{\boldsymbol{n}} c^{\dagger}_{\boldsymbol{n}\,1}(c_{\boldsymbol{n}\,2} + \mathrm{e}^{\mathrm{i}\,n_1\varphi} c_{\boldsymbol{n}+\boldsymbol{e}_2\,2} + c_{\boldsymbol{n}+\boldsymbol{e}_1+\boldsymbol{e}_2}) + \text{h.c.} + \sum_{\boldsymbol{n}\,r} e\,E\,n_1 c^{\dagger}_{\boldsymbol{n}\,r} c_{\boldsymbol{n}\,r} \qquad (2.37)$$

The matrix equations are obtained in similar fashion as done in section 2.3 for the magnetic field case. We choose periodic boundary conditions along the $\boldsymbol{e}_2$-axis and $\boldsymbol{e}_1$-axis is terminated with zig-zag boundary. The two dimension problem is reduced to solving one dimensional problem for each value of k_2. This results in finding out eigenvalues for a finite dimensional complex matrix. The complex matrix eigenvalue problem is reduced to real matrix problem by doing unitary transformation using equations 2.33 and 2.34 to improve the efficiency of the numerical routine. For the lattice computations, the energies are measured in units if 't', tight-binding overlap parameter, and the length scales is measured in the units of 'a', the lattice parameter of graphene. The equations for the matrix diagonalization are,

$$\epsilon\,\phi^{\boldsymbol{k}}_{n_1,\,1} = -2\,t\cos\left(\frac{k_2 + n_1\varphi}{2}\right)\phi^{\boldsymbol{k}}_{n_1,\,2} + \phi^{\boldsymbol{k}}_{n_1+1,\,2} + e\,E\,n_1\phi^{\mathbf{k}}_{n_1,\,1} \qquad (2.38)$$

$$\epsilon\,\phi^{\boldsymbol{k}}_{n_1,\,2} = -2\,t\cos\left(\frac{k_2 + n_1\varphi}{2}\right)\phi^{\boldsymbol{k}}_{n_1,\,1} + \phi^{\boldsymbol{k}}_{n_1-1,\,1} + e\,E\,n_1\phi^{\boldsymbol{k}}_{n_1,\,2} \qquad (2.39)$$

Fig.2.4 shows the spectrum at low energy for the cross magnetic and electric fields. The Landau levels in Fig. 2.2 acquire a linear slope w.r.t. k_y consistent with contin-

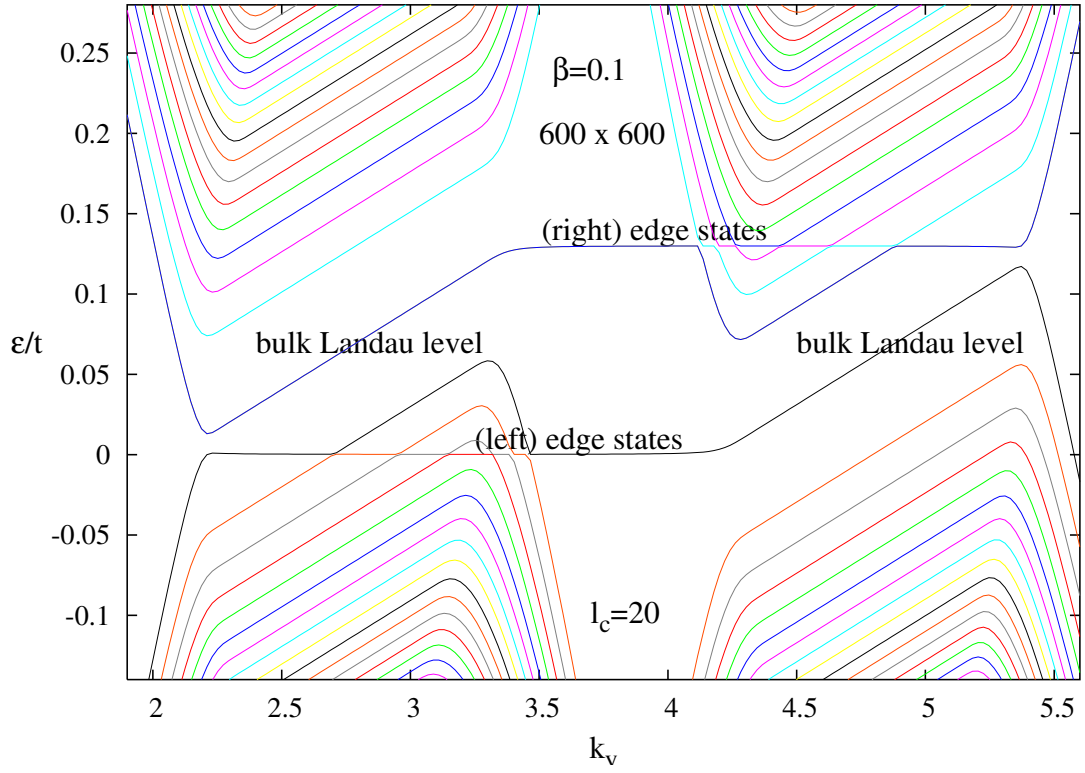

Figure 2.4: Eigenvalues of tight binding model for honeycomb lattice in presence of crossed electric and magnetic field near the two Dirac points. Here the system size is 600×600 and the magnetic field applied $B \approx 27.12\,T$, which corresponds to magnetic length $l_c = 20a$. The magnitude of applied electric field $E = 0.1 v_F B$. The eigenvalues that do not vary with k_y are the edge states that are localized at the sample edge (consequence of zig-zag edge). The eigenvalues of these localized edge states is proportional to electric field experienced by the two edges. The lines parallel to label 'bulk Landau level' are the Landau levels with positive and negative index whose degeneracy is lifted by the applied electric field. Energy eigenvalues are measured in units of 't'.

uum result Eq.(2.10). The degeneracy of zero energy localized edge states and $n = 0$ Landau level gets lifted in the presence of electric field. For small electric fields the wave-function of these edge states continues to be localized near edge of the sample. The eigenvalues of these surface states are proportional to strength of the electric field $(eEn_1a = (\sqrt{3}/2)(a^2/l_c^2)\beta n_1 t)$ experienced at the two edges of the sample. In the Fig. 2.4, the energy eigenvalue for the left edge is zero ($\because n_1 = 0$) and the right edge is ≈ 0.1299 ($n_1 = 600$). A characteristic feature of these edge states is that they do not vary with the wavevector, whereas the Landau levels develop a linear k_y dependence with electric field.

The comparison between the results from the continuum theory and the exact diagonalization is shown in Fig.2.5. We plot $\sqrt{n}$ scaling of energy eigenvalues Landau levels for various values of applied electric fields for a given k_y value. Once again for the exact numerical diagonalization, the magnetic field is chosen such that there magnetic length is large compared to lattice spacing and system size is large compared to magnetic length so that large number of cyclotron orbits can fit in the sample. For zero electric field, as we have seen earlier, there is an excellent match between continuum theory and results from the numerical diagonalization on lattice. For very small values of $\beta \sim 0.001$, there is good agreement between the results from continuum and exact diagonalization for Landau levels with small index. Now we further increase the electric field keeping the magnetic field fixed, i.e on increasing β, there is systematic deviation between lattice eigenvalues and continuum eigenvalues. This implies that gaps between the Landau levels reduces much faster than what is expected from the continuum result. The collapse of Landau levels, which happens at $\beta = 1$ for the continuum model, seem to happen at much smaller electric fields for the lattice model than what is suggested by the continuum theory. This disagreement between the lattice and continuum model is not surprising because the requirement of the slow variation of the scalar potential at lattice spacing of the continuum model is not satisfied with the large electric field. Hence we can conclude that the continuum results are reliable only for very small values of β.

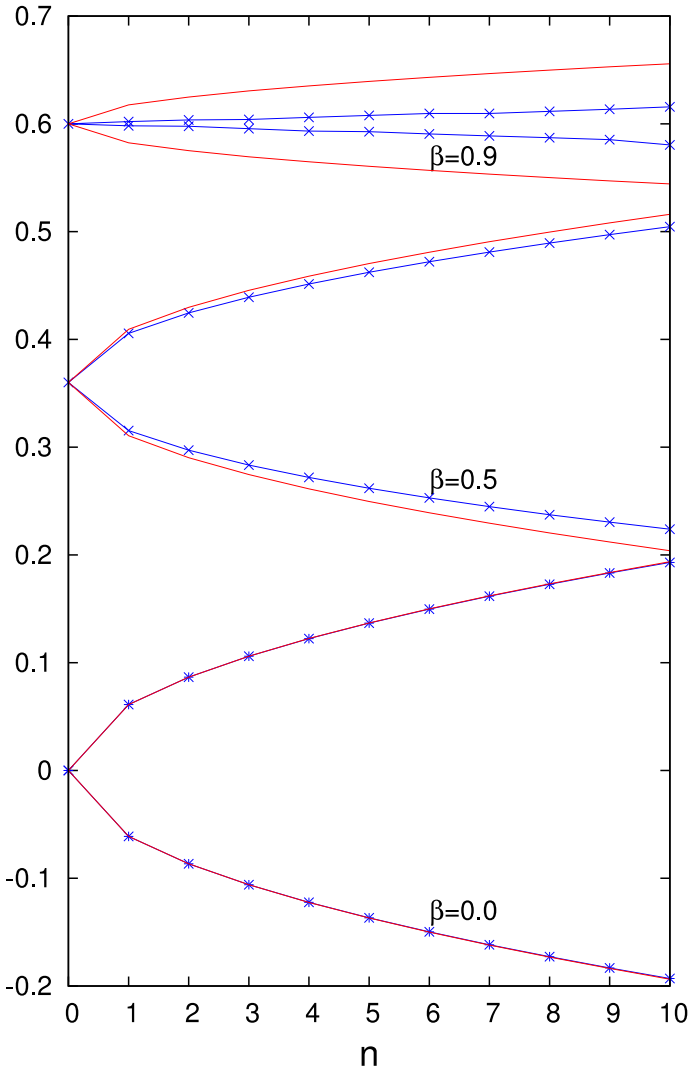

Figure 2.5: The figure shows the scaling of eigenvalues of Landau levels with Landau level index for various various electric fields. The red curve denote the results from the continuum model and blue curve are the results from exact diagonalization of the lattice model. The system size for numerical diagonalization is 600×600 and magnetic field $B \approx 27.12\,T$. The eigenvalues plotted are for one fixed value of k_y and measured in unit of 't'. Eigenvalues for three electric fields ($E = \beta v_F B$) have been shown, $\beta = 0.0, 0.5, 0.9$. A clear systematic deviation can be seen between the results from continuum model and numerical exact diagonalization as the electric field is increased.

2.5 Dielectric breakdown

In the following section we will discuss the consequences of contraction of Landau levels on the phenomena of 'dielectric breakdown' in presence of electric field for Dirac particle. We will argue that the Landau level contraction Eq. (2.10), and the n dependent guassian shift Eq. (2.12) will cause the dielectric breakdown, which is different from the conventional ones seen in the $2d$ electron gas in semi-conductors. The single particle spectrum and the corresponding eigenstates we have obtained for a given E and B, can be used to construct stable many-body quantum Hall ground states. However, the external electric field not only modifies the single particle wave function and spectrum, but can also destabilise the ground state through spontaneous creation of particle-hole pairs; i.e., by a dielectric breakdown.

Here we will show a simple argument based one particle solutions to present a simple formula for dielectric breakdown for graphene. We also compare the two cases for non-relativistic and relativistic $2D$ electron gas. The eigenvalues in Eq.(2.10) is expressed using the quantum numbers n and k_y. Another set of quantum number that can be used to express these eigenvalues are n Landau level index and x_c the centres of cyclotron motion,

$$x_c = k_y \ell_c^2 + \text{sgn}(n)\sqrt{2|n|}\frac{\ell_c \beta}{(1-\beta^2)^{\frac{1}{4}}} \tag{2.40}$$

We make a trade-off between k_y and x_c to express the eigenvalues in Eq.(2.10)

$$\epsilon_{n,x_c} = \text{sgn}(n)\sqrt{2|n|}\frac{\hbar v_F}{\ell_c}\frac{1}{(1-\beta^2)^{\frac{1}{4}}} + V(x_c) \tag{2.41}$$

Here the $V(x_c) = -eE\,x_c$ is the potential energy of the electron. Expressing the eigenvalues in Eq.(2.41) enables us to compute the gaps between the levels.

$$\Delta_n = \epsilon_{n+1,x_{c_1}} - \epsilon_{n,x_{c_2}}$$

Note that here we have taken two different cyclotron centres for the levels in order to compute the amount of energy needed to excite the electron from the ground state to lowest unoccupied state, i.e. the state with Landau level index $n+1$. The local gap is given by

$$\Delta_n = -\delta V + \text{sgn}(n)\frac{\hbar v_F}{\ell_c}\left(\frac{\sqrt{2|n+1|}}{(1-\beta_1^2)^{\frac{1}{4}}} - \frac{\sqrt{2|n|}}{(1-\beta_2^2)^{\frac{1}{4}}}\right) \tag{2.42}$$

Here $\delta V = V(x_{c_2}) - V(x_{c_1})$ represents the potential difference between the two points x_{c_1}, x_{c_2}. Here we are considering the scenario that the sample has got disorder that causes potential within a small region of sample to vary. The length scale associated with this local variation in potential is ℓ_E and this length is large compared to lattice spacing. $E_i \propto \beta_i$, is the electric field at point x_{c_i}, $i = 1, 2$. From Eq.(2.42), we can see that the local gap depends on the Landau level index, n, coupled with magnitude of field at the two points under consideration. Moreover the gaps seen by the particle and hole excitations are also different. A similar analysis for the non-relativistic electron gas will results in an expression for local gap, which is independent of Landau level index.

$$\tilde{\Delta}_n = \hbar\omega_c - \delta V + \frac{m}{2}\left(\frac{E_1^2 - E_2^2}{B^2}\right) \tag{2.43}$$

From our discussion in previous sections we had concluded that results from the continuum model are reliable for small magnitudes of electric fields, i.e. $\beta \ll 1$. The local gap Eq.(2.42) can be approximated,

$$\Delta_n \approx -\delta V + \Delta_n^0 - \frac{1}{4}\text{sgn}(n)\frac{\hbar v_F}{\ell_c}\left(\sqrt{2|n+1|}\beta_1^2 - \sqrt{2|n|}\beta_2^2\right) \tag{2.44}$$

Δ_n^0 is the gap between the Dirac-Landau levels when no external electric field applied. We arrive at an expression for the critical voltage for local breakdown by doing dimensional analysis and assuming that electric field is also slowly varying over length scale ℓ_E.

$$V_c \approx \frac{\Delta_n^0}{e}\left(1 - \kappa\, n\left(\frac{\ell_c}{\ell_E}\right)^2\right) \tag{2.45}$$

here κ is a constant which depends on the square of ratio of energy associated to the electric field fluctuations to energy associated with magnetic field ($\hbar v_F/\ell_c$) . This means that if we have an electric field, non-uniform over a nanoscopic scale ($\ell_E \sim \ell_c$), it will cause local breakdown. Such situations can be created through in plane or out of plane charged impurities or STM tips, in addition to externally applied electric fields. It is interesting that such a local breakdown is Landau level index n dependent and current required to cause such a breakdown will decrease with the increase of Landau level index. In the case of non-relativistic electron gas the critical voltage is independent of n,

$$V_c \approx \frac{\hbar\omega_c}{e}\left(1-\kappa\left(\frac{\ell_c}{\ell_E}\right)^2\right)$$

Thus we expect that the quantum Hall breakdown in graphene should be qualitatively different for $n = 0$ and $n \neq 0$ within graphene.

2.6 Experimental probing breakdown

Singh and Deshmukh [18] explored the breakdown phenomenon of quantum Hall states in graphene. Their main motivation was to probe the mechanism of breakdown in graphene which could either be from the inter-Landau level scattering due to wave function mixing or as we predicted due to local electric field effects due to defects whose sizes are comparable to the magnetic lengths. They studied the quantum Hall breakdown for Hall states $\nu = -10, -6, -2, 2, 6$ on exfoliated graphene samples with mobilities $\sim\ 11,000\,\text{cm}^2(\text{Vs})^{-1}$.

To probe the breakdown of quantum Hall effect, the sample was biased with a dc current along with a small ac current at constant magnetic field. The dc current was varied as a function of gate voltage in the vicinity of Hall plateau and voltage across the sample was measured to find the longitudinal and transverse resistance. The minina of longitudinal resistance was plotted function of dc current and the critical current for breakdown was extracted by linear extrapolation. Interpretation for the experimental data,

- The width of of the dissipationless transport reduces as the dc current is increased.
- The boundary on the either side of integer filling evolves asymmetrically.
- The critical current for the breakdown of the quantum Hall state depends on the filling factor ν. It decreases with increase in $|\nu|$.

They also compared the change in the resistance with temperature and current to ensure that local heating of the sample was not responsible for the breakdown phenomena in graphene. Hence the observed behaviour of the breakdown voltage is qualtitatively same as what we had suggested in Eq.(2.45).

2.7 Summary

Here we summarize the finding of this chapter,

1. Exact analytical solutions for Dirac particle in cross electric and magnetic field were found using the trick of Lorentz boost.
2. Numerical computations for the cross electric and magnetic field subjected to graphene on lattice were shown to confirm the effects of Landau levels is not an artifact of continuum model.
3. The phenomenon of dielectric breakdown was discussed and predictions were made about difference of dielectric breakdown for $n = 0$ and $n \neq 0$ Landau levels. And this was verified in quantum Hall experiments by Singh and Deshmukh [18]

Chapter 3

Interacting model for graphene

The integral quantum Hall plateaus at [16, 23]

$$\sigma_H = 4\left(n + \frac{1}{2}\right)\frac{e^2}{h} \tag{3.1}$$

is well understood within the framework of the one particle picture [10]. Here n takes integer values. In Eq.(3.1) the factor four is associated with degeneracy of each Landau level with index, n. Its origin are in the $SU(4)$ symmetry associated with the non-interacting continuum theory.

The samples with high mobility and at high magnetic field reveals plateaus at all integral values [21]. The inclusion of Zeeman term in the non-interacting model can possibility explain the Hall plateaus at all even integral values. The Zeeman term lifts the spin degeneracy which is part of the full $SU(4)$ symmetry. Disorder is essential ingredient to quantum Hall phenomena which results in broadening of Landau levels and believed not lift the $SU(4)$ degeneracy. An approach to resolve this issue is to study the effects of electron-electron interactions. In this chapter, we provide the motivation for the model continuum hamiltonian that is adopted in this thesis to understand the phenomena of $SU(4)$ symmetry breaking associated with quantum Hall plateaus that deviate from the

Eq.(3.1).

We begin with lattice tight binding model for the graphene and perform a systematic long wavelength expansion around Dirac points for fermion operators. The leading term obtained after continuum approximation is well studied non-interacting model for graphene. We have also derived the sub-leading term obtained from the lattice kinetic term. This terms gives correction to non-interacting continuum model with magnitude proportional to square of ratio of lattice constant and magnetic length. Hence a very small contribution when compared to leading term.

We apply continuum approximation to the electron-electron interaction term of the lattice model. We show that the leading term is $SU(4)$ symmetric and sub-leading terms breaks $SU(4)$ symmetry explicitly. The sub-leading terms are short ranged as compared to the leading term and they vary as inverse cube of distance. At short distance, point charge interactions get modified between electron because of the finite extent of the wavefunctions. We argue that physics of this symmetry breaking terms can be captured by considering the nearest neighbour interaction at lattice level. The lattice nearest neighbour interactions are incorporated in the lattice model to take into account the wave function effects of the π-electrons of the carbon atoms. This contact interaction at continuum level enables us to simplify the computations and capture the essential physics of symmetry breaking that we want to explore. We also include the Hubbard interaction term which takes into account on-site interaction between the electron wave functions. We derive the continuum approximation for lattice interactions and discuss the symmetry of our continuum model hamiltonian. We treat the nearest neighbour and Hubbard interaction strengths as tunable parameters. In presence of strong magnetic field, Zeeman splitting of spin quantum number is important, hence we have included Zeeman term in the model hamiltonian.

3.1 Continuum approximation

The π-electrons of carbon atoms which constitute the graphene are only considered in the tight binding model to understand the electronic properties. The lattice hamiltonian,

$$\mathcal{H} = -t \sum_{\boldsymbol{n},\sigma} c^{\dagger}_{\boldsymbol{n},1,\sigma} \big(c_{\boldsymbol{n},2,\sigma} + c_{\boldsymbol{n}+\boldsymbol{e}_2,2,\sigma} + c_{\boldsymbol{n}+\boldsymbol{e}_1+\boldsymbol{e}_2,2,\sigma} \big) + \text{h.c.} \tag{3.2}$$

Here $t \approx 3.033\ eV$, is the transfer integral, which is the measure of kinetic energy of the electron hopping from a lattice site to other. $c_{\boldsymbol{n},r,\sigma}$ are the fermion operator. $\boldsymbol{n}$ specifies the triangular lattice points, $r = 1, 2$, denotes the sub-lattice index associated with each lattice point and $\sigma = \uparrow, \downarrow$, is spin index. The fermion operators obey the anti-commutation relation,

$$\{ c_{\boldsymbol{n},r,\sigma}, c^{\dagger}_{\tilde{\boldsymbol{n}},\tilde{r},\tilde{\sigma}} \} = \delta_{\boldsymbol{n},\tilde{\boldsymbol{n}}} \delta_{r,\tilde{r}} \delta_{\sigma,\tilde{\sigma}}$$

The Fermi surface for the tight binding model for graphene is two points in the Brillouin zone, Dirac points, $\boldsymbol{K}_{\pm} = (\pm 2\pi/3a, \pm 2\pi/3a)$. The interesting feature of the Dirac points is that the spectrum has linear dependence on the wave vector.

To obtain low energy effective theory from the lattice hamiltonian, we project the electron operators to low energy sector and then separate the long wavelength modes from the fast varying modes.

$$c_{\boldsymbol{n},r,\sigma} \approx \mathrm{e}^{\mathrm{i}\,\boldsymbol{K}_{+}\cdot\boldsymbol{n}} \alpha^{z}_{r,s}\, \Psi_{s,+,\sigma}(\boldsymbol{n}) + \mathrm{e}^{\mathrm{i}\,\boldsymbol{K}_{-}\cdot\boldsymbol{n}} \alpha^{x}_{r,s}\, \Psi_{s,-,\sigma}(\boldsymbol{n}) \tag{3.3}$$

The label $r = 1, 2$, indicates the index of spinor structure, $\eta = +, -$ for valley index i.e. low energy excitations around Dirac points, $\boldsymbol{K}_{\pm}$. The spin is labeled by index $\sigma = \uparrow, \downarrow$. $\Psi_{r,\eta,\sigma}(\boldsymbol{n})$ are the slow varying modes around the two Dirac points.

$$\Psi_{r,\eta,\sigma}(\boldsymbol{n}) \equiv \int_{0}^{\Lambda} \mathrm{d}^2 k \left(\phi^{\mathbf{K}_\eta + \mathbf{k}, s, \sigma}(\boldsymbol{n}) \right)_r c_{\mathbf{K}_\eta + \mathbf{k}, s, \sigma} \tag{3.4}$$

Λ is the cut-off on the wave vector around the Dirac points. One can get the estimate for Λ as follows. Consider a system $N \times N$ triangular lattice with basis comprising of two carbon atoms to form honeycomb structure. It implies that we have $2 \times 2N^2$ states, first 2 is for the spin and $2N^2$ number of π-electrons. So there are $4N^2$ states in the first Brillouin zone and there are two Dirac points. An estimate for Λ is made by comparing density of states and the area of the Brillouin zone.

$$\int_0^{\Lambda} \mathrm{d}^2k \approx \frac{1}{2}\frac{\sqrt{3}}{2}\left(\frac{4\pi}{\sqrt{3}a}\right)^2$$

$$\Lambda^2 = \frac{4\pi}{\sqrt{3}}\frac{1}{a^2} \tag{3.5}$$

We substitute the projected fermion operators in lattice hamiltonian Eq.(3.2) and collect the long wavelength modes around the Dirac points to obtain the effective hamiltonian.

$$\begin{aligned}
&\left(c_{\boldsymbol{n},2,\sigma} + c_{\boldsymbol{n}+\boldsymbol{e}_2,2,\sigma} + c_{\boldsymbol{n}+\boldsymbol{e}_1+\boldsymbol{e}_2,2,\sigma}\right) \\
&\approx -\mathrm{e}^{\mathrm{i}\,\boldsymbol{K}_+\cdot\boldsymbol{n}}\Big(\Psi_{2,+,\sigma}(\boldsymbol{n}) + \mathrm{e}^{\mathrm{i}\,\boldsymbol{K}_+\cdot\boldsymbol{e}_2}\Psi_{2,+,\sigma}(\boldsymbol{n}+\boldsymbol{e}_2) + \mathrm{e}^{\mathrm{i}\,\boldsymbol{K}_+\cdot(\boldsymbol{e}_1+\boldsymbol{e}_2)}\Psi_{2,+,\sigma}(\boldsymbol{n}+\boldsymbol{e}_1+\boldsymbol{e}_2)\Big) \\
&\quad + \mathrm{e}^{\mathrm{i}\,\boldsymbol{K}_-\cdot\boldsymbol{n}}\Big(\Psi_{1,-,\sigma}(\boldsymbol{n}) + \mathrm{e}^{\mathrm{i}\,\boldsymbol{K}_-\cdot\boldsymbol{e}_2}\Psi_{1,-,\sigma}(\boldsymbol{n}+\boldsymbol{e}_2) + \mathrm{e}^{\mathrm{i}\,\boldsymbol{K}_-\cdot(\boldsymbol{e}_1+\boldsymbol{e}_2)}\Psi_{1,-,\sigma}(\boldsymbol{n}+\boldsymbol{e}_1+\boldsymbol{e}_2)\Big)
\end{aligned}$$

$\Psi_{r,\eta,\sigma}(\boldsymbol{n}+\boldsymbol{e}_i)$, varies slowly at the lattice length scale, hence can be approximated about $\boldsymbol{n}$ using Taylor expansion with lattice constant as the variable parameter.

$$\Psi_{r,\eta,\sigma}(\boldsymbol{n}+\boldsymbol{e}_i) \approx \Psi_{r,\eta,\sigma}(\boldsymbol{n}) + a\Delta_i\Psi_{r,\eta,\sigma}(\boldsymbol{n}) + \frac{a^2}{2!}\Delta_i^2\Psi_{r,\eta,\sigma}(\boldsymbol{n}) + \cdots \tag{3.6}$$

In the process of deriving the effective hamiltonian, we make use of the following relations,

$$\begin{aligned}
\mathrm{e}^{\mathrm{i}\,\boldsymbol{K}_\pm\cdot\hat{\boldsymbol{e}}_{1,2}} &= \mathrm{e}^{\pm\mathrm{i}\,\frac{2\pi}{3}} \\
1 + \mathrm{e}^{\mathrm{i}\,\frac{2\pi}{3}} + \mathrm{e}^{\mathrm{i}\,\frac{4\pi}{3}} &= 0
\end{aligned} \tag{3.7}$$

Finally we take the continuum limit, $a \to 0$, difference operators are replaced by partial

derivatives of Cartesian coordinates after taking into account coordinate transformation

$$\begin{aligned} \Delta_1 &\to \partial_x \\ \frac{1}{2}\Delta_1 + \Delta_2 &\to \frac{\sqrt{3}}{2}\partial_y \end{aligned} \tag{3.8}$$

The summation of lattice points are substituted with the integral,

$$\sum_{\boldsymbol{n}} \to \frac{1}{a^2} \iint \mathrm{d}\boldsymbol{x} \tag{3.9}$$

The field operator in continuum limit,

$$\Psi_{r,\eta,\sigma}(\boldsymbol{n}) \to a\ \Psi_{r,\eta,\sigma}(\boldsymbol{x}) \tag{3.10}$$

The leading term of the continuum approximation

$$\mathcal{H}_0 = \iint \mathrm{d}\boldsymbol{x}\ \Psi^\dagger(\boldsymbol{x}) \Big(v_F\, \boldsymbol{\alpha}\cdot\boldsymbol{p} \otimes \mathbb{1}_4 \Big) \Psi(\boldsymbol{x}) \tag{3.11}$$

Henceforth we refer $\mathcal{H}_0$ as the non-interacting continuum hamiltonian. It describes is four species of free massless Dirac particles. The speed of the massless particle is $v_F = \sqrt{3}\,a\,t/2\hbar$, the fermi velocity at the Dirac point. The field operators, $\Psi(\boldsymbol{x})$ are eight component objects and labeled as $\Psi_{r,A}(\boldsymbol{x})$, where r refers to Dirac spinor or sub-lattice index and takes values $r = 1, 2$ and A is the $SU(4)$ index with takes values $1 \ldots 4$. The matrices α^x, α^y are the 2×2 Pauli matrices for the Dirac spinor space. To clarify the notation, we explicitly write the continuum hamiltonian,

$$\mathcal{H}_0 = \iint \mathrm{d}\boldsymbol{x}\ v_F\, \Psi^\dagger_{r,A}(\boldsymbol{x}) \left(\boldsymbol{\alpha}\cdot\boldsymbol{p}\right)_{r,s} \left(\mathbb{1}_4\right)_{A,B} \Psi_{s,B}(\boldsymbol{x})$$

Under a $SU(4)$ rotation of the field operators,

$$\tilde{\Psi}_{r,A}(\boldsymbol{x}) = U_{A,B} \Psi_{r,B}(\boldsymbol{x})$$

where $U \in SU(4)$, leaves the $\mathcal{H}_0$ unchanged. Here $\mathcal{H}_0$ is invariant under $SU(4)$ rotation.

The continuum hamiltonian, Eq.(3.11), is the leading term that results after the long wavelength approximation of the lattice kinetic term. There are series of sub-leading terms, which can be expressed in power series of lattice constant a and they are lattice level correction terms. The first of the sub-leading lattice level correction term to the non-interacting model Eq.(3.11),

$$\mathcal{H}_1 = \frac{a^2 t}{8\hbar^2} \int \mathrm{d}^2x \; \Psi^\dagger(\boldsymbol{x}) \Big(\Big(\alpha^x (p_x^2 + 3p_y^2) - \alpha^y 3(p_x p_y + p_y p_x) \Big) \otimes \tau^z \Big) \Psi(\boldsymbol{x}) \tag{3.12}$$

This term will be required when to consider while considering all sub-leading terms for the mean field computations. This term does not retain the full $SU(4)$ symmetry as we had seen in the case of Eq.(3.11)

3.2 Electron-electron interactions

The electron-electron interaction for π-electron on honeycomb lattice are taken into account by considering the on-site interaction and the interaction between electron sitting on two distinct lattice points. We first consider the interaction between electrons on lattice points, it can be written in the following form,

$$\mathcal{H}_I = \frac{1}{2} \sum_{\boldsymbol{n},\boldsymbol{m}} \sum_{r,s} c^\dagger_{\boldsymbol{n},r,\sigma} c_{\boldsymbol{n},r,\sigma} \; V(|\boldsymbol{n}_r - \boldsymbol{m}_s|) \; c^\dagger_{\boldsymbol{m},s,\tilde{\sigma}} c_{\boldsymbol{m},s,\tilde{\sigma}} \tag{3.13}$$

where,

$$V(|\boldsymbol{n}_r - \boldsymbol{m}_s|) = \frac{1}{4\pi\epsilon} \frac{e^2}{|\boldsymbol{n}_r - \boldsymbol{m}_s|} \tag{3.14}$$

here $|\boldsymbol{n}_r - \boldsymbol{m}_s|$ is the distance between the two sub-lattice points under consideration. And there is constraint on summation: $r \neq s$ when $\boldsymbol{n} = \boldsymbol{m}$. The long wavelength continuum approximation for the interaction term Eq.(3.13) yields a leading $SU(4)$ symmetric term

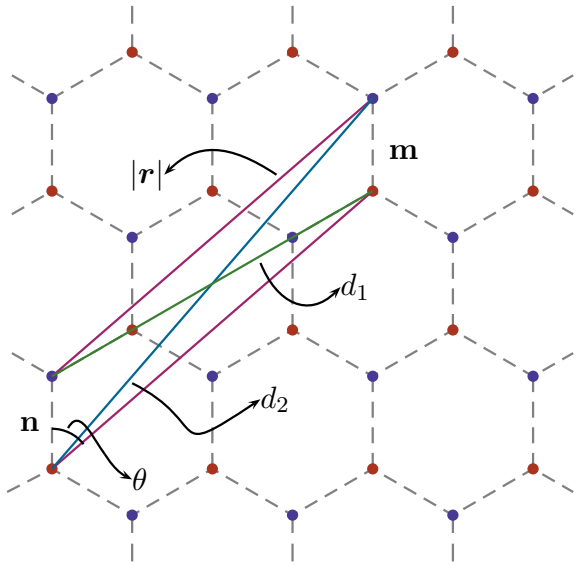

Figure 3.1: The figure shows the distance involved for Coulomb interaction between electrons at lattice points $\boldsymbol{n}$ and $\boldsymbol{m}$. $|\boldsymbol{r}|$ is the distance between the lattice point $\boldsymbol{n}$ and $\boldsymbol{m}$. d_1 and d_2 is the distance between the different sub-lattice points placed at lattice points $\boldsymbol{n}$ and $\boldsymbol{m}$. θ is the angle between carbon-carbon bond at lattice point $\boldsymbol{n}$ and vector $\boldsymbol{n}-\boldsymbol{m}$. The difference $|(|\boldsymbol{r}|-d_i)| \propto a^2/|\boldsymbol{r}|^2$, $i=1,2$, hence very small at very large $|\boldsymbol{r}|$.

(Details of derivation in Appendix C)

$$\mathcal{H}_C = \frac{1}{2}\int_{\substack{\boldsymbol{x},\boldsymbol{y}\\ \boldsymbol{x}\neq\boldsymbol{y}}} V(r)\Psi^\dagger(\boldsymbol{x})\Psi(\boldsymbol{x})\Psi^\dagger(\boldsymbol{y})\Psi(\boldsymbol{y}) \tag{3.15}$$

Here $r=|\boldsymbol{x}-\boldsymbol{y}|$ and $V(r)=\mathrm{e}^2/(4\pi\epsilon r)$. The sub-leading part of the continuum approximation,

$$\mathcal{H}_X = \frac{1}{2}\int_{\substack{\boldsymbol{x},\boldsymbol{y}\\ \boldsymbol{x}\neq\boldsymbol{y}}} V(r)\Big(\frac{1}{4}\frac{\tilde{a}^2}{r^2}(3\cos^2\theta-1)+\ldots\Big) \Big(\Psi^\dagger(\boldsymbol{x})\Psi(\boldsymbol{x})\Psi^\dagger(\boldsymbol{y})\Psi(\boldsymbol{y}) - \Psi^\dagger(\boldsymbol{x})\,\beta\tau^z\,\Psi(\boldsymbol{x})\;\Psi^\dagger(\boldsymbol{y})\,\beta\tau^z\,\Psi(\boldsymbol{y})\Big) \tag{3.16}$$

For large separation, i.e. $r >> \tilde{a}$, the effects resulting from $\mathcal{H}_X$ can be ignored when compared with that of $\mathcal{H}_C$. At shorter distances, i.e. $r \approx \tilde{a}$, the contributions can be sizable and modified when we take into account the fact that electrons are not point charge particles. The wave functions used to describe the π-orbitals have finite extent. The

Coulomb interactions between these π-orbitals will be modified as compared to point charges at same separations.

The nearest neighbour interaction at lattice level on honeycomb lattice,

$$\mathcal{H}_{\tilde{V}} = \tilde{V} \sum_{\boldsymbol{n},\sigma,\tilde{\sigma}} c^{\dagger}_{\boldsymbol{n},1,\sigma} c_{\boldsymbol{n},1,\sigma} \big(c^{\dagger}_{\boldsymbol{n},2,\tilde{\sigma}} c_{\boldsymbol{n},2,\tilde{\sigma}} + c^{\dagger}_{\boldsymbol{n}+\boldsymbol{e}_2,2,\tilde{\sigma}} c_{\boldsymbol{n}+\boldsymbol{e}_2,2,\tilde{\sigma}} + c^{\dagger}_{\boldsymbol{n}+\boldsymbol{e}_1+\boldsymbol{e}_2,2,\tilde{\sigma}} c_{\boldsymbol{n}+\boldsymbol{e}_1+\boldsymbol{e}_2,2,\tilde{\sigma}} \big) \quad (3.17)$$

which takes into account of interaction of electron wave functions at a site with its three nearest neighbours. The continuum approximation of nearest neighbour interaction (Appendix D) yields,

$$\mathcal{H}_V = \frac{3}{4} V a^2 \int_{\boldsymbol{x}} \Big(\big(\Psi^{\dagger}(\boldsymbol{x}) \Psi(\boldsymbol{x}) \big)^2 - \big(\Psi^{\dagger}(\boldsymbol{x}) \beta \tau^z \Psi(\boldsymbol{x}) \big)^2 \Big) \quad (3.18)$$

And when compared with $\mathcal{H}_X$ from Eq.(3.16), $\mathcal{H}_V$ is local interaction version of $\mathcal{H}_X$ and both of have same $SU(4)$ structure. In our model hamiltonian, we combine $\mathcal{H}_X$ with $\mathcal{H}_{\tilde{V}}$ and consider $\mathcal{H}_V$ and treat the coupling constant V as parameter which takes into account short ranged wave function effects and short ranged Coulomb interaction between the point charges. In this process of approximating $\mathcal{H}_X$ into $\mathcal{H}_V$, we forgo the variation of short ranged interaction with distance but retain the essential physics of $SU(4)$ symmetry breaking terms. Moreover the two point Coulomb interaction does not take into account the wave function extend at short distances.

The second type of electron-electron interaction for lattice model is the on-site interaction for the wave functions effects of the π-electrons of carbon atoms. It is short ranged interaction that results when the electrons with opposite spins are localized at same site. This physics is captured by the Hubbard interaction term.

$$\mathcal{H}_U = U \sum_{\boldsymbol{n}} \sum_{r} \hat{n}_{\boldsymbol{n},r,\uparrow} \hat{n}_{\boldsymbol{n},r,\downarrow} \quad (3.19)$$

A continuum approximation for Hubbard term (Details shown in Appendix. E) yields a series of local interaction terms,

$$\mathcal{H}_U = \frac{1}{4}Ua^2 \int_{\boldsymbol{x}} \Big(\big(\Psi^\dagger(\boldsymbol{x})\Psi(\boldsymbol{x})\big)^2 + \big(\Psi^\dagger(\boldsymbol{x})\beta\tau^z\Psi(\boldsymbol{x})\big)^2 + \frac{1}{2}\sum_{j,k=x,y} \big(\Psi^\dagger(\boldsymbol{x})\alpha^j\tau^k\Psi(\boldsymbol{x})\big)^2 \Big) \quad (3.20)$$

3.3 Zeeman term

The presence of magnetic field brings in the Zeeman term for the lattice model which takes into account the spin splitting,

$$\mathcal{H}_Z = -g\,\frac{\mu_B}{\hbar}\sum_{\boldsymbol{n}}\sum_{r} \mathbf{B}\cdot\mathbf{S}_{\boldsymbol{n},r} \quad (3.21)$$

The spin operator in terms of lattice fermion operator

$$S^a_{\mathbf{n},r} = \frac{\hbar}{2}\, c^\dagger_{\boldsymbol{n},r}\sigma^a c_{\boldsymbol{n},r} \quad (3.22)$$

The continuum approximation results in term that breaks the spin rotation symmetry,

$$\mathcal{H}_Z = -\frac{1}{2}\, g\,\mu_B \int_{\boldsymbol{x}} \Psi^\dagger(\boldsymbol{x})\,\boldsymbol{\sigma}\cdot\mathbf{B}\,\Psi(\boldsymbol{x}) \quad (3.23)$$

3.4 Symmetries

The model hamiltonian in presence of magnetic field that we adopt in this thesis has non-interacting term,

$$\mathcal{H}_0 = \iint \mathrm{d}\boldsymbol{x}\; \Psi^\dagger(\boldsymbol{x})\Big(v_F\,\boldsymbol{\alpha}\cdot\boldsymbol{\pi}\otimes\mathbb{1}_4\Big)\Psi(\boldsymbol{x}) \quad (3.24)$$

Here $\boldsymbol{\pi}$ is the conjugate momentum in presence of magnetic field.

$$\boldsymbol{\pi} = \boldsymbol{p} + e\boldsymbol{A}$$

$\boldsymbol{A}$ is the vector potential for the applied magnetic field. The sub-leading correction to kinetic term in presence of magnetic field,

$$\mathcal{H}_1 = \frac{a^2 t}{8\hbar^2} \int \mathrm{d}^2x \; \Psi^\dagger(\boldsymbol{x}) \Big(\Big(\alpha^x(\pi_x^2 + 3\pi_y^2) - \alpha^y 3(\pi_x\pi_y + \pi_y\pi_x) \Big) \otimes \tau^z \Big) \Psi(\boldsymbol{x}) \quad (3.25)$$

The full interacting model adopted in this thesis for variational mean field calculations

$$\mathcal{H} = \mathcal{H}_0 + \mathcal{H}_C + \mathcal{H}_V + \mathcal{H}_U + \mathcal{H}_Z + \mathcal{H}_1 \quad (3.26)$$

Here $\mathcal{H}_0$ is kinetic term given in Eq.(3.24), $\mathcal{H}_C$ takes the long ranged Coulomb interaction into account given in Eq.(3.15). The short ranged interaction are, $\mathcal{H}_V$, the nearest neighbour interaction given in Eq.(3.18) and $\mathcal{H}_U$ is the on-site Hubbard interaction term given in Eq.(3.20). $\mathcal{H}_Z$ take Zeeman splitting of spins into account given in Eq.(3.23) and finally $\mathcal{H}_1$ is sub-leading lattice correction to the kinetic term given in Eq.(3.25).

In presence of magnetic field the discrete symmetries: parity, charge conjugation and particle-hole are no longer the symmetries of the interacting model. The non-interacting term, $\mathcal{H}_0$ and long ranged Coulomb term, $\mathcal{H}_C$ are the only $SU(4)$ symmetric terms. Under $SU(4)$ transformation of fermion field operator,

$$\tilde{\Psi}_{r,A}(\boldsymbol{r}) = \mathcal{U}_{A,B}\Psi_{r,B}(\boldsymbol{r}) \quad (3.27)$$

where $\mathcal{U} \in SU(4)$, is the unitary operator. Both $\mathcal{H}_0$ and $\mathcal{H}_C$ are invariant under this transformation, Eq.(3.27).

The short ranged interaction terms break this $SU(4)$ symmetry. Both $\mathcal{H}_V$ and $\mathcal{H}_U$ are

invariant under $U(1) \times SU(2)$, i.e.

$$\mathcal{U} = \mathrm{e}^{-\frac{\mathrm{i}}{2}\theta_\tau \tau^z} \otimes U_\sigma \tag{3.28}$$

Here U_σ denotes a unitary rotation in $SU(2)$ spin space. There is also a discrete symmetry that leaves only the short ranged interactions invariant,

$$\mathcal{U} = \tau^x \otimes U_\sigma \tag{3.29}$$

This transformation amounts to interchanging the valley indices of the field operators. The group that leave the contact interaction terms invariant is a semi-direct product of $Z_2 \rtimes U(1) \otimes SU(2)$

The sub-leading correction to kinetic term, $\mathcal{H}_1$ is only invariant under $U(1) \otimes SU(2)$.

The Zeeman term, $\mathcal{H}_Z$ breaks the spin symmetry and only $U(1)$ symmetry of spin rotation is remnant of the $SU(2)$ spin rotation and leaves the $SU(2)$ valley unbroken. Hence the

$$\mathcal{U} = U_\tau \otimes \mathrm{e}^{-\frac{\mathrm{i}}{2}\theta_\sigma \sigma^z} \tag{3.30}$$

is the transformation on field operator that leaves the Zeeman term invariant. Here U_τ is a unitary rotation in $SU(2)$ valley space

The symmetry under which our model hamiltonian Eq.(3.26) is invariant is $U(1) \times U(1)$. The transformation

$$\mathcal{U} = \mathrm{e}^{-\frac{\mathrm{i}}{2}\theta_\tau \tau^z} \otimes \mathrm{e}^{-\frac{\mathrm{i}}{2}\theta_\sigma \sigma^z} \tag{3.31}$$

on the field operators leaves $\mathcal{H}$ invariant.

3.5 Summary

We have shown in this chapter a systematic continuum approximation for the interacting lattice model for graphene. The lattice interaction terms yields a leading $SU(4)$ terms and sub-leading part. We justified replacing the sub-leading part with the terms resulting from the nearest neighbour interaction to take into account the wave function effects at the short distances. We have presented the interacting continuum model that we study in this thesis in Eq.(3.26)

Chapter 4

Variational wave function

In this thesis, we study the interacting model Eq.(3.26) described in the previous chapter to explore the possible nature of ground state for the Hall conductivity at $\sigma_H = 0, \pm 1$. The route taken is that of variational mean field theory. We first motivate our choice of single particle wave functions for massive Dirac particle in magnetic field to construct the many body variational ground state wave functions. The variational ground state comprises of the Landau level indices with negative integers, which is referred as filled Dirac sea. And partially filled quartet $n = 0$ Landau level that corresponds to the particular Hall conductivity under consideration. Henceforth, the reference to partially filled quartet $n = 0$ Landau level indicates, for example, one of the four $SU(4)$ levels (sub-levels) is occupied and orbital degeneracy is saturated in case of $\sigma_H = -1$. In the case for $\sigma_H = 0$, two of $SU(4)$ levels of $n = 0$ Landau levels are filled with orbital degeneracy saturated. Though the filled Dirac sea has Landau levels with all negative indices is a feature of the effective continuum Dirac theory for graphene, we have a cut-off for the highest Landau level with negative index occupied. Justification for this ultraviolet cut-off comes from the lattice model for the graphene. We construct the variational wave functions for the Hall conductivity at $\sigma_H = 0, \pm 1$ and discuss their parameterization.

To compute the variational mean field energy with the filled Dirac sea, a convenient route

is to evaluate the equal time Euclidean Feynman propagator for a massive Dirac particle in magnetic field. We derive the two point correlator for a massive Dirac particle in presence of magnetic field with filled Dirac sea. The Wick's decomposition of the four fermion terms for the interaction can be expressed in terms of two point correlation functions. And these correlation functions are computed from the imaginary time representation of propagators. The two point correlation function and the coincident correlation function are evaluated and used to compute the mean field energy and particle-hole excitation gaps.

4.1 Charge and spin ordering of $n = 0$ Landau level

In this thesis, we are interested in understanding the ground states for the Hall conductivity $\sigma_H = 0, \pm 1$. At single particle level, this can be understood by occupying the sub-levels of Landau level with index $n = 0$ with the orbital degeneracy saturated for filled sub-level. The Landau level with index $n = 0$ for a massless Dirac particle (Appendix. A)

$$\phi^{0,l}(\boldsymbol{x}) = \begin{pmatrix} 0 \\ \\ \varphi_{0,l}(\boldsymbol{x}) \end{pmatrix} \tag{4.1}$$

is special when compared with Landau levels with non-zero index. It has a staggered charge distribution. The measure of the staggered charge for filled $n = 0$ Landau level with saturated orbital degeneracy,

$$\int \mathrm{d}\boldsymbol{x} \sum_{l=0}^{\infty} \left(\phi^{0,l}(\boldsymbol{x})\right)^{\dagger} \beta \, \phi^{0,l}(\boldsymbol{x}) = -1 \tag{4.2}$$

This staggered charge is absent for the Landau levels with non-zero integer indices, $|n| \neq 0$,

$$\int \mathrm{d}\boldsymbol{x} \sum_{l=-n}^{\infty} \left(\phi^{n,l}(\boldsymbol{x})\right)^{\dagger} \beta \, \phi^{n,l}(\boldsymbol{x}) = 0 \tag{4.3}$$

In the case of graphene, the eigen vectors also carry the $SU(4)$ index as they are good quantum numbers for non-interacting model,

$$\Phi^{n,l,q}(\boldsymbol{x}) = \phi^{n,l}(\boldsymbol{x})\,\chi^{q} \tag{4.4}$$

Here χ^q is four component vector corresponding to $SU(4)$ part of the hamiltonian. The quantity that is physically relevant is the staggered charge on the two sub-lattice for graphene and its measure is given by,

$$\int \mathrm{d}\boldsymbol{x} \sum_{l=0}^{\infty} \left(\Phi^{0,l,q}(\boldsymbol{x})\right)^{\dagger} \beta\tau^{z}\, \Phi^{0,l,q}(\boldsymbol{x}) = \pm 1 \tag{4.5}$$

Here we are assumed for simplicity that χ^q is eigenvector of τ^z, i.e. valley is good quantum number. At lattice level for graphene, this means that a filled $n = 0$ Landau level sub-level with orbital degeneracy saturated will result in charge localized on one of the sub-lattice points. Thus leading to staggered charge distribution for graphene sub-lattice points and average of the operator, $\beta\,\tau^z$, gives the measure for it. Another quantity which is significance is the staggered spin on the two sub-lattice points and the operator $\beta\,\tau^z\,\sigma^z$ gives its measure. In the case, when χ^q is the eigenvector for the operator $\tau^z\,\sigma^z$, then

$$\int \mathrm{d}\boldsymbol{x} \sum_{l=0}^{\infty} \left(\Phi^{0,l,q}(\boldsymbol{x})\right)^{\dagger} \beta\,\tau^{z}\,\sigma^{z}\, \Phi^{0,l,q}(\boldsymbol{x}) = \pm 1 \tag{4.6}$$

Third quantity that can be readily seen is the total spin, and the operator σ^z is a good measure and once again it will depend on eigenstate of the vector χ^q.

The profile at lattice level for a occupied sub-level of $n = 0$ Landau level resides in the eigenstate of $SU(4)$ component. The Fig.4.1 shows the caricature at lattice level when χ^q is an eigenstate of the operator $\tau^z\,\sigma^z$. This particular choice gives a non-zero value for the operators, $\beta\,\tau^z$, $\beta\tau^z\sigma^z$ and σ^z. The vector χ^q could have pointed in any direction in the $SU(4)$ space. For example, χ^q could have been a linear superposition of eigenstates of $\tau^z\,\sigma^z$.

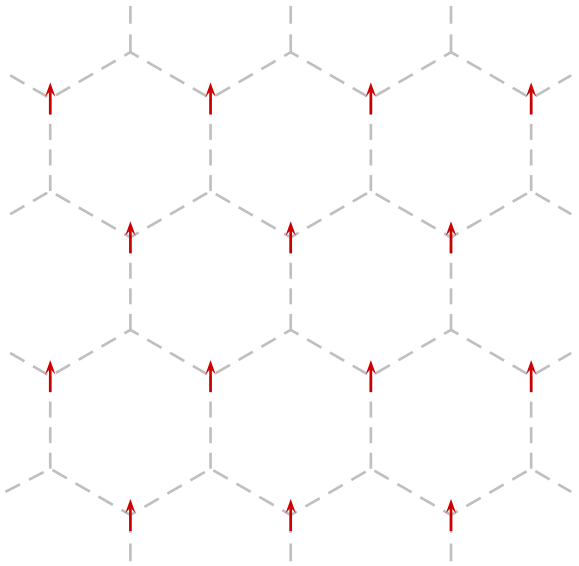

Figure 4.1: This figure shows a profile for one of the $n = 0$ Landau level wave function. The up arrow is caricature of the wave function that is localized on one of the sub-lattice point with spin pointing along the z-axis.

In the case when two sub-levels of $n = 0$ Landau level are occupied, there are several possibilities that can result in a profile at lattice level. We enumerate a few here. The possible scenario that if both the sub-levels are eigenstates of operator σ^z and have same eigenvalue. This results in a ferromagnetic ordering of spins at the lattice level as both the sub-lattice points have spins pointing along z-axis. In the scenario when both the sub-levels are eigenstates of operator τ^z with same eigenvalue, then we have got a charge ordered state. In this state, both the sub-levels are localized on one of the sub-lattice point with spin pointing in opposite direction. Another possibility is when the two occupied sub-levels result in a staggered spin orientation on two sub-lattice. This will result if both the sub-levels have same eigenvalue for the operator $\tau^z\,\sigma^z$.

An important point to note is that in case of all four sub-levels of $n = 0$ Landau levels are occupied then the staggered charge distribution vanishes.

$$\int \mathrm{d}\boldsymbol{x} \sum_{q=1}^{4} \sum_{l=0}^{\infty} \left(\Phi^{0,l,q}(\boldsymbol{x})\right)^{\dagger} \beta\tau^z\, \Phi^{0,l,q}(\boldsymbol{x}) = 0 \tag{4.7}$$

And so does the staggered spin distribution distribution. In the scenario when all the

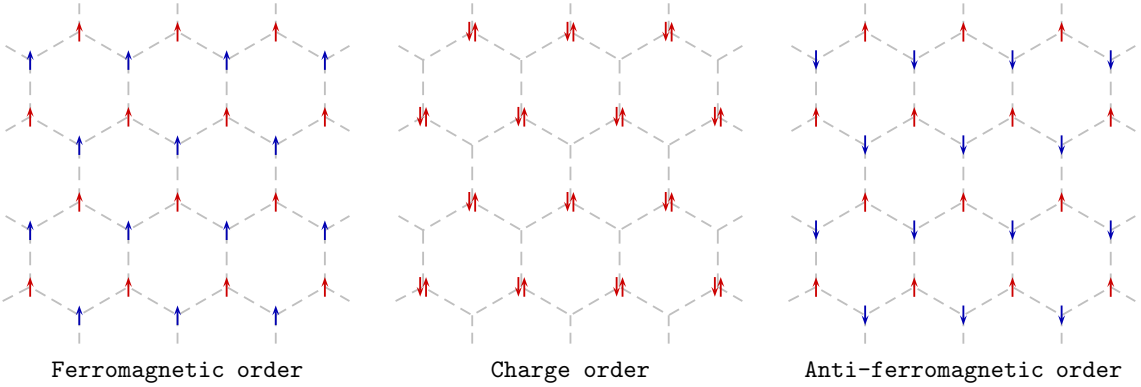

Figure 4.2: This figure shows a profile for two occupied of the $n = 0$ Landau level wave function. The figure shows the possible ferromagnetic, charge and anti-ferromagnetic ordering that can occur the way two sub-levels are filled.

$n = 0$ sub-levels are occupied we have a $SU(4)$ singlet and no interesting lattice level profile.

The case when three of sub-levels are occupied can be viewed from the hole perspective, i.e. the wave function profile of the only unoccupied sub-level. The results will be same as that of only one of $n = 0$ sub-level is occupied.

For massless Dirac particle with Landau level index $n \neq 0$, for each filled sub-level, the staggered charge always vanishes,

$$\int \mathrm{d}\boldsymbol{x} \sum_{l=-n}^{\infty} \left(\Phi^{n,l,q}(\boldsymbol{x})\right)^{\dagger} \beta\tau^{z} \Phi^{n,l,q}(\boldsymbol{x}) = 0 \tag{4.8}$$

And so does the staggered spin distribution, $\beta\tau^{z}\sigma^{z}$.

The ground state for the Hall conductivity $\sigma_H = 0, \pm 1$, can be viewed having two components: first partially filled sub-levels of $n = 0$ Landau levels occupied. The second component is all the Landau levels with negative index are filled, that is, for each index n, the sub-level and sub-band degeneracy is saturated. The case when all the four sub-levels of the Landau level for any index n for the massless Dirac particle forms a $SU(4)$ singlet, i.e. invariant under any $SU(4)$ rotation. The construction of variational state for Hall conductivity, $\sigma_H = 0, \pm 1$ with Landau levels for massless Dirac particles results in

variational ground state where $SU(4)$ symmetry is broken for $n = 0$ and $SU(4)$ singlet for all $n < 0$.

Taking hint from the staggered nature of $n = 0$ Landau level, we consider the ansatz that electron-electron interaction induces mass to the massless Dirac particle of the non-interacting theory. We will show self-consistently that indeed the non-zero value of mass minimizes the ground state energy for the Hall conductivity under consideration in this thesis. Moreover it provides a possibility of same symmetry for the partially occupied sub-levels of $n = 0$ Landau level and the filled Dirac sea.

4.2 Landau levels for massive Dirac particle in graphene

In this section, we discuss the features of eigenvectors of massive Dirac particles for the graphene in presence of magnetic field. These Landau states for massive Dirac particle will be used to construct variational ground state in the next section. One particle hamiltonian for massive Dirac particles in graphene in presence of magnetic field,

$$\mathrm{h} = v_F \, \boldsymbol{\alpha} \cdot \boldsymbol{\pi} \otimes \mathbb{1}_4 + \beta \otimes M \tag{4.9}$$

Here the $\mathbb{1}_4$ and M are 4×4 matrices corresponding to the $SU(4)$ space. And $\boldsymbol{\pi} = \boldsymbol{p} + e\boldsymbol{A}$ is the conjugate momenta in presence of magnetic field. The only assumption made about the matrix M is that it is hermitian to ensure the hermiticity of the hamiltonian. Hence there exist a basis where M is diagonal and can be expressed as,

$$M = \sum_{q=1}^{4} m_q |q\rangle\langle q| \tag{4.10}$$

The eigenvalues m_q are the mass of Dirac particles and $|q\rangle$ are the corresponding eigenvectors.

The eigenvalues and eigenvectors for the hamiltonian Eq.(4.9),

$$\epsilon_{n,l,q} = \text{sgn}(n)\sqrt{2|n| + m_q^2} \tag{4.11}$$

$$\Phi^{n,l,q}(\boldsymbol{x}) = \frac{1}{\sqrt{2\epsilon_{n,l,q}(\epsilon_{n,l,q} + m_q)}} \begin{pmatrix} (\epsilon_{n,l,q} + m_q)\varphi_{n-1,l+1}(\boldsymbol{x}) \\ \mathrm{i}\sqrt{2|n|}\varphi_{n,l}(\boldsymbol{x}) \end{pmatrix} \chi^q \tag{4.12}$$

And for $n = 0$

$$\epsilon_{0,l,q} = -m_q \tag{4.13}$$

$$\Phi^{0,l,q}(\boldsymbol{x}) = \begin{pmatrix} 0 \\ \varphi_{0,l}(\boldsymbol{x}) \end{pmatrix} \chi^q \tag{4.14}$$

Here the energies, $\epsilon_{n,l,q}$ and masses m_q are measured in the units of $(\hbar\, v_F/\ell_c)$. So they are dimensionless quantities. χ^q are four component vectors.

An interesting feature of the Landau levels for the massive Dirac particles is that they can be expressed as the linear combination of Landau levels for massless Dirac particle. The eigenstates Eq.(4.12), any $n \neq 0$,

$$\Phi^{n,l.q}(\boldsymbol{x}) = A_{n,m_q} \begin{pmatrix} \varphi_{n-1,l+1}(\boldsymbol{x}) \\ \mathrm{i}\,\varphi_{n,l}(\boldsymbol{x}) \end{pmatrix} \chi^q + B_{n,m_q} \begin{pmatrix} \varphi_{n-1,l+1}(\boldsymbol{x}) \\ -\mathrm{i}\,\varphi_{n,l}(\boldsymbol{x}) \end{pmatrix} \chi^q \tag{4.15}$$

The coefficients

$$\begin{aligned} A_{n,m_q} &= \frac{1}{2}\Big(\Big(1 + \frac{m_q}{\epsilon_{n,l.q}}\Big)^{\frac{1}{2}} + \Big(1 - \frac{m_q}{\epsilon_{n,l.q}}\Big)^{\frac{1}{2}}\Big) \\ B_{n,m_q} &= \frac{1}{2}\Big(\Big(1 + \frac{m_q}{\epsilon_{n,l.q}}\Big)^{\frac{1}{2}} - \Big(1 - \frac{m_q}{\epsilon_{n,l.q}}\Big)^{\frac{1}{2}}\Big) \end{aligned} \tag{4.16}$$

This shows that for $n \neq 0$ the Landau level with index n of massive Dirac particle are obtained by mixing positive and negative Landau levels of massless Dirac particle with same index. This amounts to mixing massless Dirac particle and hole states with same Landau level index. The breaking of particle-hole symmetry is justified as in presence of

magnetic field, the non-interacting model no longer retains the particle-hole symmetry.

The $n = 0$ Landau level for massive Dirac particle is exactly same as that of massless ones, hence it retains the staggered charge and spin ordering that we discussed in the previous section. The $n \neq 0$ Landau levels for the massive Dirac particles, the staggered charge distribution on two sub-lattice points is,

$$\int \mathrm{d}\boldsymbol{x} \sum_{l=-n}^{\infty} \left(\Phi^{n,l,q}(\boldsymbol{x})\right)^{\dagger} \beta\tau^{z}\, \Phi^{n,l,q}(\boldsymbol{x}) = \frac{m_q}{\epsilon_{n,l,q}}\, (\chi^{q})^{\dagger}\tau^{z}\chi^{q} \tag{4.17}$$

And the staggered spin distribution is,

$$\int \mathrm{d}\boldsymbol{x} \sum_{l=-n}^{\infty} \left(\Phi^{n,l,q}(\boldsymbol{x})\right)^{\dagger} \beta\tau^{z}\sigma^{z}\, \Phi^{n,l,q}(\boldsymbol{x}) = \frac{m_q}{\epsilon_{n,l,q}}\, (\chi^{q})^{\dagger}\tau^{z}\sigma^{z}\chi^{q} \tag{4.18}$$

This shows that $n \neq 0$ Landau levels also have staggered charge and spin distribution. The symmetries partially occupied $n = 0$ Landau levels are translated to that of $n \neq 0$ with the choice of massive Dirac eigenstates and magnitude of $SU(4)$ polarization of the filled Dirac sea is proportional to the magnitude of eigenvalues m_q. The quantities that completely specify the matrix M are the variational parameters for ground state that we are going to construct for Hall conductivity $\sigma_H = 0, \pm 1$. The hermitian matrix M required sixteen parameters to be completely specified but the additional symmetry constraints for specific Hall conductivity will reduce the number of variational parameters required for each case, which we discuss in the next section.

4.3 Variational states

The Landau level wave functions for massive Dirac particles are used to expand the field operators,

$$\Psi_{r,A}(\boldsymbol{x}) = \sum_{n,l,q} \Phi^{n,l,q}_{r,A}(\boldsymbol{x})\; \psi_{n,l,q} \tag{4.19}$$

Here the first subscript r is used for Dirac spinor index and second A is used to specify the $SU(4)$ spinor index. $\psi_{n,l,q}$ is annihilation operator for fermion with Landau level index n, orbit degeneracy index l and the $SU(4)$ quantum number q.

In this thesis we will be only investigating the nature of ground state and excitations about the states for Hall conductivity $\sigma_H = 0$ and $\sigma_H = -1$. The state for $\sigma_H = +1$ is charge conjugate state of $\sigma_H = -1$, so we are only going to study the $\sigma_H = -1$ here.

$$|\sigma_H = 0\rangle = \Big(\prod_{q=1}^{2}\prod_{l=0}^{\infty}\psi^{\dagger}_{0,l,1}\Big)\Big(\prod_{n=-N_c}^{-1}\prod_{q=1}^{4}\prod_{l=-|n|}^{\infty}\psi^{\dagger}_{n,l,q}\Big)|0\rangle \tag{4.20}$$

$$|\sigma_H = -1\rangle = \Big(\prod_{l=0}^{\infty}\psi^{\dagger}_{0,l,1}\Big)\Big(\prod_{n=-N_c}^{-1}\prod_{q=1}^{4}\prod_{l=-|n|}^{\infty}\psi^{\dagger}_{n,l,q}\Big)|0\rangle \tag{4.21}$$

These states have partially occupied sub-levels of $n = 0$ Landau level and a filled Dirac sea operators acting on the vacuum, $|0\rangle$, zero particle state. The Dirac theory has a sea with no lower bound, but here the $(2+1)d$ Dirac theory is an effective theory resulting from the underlying lattice model. The lattice model set an ultraviolet cutoff which is proportional to the inverse of the lattice constant. We estimate a cutoff for Landau level index by equating the number of states of the lattice model to that of continuum model.

$$2_{\text{valley}} \times 2_{\text{spin}} \times 2_{bands,\pm} \int_0^{\Lambda} \frac{\mathrm{d}^2k}{(2\pi)^2} = 2_{\text{valley}} \times 2_{\text{spin}} \times \frac{2N_c + 1}{2\pi\ell_c^2} \tag{4.22}$$

In Eq.(4.22), LHS is number density of the states for the continuum model after equating with lattice model

$$\Lambda^2 = \frac{4\pi}{\sqrt{3}a^2}$$

Λ is the ultraviolet cutoff on the wavevector. RHS is total number density of states resulting from the non-interacting model in presence of magnetic field. The cutoff on the Landau level index,

$$N_c = \frac{2\pi}{\sqrt{3}}\Big(\frac{\ell_c}{a}\Big)^2 \tag{4.23}$$

The variational ground states described in Eq.(4.20) and Eq.(4.21) is parameterized by

the elements that specifies the mass matrix M. As discussed earlier in previous section that 4×4 hermitian matrix M required sixteen parameters to be specified completely. A hermitian matrix will have a unitary matrix, $\mathcal{U}$, that will diagonalize it.

$$M = \mathcal{U}\, M_D\, \mathcal{U}^\dagger \tag{4.24}$$

Here $M_D = \{m_1, m_2, m_3, m_4\}$ is diagonal matrix, which accounts for four parameters. In general $n \times n$ unitary matrix requires n^2 parameters to specify it. In our case, a sixteen parameters will be required for unitary matrix, $\mathcal{U}$. This suggests that we have over counting of parameter on the RHS of Eq.(4.24). The extra four parameters can be accounted for by choice of matrix $\mathcal{U}$. The matrix $\mathcal{U}$ is not unique as we free to choose as a product of two unitary matrices,

$$\mathcal{U} = \tilde{\mathcal{U}}\, \tilde{\mathcal{V}}$$

such that it $\tilde{\mathcal{V}}$ leaves the M_D invariant, i.e. $\tilde{\mathcal{V}} M_D \tilde{\mathcal{V}}^\dagger = M_D$. This is possible choosing a diagonal form for $\tilde{\mathcal{V}} = \{\mathrm{e}^{\mathrm{i}\,\theta_1}, \mathrm{e}^{\mathrm{i}\,\theta_2}, \mathrm{e}^{\mathrm{i}\,\theta_3}, \mathrm{e}^{\mathrm{i}\,\theta_4}\}$. This takes into account of four parameters and we need only twelve parameters to specify the matrix $\tilde{\mathcal{U}}$. So we have shown that we actually only need twelve parameters to completely specify matrix $\mathcal{U}$ in Eq.(4.24) and taking into account of parameter counting on either side of this equation.

An alternative route to confirm that we only need the twelve parameters for matrix $\mathcal{U}$, up to a right multiplication by a diagonal unitary matrix, is by counting the parameters required to construct unitary matrix from the eigenvectors up to overall phases. An eigenvector of matrix M is four component column vector with complex entries and taking orthonormality into account implies that we need seven real parameters to describe it completely. Four eigenvectors of M takes the count to twenty eight to construct $\mathcal{U}$. The requirement, $\mathcal{U}\,\mathcal{U}^\dagger = \mathbb{1}_4$ results in sixteen constraint equations. This leaves with twelve independent parameters to describe an unitary matrix $\mathcal{U}$ up to a multiplication by a diagonal unitary matrix.

In general, full parameterization of mass matrix M can be done by four parameters to specify the eigenvalues and twelve to describe the four eigenvectors. There are some more symmetry consideration that will reduce the sixteen parameters to parameterize M for our variational states as we shall see in following discussion.

4.3.1 Parameterization for ground state at $\sigma_H = -1$

The ground state for Hall conductivity $\sigma_H = -1$ requires only one of four sub-levels of $n = 0$ Landau level to be occupied and rest three unoccupied. This choice implies that $n = 0$ Landau level should be invariant under a subgroup, $U(1) \times SU(3)$, of $SU(4)$. This amounts that there is $U(1)$ transformation for occupied sub-level of $n = 0$ Landau level and $SU(3)$ transformation for the unoccupied sub-levels should leave the ground state invariant. The invariance of ground state under $U(1)\times SU(3)$ is ensured by the structure of mass matrix M. The diagonal matrix $M_D = \{m_o, -m_u, -m_u, -m_u\}$ and the associated unitary matrix that diagonalize M, belongs to the subgroup $U(1) \times SU(3)$. Here $m_o > 0$ and $m_u > 0$. The negative sign indicates the unoccupied levels for $n = 0$. This ensures that ground state Eq.(4.21) is invariant under transformation $SU(1) \times SU(3)$. Thus the set of all such mass matrix is a coset space $SU(4)/(U(1) \times SU(3))$. This counting of parameters for the coset space is equivalent to that of $U(4)/(U(1) \times U(3))$, which is $4^2 - 1^2 - 3^2 = 6$.

The mass matrix that is invariant under subgroup $U(1)\times SU(3)$ can be constructed explicitly by specifying the $SU(4)$ component of the occupied level. A general four component vector required four complex numbers to be specified. Orthonormality and an overall phase factor gets rid of two and leaving with six parameters to specify single $SU(4)$ component,

$$|1\rangle = \cos(\frac{\gamma_1}{2})|+\rangle|\boldsymbol{n}_1\rangle + \mathrm{e}^{\mathrm{i}\,\Omega_1}\sin(\frac{\gamma_1}{2})|-\rangle|-\boldsymbol{n}_2\rangle \tag{4.25}$$

Here $|\pm\rangle|\boldsymbol{n}_i\rangle = |\pm\rangle \otimes |\boldsymbol{n}_i\rangle$. And $|\pm\rangle$ are the eigenvectors of valley operator τ^z. $|\boldsymbol{n}_i\rangle$ is

an vector pointing in arbitrary direction in spin space.

$$|\boldsymbol{n}_i\rangle = \cos(\frac{\theta_i}{2})|\uparrow\rangle + \mathrm{e}^{\mathrm{i}\,\phi_i}\sin(\frac{\theta_i}{2})|\downarrow\rangle \tag{4.26}$$

Here $|\uparrow\rangle$ and $|\downarrow\rangle$ are the eigenvector for spin operator σ^z.

The mass matrix for the Hall conductivity $\sigma_H = -1$ is

$$M = (m_o + m_u)|1\rangle\langle 1| - m_u \mathbb{1}_4 \tag{4.27}$$

Here we made use of the fact, $\sum_{q=1}^{4} |q\rangle\langle q| = \mathbb{1}_4$

The two parameters m_o and m_u for the eigenvalues of M and six angle parameters for vector $|1\rangle$ makes it eight variational parameters to describe the ground state in Eq.(4.21).

4.3.2 Parameterization for ground state at $\sigma_H = 0$

In case of hall conductivity at $\sigma_H = 0$, two of the sub-levels of $n = 0$ Landau level are occupied and two are unoccupied. The subgroup that leaves the $n = 0$ Landau levels invariant is $SU(2) \times SU(2)$, which means that both the occupied and unoccupied sub-levels are invariant under $SU(2)$ rotations among themselves. To achieve same invariance under unitary rotation for the filled Dirac sea, for each Landau level with negative index, the diagonal mass matrix takes the form, $M_D = \{m_o, m_o, -m_u, -m_u\}$. The unitary matrix that bring the mass matrix M to this form is a subgroup $SU(4)$, same as for $n = 0$ Landau level, i.e. $SU(2) \times SU(2)$. The number of parameters need to describe this subgroup from a coset space $SU(4)/(SU(2)\times SU(2))\times U(1)$. This counting is equivalent to counting the coset space for $U(4)/(U(2) \times U(2))$, which amounts to $4^2 - 2^2 - 2^2 = 8$. In addition there are two parameters for the eigenvalues of mass matrix m_o and m_u. Thus we need ten parameters to describe the variational ground state Eq.(4.20).

Similar to what we saw in previous subsection, we can construct the unitary matrix from

the orthonormal four component column vectors with eight parameters. This can be done by selecting a four component vector with six parameters as we did for the case of $\sigma_H = -1$ and then choosing a second that is orthonormal to the first with addition of two more parameters,

$$|1\rangle = \cos(\frac{\gamma_1}{2})|+\rangle|\boldsymbol{n}_1\rangle + \mathrm{e}^{\mathrm{i}\,\Omega_1}\sin(\frac{\gamma_1}{2})|-\rangle|-\boldsymbol{n}_2\rangle \tag{4.28}$$

$$|2\rangle = \cos(\frac{\gamma_2}{2})|+\rangle|-\boldsymbol{n}_1\rangle + \mathrm{e}^{\mathrm{i}\,\Omega_2}\sin(\frac{\gamma_2}{2})|-\rangle|\boldsymbol{n}_2\rangle \tag{4.29}$$

Parameter count for these two orthonormal vectors is eight.

The mass matrix for Hall conductivity $\sigma_H = 0$ has ten variational parameters,

$$M = (m_o + m_u)\big(|1\rangle\langle 1| + |2\rangle\langle 2|\big) - m_u\mathbb{1}_4 \tag{4.30}$$

The choice of massive Dirac particle for constructing the variational wave function with mass matrix as the variational parameter allows us to have same $SU(4)$ polarization for both partially filled $n = 0$ Landau level and the filled Dirac sea. The specific values taken by the variational parameters i.e. the mass matrix M, which will be decided by the minimization of variational mean field energy is going to decide the $SU(4)$ polarization of the ground state.

4.4 Propagator for massive Dirac particle in presence of magnetic field

In this section, we digress to evaluate the two point correlator using time ordered Feynman propagator for a massive Dirac particle in presence of magnetic field. This two point correlator that is encountered while computing the ground state energies. Here we are considering a massive Dirac particle in $(2+1)d$ and subjected to magnetic field along the

z-axis. The hamiltonian,

$$\mathrm{h} = \frac{\hbar v_F}{\ell_c} \begin{pmatrix} m & \pi_x - \mathrm{i}\,\pi_y \\ \pi_x + \mathrm{i}\,\pi_y & -m \end{pmatrix} \tag{4.31}$$

Here $m > 0$ is expressed in units of $\hbar v_F/\ell_c$, and the eigenvalues are,

$$\begin{aligned} \epsilon_{n,l} &= \mathrm{sgn}(n)\big(\frac{\hbar\, v_F}{\ell_c}\big)\sqrt{2|n| + m^2} \\ \epsilon_{0,l} &= -m \end{aligned} \tag{4.32}$$

The completeness relation

$$\mathbb{1}_2 = \sum_{n=-\infty}^{\infty} \sum_{l=-|n|}^{\infty} \Big(\Theta(-\epsilon_n)|n,l\rangle\langle n,l| + \Theta(\epsilon_n)\|n,l\rangle\langle n,l|\Big) \tag{4.33}$$

Here $\mathbb{1}_2$ is 2×2 identity matrix, $\epsilon_n > 0$ and the first term is summation over all negative energy eigenvalue states which includes all the Landau levels with negative indices and the $n = 0$ Landau level since the eigenvalue is $-m$ with $m > 0$. The second term is for states with positive energies i.e. Landau levels with indices $n > 0$.

We are interested in constructing two point correlator,

$$G_{s,s'}(\boldsymbol{r}, \boldsymbol{r}_0) = \frac{1}{2}\langle 0|[\Psi_s^\dagger(\boldsymbol{r}), \Psi_{s'}(\boldsymbol{r}_0)]|0\rangle \tag{4.34}$$

Here $|0\rangle$, the vacuum is constructed by occupying Landau levels with index $n = 0$ and $n < 0$ that is all the Landau levels with negative energy eigenvalues. This definition takes into account the subtraction of background charge from the positive charged ions.

$$G = \frac{1}{2}\sum_{n=-\infty}^{\infty} \sum_{l=-|n|}^{\infty} \big(\Theta(-\epsilon_n) - \Theta(\epsilon_n)\big)|n,l\rangle\langle n,l| \tag{4.35}$$

Let

$$K = \Theta(-\epsilon_n) - \Theta(\epsilon_n) \tag{4.36}$$

K can be defined as following by considering the equal time for time ordered Feynman propagator,

$$K = \lim_{\tau \to 0^-} \mathrm{e}^{-\tau\epsilon_n}\Theta(-\tau)\Theta(-\epsilon_n) - \lim_{\tau \to 0^+} \mathrm{e}^{-\tau\epsilon_n}\Theta(\tau)\Theta(\epsilon_n) \tag{4.37}$$

Define

$$K(\tau) = \mathrm{e}^{-\tau\epsilon_n}\Theta(-\tau)\Theta(-\epsilon_n) - \mathrm{e}^{-\tau\epsilon_n}\Theta(\tau)\Theta(\epsilon_n) \tag{4.38}$$

$$K = \lim_{\tau \to 0^-} K(\tau) + \lim_{\tau \to 0^+} K(\tau) \tag{4.39}$$

$$K(\tau) = -\int_{-\infty}^{+\infty} \frac{\mathrm{d}\omega}{2\pi} \frac{\mathrm{e}^{\mathrm{i}\,\omega\tau}}{\epsilon_n + \mathrm{i}\,\omega} \tag{4.40}$$

$$= -\int_{-\infty}^{+\infty} \frac{\mathrm{d}\omega}{2\pi} \mathrm{e}^{\mathrm{i}\,\omega\tau}(\epsilon_n - \mathrm{i}\,\omega) \int_0^{\infty} \mathrm{d}s\ \mathrm{e}^{-s(\epsilon_n^2+\omega^2)} \tag{4.41}$$

Here we make use the integral representation,

$$\frac{1}{\epsilon_n^2 + \omega^2} = \int_0^{\infty} \mathrm{d}s\ \mathrm{e}^{-s(\epsilon_n^2+\omega^2)} \tag{4.42}$$

$$K(\tau) = -\frac{1}{2\sqrt{\pi}} \int_0^{\infty} \frac{\mathrm{d}s}{\sqrt{s}}\ \mathrm{e}^{-(s\epsilon_n^2 + \frac{\tau^2}{4s})}\big(\epsilon_n + \frac{\tau}{2s}\big) \tag{4.43}$$

Hence using Eq.(4.39)

$$K = -\frac{1}{\sqrt{\pi}}\epsilon_n \int_0^{\infty} \frac{\mathrm{d}s}{\sqrt{s}}\ \mathrm{e}^{-s\epsilon_n^2} \tag{4.44}$$

using it in Eq.(4.35), we obtain the correlator,

$$G = -\frac{1}{2\sqrt{\pi}} \int_0^{\infty} \frac{\mathrm{d}s}{\sqrt{s}}\ \mathrm{h}\,\mathrm{e}^{-s\mathrm{h}^2} \tag{4.45}$$

This is the so called 'heat kernel' representation.

Now the task is find the real space representation for the heat kernel operator $\mathrm{e}^{-s\mathrm{h}^2}$.

$$\mathrm{h} = \epsilon \begin{pmatrix} m & \pi_x - \mathrm{i}\,\pi_y \\ \pi_x + \mathrm{i}\,\pi_y & -m \end{pmatrix} \tag{4.46}$$

Here $\epsilon = (\hbar v_F)/\ell_c$ and h^2 is diagonal.

$$\mathrm{h}^2 = \epsilon^2 \begin{pmatrix} m^2 + \pi_x^2 + \pi_y^2 + 1 & 0 \\ 0 & m^2 + \pi_x^2 + \pi_y^2 - 1 \end{pmatrix} \tag{4.47}$$

From the knowledge of imaginary time, i.e. $t = -\mathrm{i}\,\hbar\beta$ propagator for hamiltonian $(\pi_x^2 + \pi_y^2)(\hbar\omega_c/2)$ in configuration space [8], Appendix. F

$$\sum_{n,l} \varphi^*_{n,l}(\boldsymbol{r}_0)\mathrm{e}^{-\beta(\frac{\hbar\omega_c}{2})(\pi_x^2+\pi_y^2)}\varphi_{n,l}(\boldsymbol{r}) = \frac{1}{2\pi\ell_c^2}\frac{\mathrm{e}^{-\frac{1}{4\ell_c^2}|\boldsymbol{r}-\boldsymbol{r}_0|^2\coth(\frac{\beta\hbar\omega_c}{2})}}{2\sinh(\frac{\beta\hbar\omega_c}{2})}\mathrm{e}^{\frac{\mathrm{i}}{2\ell_c^2}(xy_0-yx_0)} \tag{4.48}$$

This enables us to write $\mathrm{e}^{-s\mathrm{h}^2}$ in configuration space,

$$\langle \boldsymbol{r_0}|\mathrm{e}^{-s\mathrm{h}^2}|\boldsymbol{r}\rangle = \frac{1}{2\pi\ell_c^2}\frac{\mathrm{e}^{-\frac{1}{4\ell_c^2}|\boldsymbol{r}-\boldsymbol{r}_0|^2\coth(s\epsilon^2)}}{2\sinh(s\epsilon^2)}\mathrm{e}^{\frac{\mathrm{i}}{2\ell_c^2}(xy_0-yx_0)} \begin{pmatrix} \mathrm{e}^{-s(m^2+1)\epsilon^2} & 0 \\ 0 & \mathrm{e}^{-s(m^2-1)\epsilon^2} \end{pmatrix} \tag{4.49}$$

For our convenience, we rewrite the above equation in more compact notation. Since s has dimension of inverse of energy square and $\boldsymbol{r}$ has the dimension of length, we employ.

$$\frac{s}{\epsilon^2} \to s, \qquad \frac{\boldsymbol{r}}{\ell_c} \to \boldsymbol{r}$$

and define,

$$\zeta_s(\boldsymbol{r}, \boldsymbol{r}_0) = \mathrm{e}^{-\frac{1}{4}|\mathbf{r}-\mathbf{r}_0|^2\coth(s)}\ \mathrm{e}^{\frac{\mathrm{i}}{2}(xy_0-yx_0)} \tag{4.50}$$

The net result so far in compact notation,

$$\langle \boldsymbol{r_0}|\mathrm{e}^{-s\mathrm{h}^2}|\boldsymbol{r}\rangle = \frac{1}{2\pi\ell_c^2}\zeta_s(\boldsymbol{r},\boldsymbol{r}_0)\frac{\mathrm{e}^{-sm^2}}{2\sinh(s)}\begin{pmatrix}\mathrm{e}^{-s} & 0\\ 0 & \mathrm{e}^{s}\end{pmatrix} \tag{4.51}$$

To obtain the propagator, we need to evaluate $\mathrm{h}\,\mathrm{e}^{-s\mathrm{h}^2}$. This achieved by finding the action of operators π_+ and π_- on $\zeta_s(\boldsymbol{r},\boldsymbol{r}_0)$. To accomplish this we express the operators $\pi_\pm$ in terms of complex variable $z = x + \mathrm{i}\,y$ and its conjugate $\bar{z}$.

$$\begin{aligned}\pi_+ &= (p_x - \frac{1}{2}y) + \mathrm{i}\,(p_y + \frac{1}{2}x) = -\mathrm{i}\,2\,\partial_{\bar{z}} + \frac{\mathrm{i}}{2}z\\ \pi_- &= (p_x - \frac{1}{2}y) - \mathrm{i}\,(p_y + \frac{1}{2}x) = -\mathrm{i}\,2\,\partial_{z} - \frac{\mathrm{i}}{2}\bar{z}\end{aligned} \tag{4.52}$$

And expressing $\zeta_s(\boldsymbol{r},\boldsymbol{r}_0)$ in terms of complex variables,

$$\zeta_s(\boldsymbol{r},\boldsymbol{r}_0) = \mathrm{e}^{-\frac{1}{4}|z-z_0|^2\coth(s)}\,\mathrm{e}^{\frac{1}{4}(\bar{z}z_0 - z\bar{z}_0)} \tag{4.53}$$

We obtain,

$$\begin{aligned}\pi_+\zeta_s(\boldsymbol{r},\boldsymbol{r}_0) =& \frac{\mathrm{i}}{2}(z-z_0)(\coth(s)+1)\zeta_s(\boldsymbol{r},\boldsymbol{r}_0)\\ =& \frac{\mathrm{i}}{2}(z-z_0)\frac{\mathrm{e}^{s}}{\sinh(s)}\zeta_s(\boldsymbol{r},\boldsymbol{r}_0)\end{aligned} \tag{4.54}$$

$$\begin{aligned}\pi_-\zeta_s(\boldsymbol{r},\boldsymbol{r}_0) =& \frac{\mathrm{i}}{2}(\bar{z}-\bar{z}_0)(\coth(s)-1)\zeta_s(\boldsymbol{r},\boldsymbol{r}_0)\\ =& \frac{\mathrm{i}}{2}(\bar{z}-\bar{z}_0)\frac{\mathrm{e}^{-s}}{\sinh(s)}\zeta_s(\boldsymbol{r},\boldsymbol{r}_0)\end{aligned} \tag{4.55}$$

The operator $\mathrm{he}^{-s\mathrm{h}^2}$ in configuration space,

$$\langle \boldsymbol{r}_0|\mathrm{h}\,\mathrm{e}^{-s\mathrm{h}^2}|\boldsymbol{r}\rangle = \frac{1}{2\pi\ell_c^2}\frac{\zeta_s(\boldsymbol{r},\boldsymbol{r}_0)}{2\sinh(s)}\begin{pmatrix} m\,\mathrm{e}^{-s(m^2+1)} & \frac{\mathrm{i}\,(\bar{z}-\bar{z}_0)}{2}\,\frac{\mathrm{e}^{-sm^2}}{\sinh(s)}\\ \frac{\mathrm{i}\,(z-z_0)}{2}\,\frac{\mathrm{e}^{-sm^2}}{\sinh(s)} & -m\,\mathrm{e}^{-s(m^2-1)}\end{pmatrix} \tag{4.56}$$

The correlator in Eq.(4.45) the limits of integration for s were $(0, \infty)$. s has the dimensions of inverse square of energy. We have to take into account the ultra-violet cut-off because of the underlying lattice structure of graphene lattice. This is taken into account by taking the limits of integration from $1/2N_C$ to infinity for s. Hence the correlator for the massive Dirac particle in magnetic field is,

$$G = -\frac{1}{2\sqrt{\pi}} \int\limits_{\frac{1}{2N_C}}^{\infty} \frac{\mathrm{d}s}{\sqrt{s}} \, \mathrm{h} \, \mathrm{e}^{-s\mathrm{h}^2} \tag{4.57}$$

In configuration space the equal time two point correlator, $\langle \boldsymbol{r}_2 | G | \boldsymbol{r}_1 \rangle = G_m(\boldsymbol{r}_1, \boldsymbol{r}_2)$

$$G_m(\boldsymbol{r}_1, \boldsymbol{r}_2) = -\frac{1}{2\pi\ell_c^2} \frac{1}{2\sqrt{\pi}} \int\limits_{\frac{1}{2N_C}}^{\infty} \frac{\mathrm{d}s}{\sqrt{s}} \, \zeta_s(\boldsymbol{r}_1, \boldsymbol{r}_2) \frac{\mathrm{e}^{-sm^2}}{2\sinh(s)} \begin{pmatrix} m\,\mathrm{e}^{-s} & \frac{\mathrm{i}\,(\bar{z}_1 - \bar{z}_2)}{2\sinh(s)} \\ \frac{\mathrm{i}\,(z_1 - z_2)}{2\sinh(s)} & -m\,\mathrm{e}^{s} \end{pmatrix} \tag{4.58}$$

The $\zeta_s(\boldsymbol{r}_1, \boldsymbol{r}_2)$ is defined in Eq.(4.50).

Another quantity that we will require when we compute the mean field energy for the contact terms in the interacting hamiltonian is coincident correlator. That is obtained by evaluating propagator for a given point, $\langle \boldsymbol{r}_0 | G | \boldsymbol{r}_0 \rangle = G(\boldsymbol{r}_0, \boldsymbol{r}_0)$

$$G_m(0) = -\frac{1}{2\pi\ell_c^2} \frac{1}{2\sqrt{\pi}} \int\limits_{\frac{1}{2N_C}}^{\infty} \frac{\mathrm{d}s}{\sqrt{s}} \, \frac{\mathrm{e}^{-sm^2}}{2\sinh(s)} \begin{pmatrix} m\,\mathrm{e}^{-s} & 0 \\ 0 & -m\,\mathrm{e}^{s} \end{pmatrix} \tag{4.59}$$

The coincident correlator for Dirac particle is independent of position. The correlator obtained in this section are for a single Dirac particle. To obtain the correlator for the Dirac particles in graphene we need to take into account the $SU(4)$ structure of the eigen functions. We will use these two point correlator and coincident one to construct the correlator for the case of graphene in next section.

4.5 Two point correlation functions

The computation of mean field energy requires the knowledge of two point correlation function, which is expectation value of the two point field operators. This results from Wick decomposition applied to four fermion terms in the interacting model. For example, consider the case four fermion term occurring in Coulomb interaction term,

$$\langle \Psi^{\dagger}_{r,A}(\boldsymbol{x})\Psi_{r,A}(\boldsymbol{x})\Psi^{\dagger}_{s,B}(\boldsymbol{x})\Psi_{s,B}(\boldsymbol{x})\rangle = \langle \Psi^{\dagger}_{r,A}(\boldsymbol{x})\Psi_{r,A}(\boldsymbol{x})\rangle\langle \Psi^{\dagger}_{s,B}(\boldsymbol{x})\Psi_{s,B}(\boldsymbol{x})\rangle - \langle \Psi^{\dagger}_{r,A}(\boldsymbol{x})\Psi_{s,B}(\boldsymbol{x})\rangle\langle \Psi^{\dagger}_{s,B}(\boldsymbol{x})\Psi_{r,A}(\boldsymbol{x})\rangle \quad (4.60)$$

Here the notation $\langle \ldots \rangle$ stands for the expectation value $\langle GS|\ldots|GS\rangle$ and $|GS\rangle$ is the ground state under consideration. This requires the expectation value of two point fermion operators,

$$\langle \Psi^{\dagger}_{s,B}(\boldsymbol{y})\Psi_{r,A}(\boldsymbol{x})\rangle = \sum_{(n,l,q)\in \text{occ}} \Phi^{n,l,q^*}_{s,B}(\boldsymbol{y})\, \Phi^{n,l,q}_{r,A}(\boldsymbol{x}) \quad (4.61)$$

Here the summation is over all the occupied states. We define an quantity, *two-point correlation function*,

$$\Gamma(\boldsymbol{x},\boldsymbol{y}) = \sum_{(n,l,q)\in \text{occ}} \Phi^{n,l,q}(\boldsymbol{x})\big(\Phi^{n,l,q}(\boldsymbol{y})\big)^{\dagger} \quad (4.62)$$

By construction $\Gamma(\boldsymbol{x},\boldsymbol{y})$ is 8×8 matrix and this will be computed from the propagator for massive Dirac particle in magnetic field obtained in the previous section. For the Hall conductivity we are considering in this thesis, is encoded in the mass matrix M, for the masses of Dirac particles for graphene.

$$M = \sum_{q=1}^{4} m_q \chi^q \chi^{q\dagger} \quad (4.63)$$

here χ^q is eigenvector corresponding to m_q. For Hall conductivity $\sigma_H = 0$, $m_1 = m_2 = m_o$ and $m_3 = m_4 = -m_u$. And in the case for $\sigma_H = -1$ $m_1 = m_o$, $m_2 = m_3 = m_4 =$

$-m_u$. We define projection operator,

$$P_q = \chi^q \chi^{q\dagger} \tag{4.64}$$

which satisfies $P_q^2 = P_q$ and the completeness relation,

$$\mathbb{1}_4 = \sum_{q=1}^{4} P_q \tag{4.65}$$

Using Eq.(4.58) to construct the correlator for the desired Hall conductivity,

$$\Gamma(\boldsymbol{r}_1, \boldsymbol{r}_2) = \sum_{q=1}^{4} G_{m_q}(\boldsymbol{r}_1, \boldsymbol{r}_2) P_q \tag{4.66}$$

$$\Gamma(\boldsymbol{r}_1, \boldsymbol{r}_2) = \frac{1}{2}\frac{1}{2\pi\ell_c^2} \sum_{q=1}^{4} \begin{pmatrix} -f_{m_q}(\boldsymbol{r}_1, \boldsymbol{r}_2) & d_{m_q}(\boldsymbol{r}_1, \boldsymbol{r}_2) \\ b_{m_q}(\boldsymbol{r}_1, \boldsymbol{r}_2) & g_{m_q}(\boldsymbol{r}_1, \boldsymbol{r}_2) \end{pmatrix} P_q \tag{4.67}$$

Here,

$$f_{m_q}(\boldsymbol{r}_1, \boldsymbol{r}_2) = \frac{m_q}{2\sqrt{\pi}} \int\limits_{\frac{1}{2N_C}}^{\infty} \frac{\mathrm{d}s}{\sqrt{s}} \frac{\mathrm{e}^{-s(m_q^2+1)}}{\sinh(s)} \zeta_s(\boldsymbol{r}_1, \boldsymbol{r}_2) \tag{4.68}$$

$$g_{m_q}(\boldsymbol{r}_1, \boldsymbol{r}_2) = \frac{m_q}{2\sqrt{\pi}} \int\limits_{\frac{1}{2N_C}}^{\infty} \frac{\mathrm{d}s}{\sqrt{s}} \frac{\mathrm{e}^{-s(m_q^2-1)}}{\sinh(s)} \zeta_s(\boldsymbol{r}_1, \boldsymbol{r}_2) \tag{4.69}$$

$$b_{m_q}(\boldsymbol{r}_1, \boldsymbol{r}_2) = -\mathrm{i}\, \frac{(z_1 - z_2)}{4\sqrt{\pi}} \int\limits_{\frac{1}{2N_C}}^{\infty} \frac{\mathrm{d}s}{\sqrt{s}} \frac{\mathrm{e}^{-sm_q^2}}{\sinh^2(s)} \zeta_s(\boldsymbol{r}_1, \boldsymbol{r}_2) \tag{4.70}$$

$$d_{m_q}(\boldsymbol{r}_1, \boldsymbol{r}_2) = -\mathrm{i}\, \frac{(\bar{z}_1 - \bar{z}_2)}{4\sqrt{\pi}} \int\limits_{\frac{1}{2N_C}}^{\infty} \frac{\mathrm{d}s}{\sqrt{s}} \frac{\mathrm{e}^{-sm_q^2}}{\sinh^2(s)} \zeta_s(\boldsymbol{r}_1, \boldsymbol{r}_2) \tag{4.71}$$

The coincident correlator,

$$\Gamma = \frac{1}{2}\frac{1}{2\pi\ell_c^2} \sum_{q=1}^{4} \begin{pmatrix} -f_{m_q} & 0 \\ 0 & g_{m_q} \end{pmatrix} P_q \tag{4.72}$$

Here,

$$f_{m_q} = \frac{m_q}{2\sqrt{\pi}} \int\limits_{\frac{1}{2N_C}}^{\infty} \frac{\mathrm{d}s}{\sqrt{s}} \frac{\mathrm{e}^{-s(m_q^2+1)}}{\sinh(s)} \tag{4.73}$$

$$g_{m_q} = \frac{m_q}{2\sqrt{\pi}} \int\limits_{\frac{1}{2N_C}}^{\infty} \frac{\mathrm{d}s}{\sqrt{s}} \frac{\mathrm{e}^{-s(m_q^2-1)}}{\sinh(s)} \tag{4.74}$$

$$\Gamma = \frac{1}{2\pi\ell_c^2} \frac{1}{2} \sum_{q=1}^{4} \Big(u_{m_q} \mathbb{1}_2 - v_{m_q} \beta \Big) \otimes P_q \tag{4.75}$$

Here,

$$u_{m_q} = \frac{m_q}{2\sqrt{\pi}} \int\limits_{\frac{1}{2N_C}}^{\infty} \frac{\mathrm{d}s}{\sqrt{s}} \, \mathrm{e}^{-sm_q^2}$$

$$v_{m_q} = \frac{m_q}{2\sqrt{\pi}} \int\limits_{\frac{1}{2N_C}}^{\infty} \frac{\mathrm{d}s}{\sqrt{s}} \, \mathrm{e}^{-sm_q^2} \coth(s)$$

For numerical evaluation it convenient to rewrite above equations,

$$v_{m_q} = \frac{m_q}{\sqrt{\pi}} \int\limits_{\frac{1}{\sqrt{2N_C}}}^{\infty} \mathrm{d}\xi \, \mathrm{e}^{-m_q^2\xi^2} \Big(\frac{1+\mathrm{e}^{-2\xi^2}}{1-\mathrm{e}^{-2\xi^2}} \Big) \tag{4.76}$$

$$u_{m_q} = \frac{m_q}{\sqrt{\pi}} \int\limits_{\frac{1}{\sqrt{2N_C}}}^{\infty} \mathrm{d}\xi \, \mathrm{e}^{-m_q^2\xi^2} = \frac{\mathrm{sgn}(m_q)}{2} \, \mathrm{erfc}\big(\frac{|m_q|}{\sqrt{2N_C}} \big) \tag{4.77}$$

The complementary error function is defined as

$$\mathrm{erfc}(x) = \frac{2}{\sqrt{\pi}} \int\limits_{x}^{\infty} \mathrm{d}t \, \mathrm{e}^{-t^2} \tag{4.78}$$

Making use of the structure of mass matrix M for the Hall conductivity under considera-

tion here the two point coincident correlator can be written in convenient form

$$\Gamma = \frac{1}{2\pi\ell_c^2}\frac{1}{2}\Big(\big((u_{m_o}+u_{m_u})\,\mathbb{1}_2 - (v_{m_o}+v_{m_u})\beta\big) \otimes \sum_{j\in \text{occ}} P_j \\ - (u_{m_u}\mathbb{1}_2 - v_{m_u}\beta)\otimes \mathbb{1}_4 \Big) \quad (4.79)$$

Here the summation over $j = 1$ for $\sigma_H = -1$ and $j = 1, 2$ for $\sigma_H = 0$.

4.6 Summary

We summarize the features of framework that we developed in this chapter to be used in subsequent chapter for mean field computations,

1. We showed that Landau levels for massive Dirac particle will provided the same $SU(4)$ polarization for both partially occupied $n = 0$ Landau levels and filled Dirac sea.

2. We described the number of parameters needed for the variational ground states for the Hall conductivity $\sigma_H = 0$ and $\sigma_H = -1$.

3. Using the heat kernel method we developed a convenient expression for two point correlator for a massive Dirac particle in magnetic field.

4. With the knowledge of two point correlator for a massive Dirac particle we constructed the two point correlator and coincident correlator for Dirac particle in graphene to be used for variational mean field computations.

Chapter 5

$SU(4)$ symmetric model

In this chapter, we consider the $SU(4)$ symmetric model for graphene, which includes the leading terms from the kinetic and Coulomb terms in the continuum approximation. The model used in this chapter

$$\mathcal{H} = \mathcal{H}_0 + \mathcal{H}_C \tag{5.1}$$

The kinetic term,

$$\mathcal{H}_0 = \int_{\boldsymbol{r}} \Psi^\dagger(\boldsymbol{r}) \big(v_F \, \boldsymbol{\alpha} \cdot \boldsymbol{\pi} \otimes \mathbb{1}_4 \big) \Psi(\boldsymbol{r}) \tag{5.2}$$

The $SU(4)$ symmetric part of electron-electron interaction,

$$\mathcal{H}_C = \frac{1}{2} \int_{\boldsymbol{r}_1, \boldsymbol{r}_2} V_C(|\boldsymbol{r}_1 - \boldsymbol{r}_2|) \Big(\Psi^\dagger(\boldsymbol{r}_1)\Psi(\boldsymbol{r}_1)\Psi^\dagger(\boldsymbol{r}_2)\Psi(\boldsymbol{r}_2) - 2\bar{\rho}\Psi^\dagger(\boldsymbol{r}_1)\Psi(\boldsymbol{r}_1) + \bar{\rho}^2 \Big) \tag{5.3}$$

here $\bar{\rho}$ is the average charge density. This has been incorporated to take into account the average background charge due to positive charge of the ions. Both $\mathcal{H}_0$ and $\mathcal{H}_C$ are invariant under $SU(4)$ rotation performed on the field operator, i.e. $\mathcal{U}_{A,B}\Psi(\boldsymbol{x})_{r,B}$, leaves both terms unchanged.

We will show that, the $SU(4)$ symmetric model spontaneously breaks the $SU(4)$ symmetry to $SU(3) \otimes U(1)$ for Hall conductivity at $\sigma_H = -1$ and $SU(2) \otimes SU(2)$ for Hall

conductivity $\sigma_H = 0$. It does not throw light on the nature of the ground states of the Hall conductivity for $\sigma_H = 0, \pm 1$. The mean field energies for ground state turns out to be independent of the angle parameters. These angle parameters are responsible for indicating the direction of the ground states in the $SU(4)$ space i.e. the $SU(4)$ polarization of the ground states in not completely specified. In the case of particle-hole excitations also gaps also turns out to be independent of the angle parameters. We will show that leading contributions to the magnitude of the gaps comes from the Coulomb term but the $SU(4)$ component of the excitations are left unspecified.

5.1 Expectation value for symmetric model

In this section we use the two point correlator Eq.(4.67) to compute the expectation value of kinetic and Coulomb term. We will show that the expectation value for the $SU(4)$ symmetric terms is independent of angle parameters that specify the $SU(4)$ polarization. The expectations values are reduced to evaluating the integration of s variable of the correlator, Eq.(4.67), which is done numerically.

5.1.1 Kinetic term

The kinetic term has local fermion field operators and the expectation value can be expressed as,

$$\langle \mathcal{H}_0 \rangle = \int_{\boldsymbol{r}} \mathrm{h}_{r,A;s,B} \langle \Psi^\dagger_{r,A}(\boldsymbol{r}) \Psi_{s,B}(\boldsymbol{r}) \rangle \tag{5.4}$$

From Eq.(5.2), $\mathrm{h}_{r,A;s,B} = v_F \left(\boldsymbol{\alpha} \cdot \boldsymbol{\pi}\right)_{r,s} \left(\mathbb{1}_4\right)_{A,B}$. To compute average of kinetic term we need to take into account the action of operator h which makes it non-local because of the action of conjugate momentum operator. We cannot apply the coincident correlator here instead we compute the action of operator h on the two point correlator and take the

coincident limit.

$$\langle \mathcal{H}_0 \rangle = \int_{\boldsymbol{r}} \lim_{\boldsymbol{r}\to\boldsymbol{r}_0} \mathrm{Tr}[\mathrm{h}\,\Gamma(\boldsymbol{r},\boldsymbol{r}_0)] \tag{5.5}$$

Since the operator $\boldsymbol{\alpha}\cdot\boldsymbol{\pi}$ has only off-diagonal elements, hence

$$\mathrm{Tr}[\mathrm{h}\,\Gamma(\boldsymbol{r},\boldsymbol{r}_0)] = \frac{1}{2\pi\ell_c^2}\frac{1}{2}\Big(\frac{\hbar v_F}{\ell_c}\Big)\sum_{q=1}^{4}\big(\pi_- b_{m_q}(\boldsymbol{r},\boldsymbol{r}_0) + \pi_+ d_{m_q}(\boldsymbol{r},\boldsymbol{r}_0)\big) \tag{5.6}$$

Here $\pi_\pm = \pi_x \pm \mathrm{i}\,\pi_y$ and its action on the off-diagonal elements of the two-point correlator provides the contributions. $\boldsymbol{\pi} = \boldsymbol{p} + e\boldsymbol{A}$ is the conjugate momenta in presence of magnetic field. The action of $\pi_\pm$ can be easily obtained by expressing them as derivatives of complex variable $z = x + \mathrm{i}\,y$ and its conjugate $\bar{z}$ as shown in Eq.(4.52) and using the Eq.(4.54) and Eq.(4.55), we obtain

$$\pi_+\big((\bar{z}-\bar{z}_0)\zeta_s(z,z_0)\big) = \mathrm{i}\,\big(-2-\frac{1}{2}z(\bar{z}-\bar{z}_0)+\frac{1}{2}|z-z_0|^2(\coth(s)+1)\big)\zeta_s(z,z_0)$$
$$\pi_-\big((z-z_0)\zeta_s(z,z_0)\big) = \mathrm{i}\,\big(-2-\frac{1}{2}\bar{z}(z-z_0)+\frac{1}{2}|z-z_0|^2(\coth(s)-1)\big)\zeta_s(z,z_0)$$

Now taking limit $z \to z_0$ and we obtain,

$$\lim_{\boldsymbol{r}\to\boldsymbol{r}_0}\pi_- b_{m_q}(\boldsymbol{r},\boldsymbol{r}_0) = -\frac{1}{2\sqrt{\pi}}\int_s \frac{\mathrm{e}^{-sm_q^2}}{\sqrt{s}\sinh^2(s)} \tag{5.7}$$

$$\lim_{\boldsymbol{r}\to\boldsymbol{r}_0}\pi_+ d_{m_q}(\boldsymbol{r},\boldsymbol{r}_0) = -\frac{1}{2\sqrt{\pi}}\int_s \frac{\mathrm{e}^{-sm_q^2}}{\sqrt{s}\sinh^2(s)} \tag{5.8}$$

The spatial integration in Eq.(5.5) is trivial and results in V, volume of the system

$$\langle \mathcal{H}_0 \rangle = -\frac{\mathrm{V}}{2\pi\ell_c^2}\Big(\frac{\hbar v_F}{\ell_c}\Big)\frac{1}{2\sqrt{\pi}}\sum_{q=1}^{4}\int_{\frac{1}{2N_C}}^{\infty}\mathrm{d}s\,\frac{\mathrm{e}^{-sm_q^2}}{\sqrt{s}\sinh^2(s)} \tag{5.9}$$

The integrand in Eq.(5.9), is a diverging function of s near zero. Although the point of divergence, $s = 0$, is not part of range of integration but it diverges very rapidly in the proximity of the lower limit of the integration. We note that leading contribution of this integration is independent of variational parameter, which is just a constant from the min-

imization point of view. Hence we remove this constant in the process of computing the coefficients with variational parameter dependence and to keep the integration going out of bounds for numerical computation. The integration can be rearranged in the following way,

$$\int_{\frac{1}{2N_C}}^{\infty} \mathrm{d}s \, \frac{\mathrm{e}^{-sm_q^2}}{\sqrt{s}\sinh^2(s)} = \int_{\frac{1}{2N_C}}^{\infty} \mathrm{d}s \, \frac{1}{\sqrt{s}\sinh^2(s)} - \int_{\frac{1}{2N_C}}^{\infty} \mathrm{d}s \, \frac{(1-\mathrm{e}^{-sm_q^2})}{\sqrt{s}\sinh^2(s)}$$

The first term in the above equation is independent of variational parameter so we drop it and second one carries the complete variational parameter dependence. The expectation value of the kinetic term that has variational parameter dependence can be expressed as,

$$\langle \mathcal{H}_0 \rangle = \frac{\mathrm{V}}{2\pi\ell_c^2}\Big(\frac{\hbar v_F}{\ell_c}\Big) \sum_{q=1}^{4} \eta_t(m_q) \tag{5.10}$$

The quantity

$$\eta_t(m_q) = \frac{4}{\sqrt{\pi}} \int_{\frac{1}{\sqrt{2N_C}}}^{\infty} \mathrm{d}\xi \, \frac{(1-\mathrm{e}^{-m_q^2\xi^2})\mathrm{e}^{-2\xi^2}}{(1-\mathrm{e}^{-2\xi^2})^2} \tag{5.11}$$

is expressed with change of variable which suited best for it to be computed numerically. Also note that the coefficient $\eta_t(m_q)$ will yield positive values for range of integration and parameter values that are of our interest.

5.1.2 Coulomb term

The expectation value of Coulomb term, Eq.(5.3),

$$\begin{aligned}\langle \mathcal{H}_C \rangle = \frac{1}{2}\frac{e^2}{4\pi\varepsilon} \int_{\boldsymbol{r}_1}\int_{\boldsymbol{r}_2} \frac{1}{|\boldsymbol{r}_1-\boldsymbol{r}_2|}\Big(&\langle \Psi^\dagger_{r,A}(\boldsymbol{r}_1)\Psi_{r,A}(\boldsymbol{r}_1)\rangle\langle \Psi^\dagger_{s,B}(\boldsymbol{r}_2)\Psi_{s,B}(\boldsymbol{r}_2)\rangle \\ &- \langle \Psi^\dagger_{r,A}(\boldsymbol{r}_1)\Psi_{s,B}(\boldsymbol{r}_2)\rangle\langle \Psi^\dagger_{s,B}(\boldsymbol{r}_2)\Psi_{r,A}(\boldsymbol{r}_1)\rangle \\ &- 2\bar{\rho}\langle \Psi^\dagger_{r,A}(\boldsymbol{r}_1)\Psi_{r,A}(\boldsymbol{r}_1)\rangle + \bar{\rho}^2 \end{aligned} \tag{5.12}$$

In above equation four fermion term has undergone Wick's decomposition. By definition $\bar{\rho} = \mathrm{Tr}[\Gamma(\boldsymbol{r}, \boldsymbol{r})]$, the average charge. This leads to cancellation of the first and last two terms. The mean field energy contributions from the Coulomb term comes from the exchange term and can be expressed in terms of the two point correlator,

$$\langle \mathcal{H}_C \rangle = -\frac{1}{2}\frac{e^2}{4\pi\varepsilon}\int_{\boldsymbol{r}_1}\int_{\boldsymbol{r}_2}\frac{1}{|\boldsymbol{r}_1 - \boldsymbol{r}_2|}\mathrm{Tr}[\Gamma(\boldsymbol{r}_1, \boldsymbol{r}_2)\,\Gamma(\boldsymbol{r}_2, \boldsymbol{r}_1)] \tag{5.13}$$

We use the fact, $\mathrm{Tr}[P_q P_{\tilde{q}}] = \delta_{q,\tilde{q}}$, to evaluate the trace of correlator,

$$\begin{aligned}\mathrm{Tr}[\Gamma(\boldsymbol{r}_1, \boldsymbol{r}_2)\Gamma(\boldsymbol{r}_2, \boldsymbol{r}_1)] = \frac{1}{(2\pi\ell_c^2)^2}\frac{1}{4}\sum_{q=1}^{4}\Big(f_{m_q}(\boldsymbol{r}_1, \boldsymbol{r}_2)f_{m_q}(\boldsymbol{r}_2, \boldsymbol{r}_1) \\ + g_{m_q}(\boldsymbol{r}_1, \boldsymbol{r}_2)g_{m_q}(\boldsymbol{r}_2, \boldsymbol{r}_1) + b_{m_q}(\boldsymbol{r}_1, \boldsymbol{r}_2)d^*_{m_q}(\boldsymbol{r}_2, \boldsymbol{r}_1) + d_{m_q}(\boldsymbol{r}_1, \boldsymbol{r}_2)b^*_{m_q}(\boldsymbol{r}_2, \boldsymbol{r}_1)\Big)\end{aligned} \tag{5.14}$$

This indicated that the Coulomb expectation value is independent of the angle parameters.

Now consider the integral

$$\begin{aligned}\mathcal{I}_1 = \Big(\frac{1}{2}\frac{e^2}{4\pi\varepsilon}\Big)\frac{1}{(2\pi\ell_c^2)^2}\frac{1}{4}\iint_{\boldsymbol{r}_1,\boldsymbol{r}_2}\frac{1}{|\boldsymbol{r}_1 - \boldsymbol{r}_2|}\Big(f_{m_q}(\boldsymbol{r}_1, \boldsymbol{r}_2)f_{m_q}(\boldsymbol{r}_2, \boldsymbol{r}_1) \\ + g_{m_q}(\boldsymbol{r}_2, \boldsymbol{r}_1)g_{m_q}(\boldsymbol{r}_1, \boldsymbol{r}_2)\Big)\end{aligned} \tag{5.15}$$

Once again we plug in $f_{m_q}(\boldsymbol{r}_1, \boldsymbol{r}_2)$ from Eq.(4.68) and $g_{m_q}(\boldsymbol{r}_1, \boldsymbol{r}_2)$ from Eq.(4.69) in the above equation,

$$\begin{aligned}\mathcal{I}_1 = \Big(\frac{1}{2}\frac{e^2}{4\pi\varepsilon\ell_c}\Big)\frac{1}{(2\pi\ell_c^2)^2}\frac{m_q^2}{8\pi}\iint_{s_1,s_2}\frac{\mathrm{e}^{-(s_1+s_2)m_q^2}\,\cosh(s_1+s_2)}{\sqrt{s_1\,s_2}\,\sinh(s_1)\sinh(s_2)} \\ \iint_{\boldsymbol{r}_1,\boldsymbol{r}_2}\frac{\mathrm{e}^{-\frac{1}{4}|\boldsymbol{r}_1-\boldsymbol{r}_2|^2(\coth(s_1)+\coth(s_2))}}{|\boldsymbol{r}_1 - \boldsymbol{r}_2|}\end{aligned} \tag{5.16}$$

The spatial integration involves only the magnitude of relative position coordinates, hence we transform the spatial integration from two position coordinates to center of mass and relative coordinates. The center of mass coordinate is trivial and yields the volume of the

system and the relative coordinate is a gaussian integral.

$$\begin{aligned}\mathcal{I}_1 &= \Big(\frac{1}{2}\frac{e^2}{4\pi\varepsilon\ell_c}\Big)\frac{\mathrm{V}}{2\pi\ell_c^2}\frac{m_q^2}{8\sqrt{\pi}}\iint_{s_1,s_2}\frac{\mathrm{e}^{-(s_1+s_2)m_q^2}}{\sqrt{s_1\,s_2}\,\sinh(s_1)\sinh(s_2)}\frac{\cosh(s_1+s_2)}{\sqrt{\coth(s_1)+\coth(s_2)}}\\ &= \Big(\frac{1}{2}\frac{e^2}{4\pi\varepsilon\ell_c}\Big)\frac{\mathrm{V}}{2\pi\ell_c^2}\frac{m_q^2}{8\sqrt{\pi}}\iint_{s_1,s_2}\frac{\mathrm{e}^{-(s_1+s_2)m_q^2}}{\sqrt{s_1\,s_2}}\frac{\cosh(s_1+s_2)}{\sqrt{\sinh(s_1)\sinh(s_2)\sinh(s_1+s_2)}}\\ &= \Big(\frac{1}{2}\frac{e^2}{4\pi\varepsilon\ell_c}\Big)\frac{\mathrm{V}}{2\pi\ell_c^2}\,\eta_{fg}(m_q)\end{aligned} \tag{5.17}$$

The variational parameter dependent $\eta_{fg}(m_q)$ is computed numerically by implementing the double integral

$$\eta_{fg}(m_q) = m_q^2\sqrt{\frac{2}{\pi}}\int\limits_{\frac{1}{\sqrt{2N_C}}}^{\infty}\mathrm{d}\xi_1\frac{\mathrm{e}^{-\xi_1^2m_q^2}}{\sqrt{(1-\mathrm{e}^{2\xi_1^2})}}\int\limits_{\frac{1}{\sqrt{2N_C}}}^{\xi_1}\mathrm{d}\xi_2\frac{\mathrm{e}^{-\xi_2^2m_q^2}(1+\mathrm{e}^{-2(\xi_1^2+\xi_2^2)})}{\sqrt{(1-\mathrm{e}^{2\xi_2^2})(1-\mathrm{e}^{-2(\xi_1^2+\xi_2^2)})}} \tag{5.18}$$

Now consider the integral,

$$\begin{aligned}\mathcal{I}_2 = \Big(\frac{1}{2}\frac{e^2}{4\pi\varepsilon\ell_c}\Big)\frac{1}{(2\pi\ell_c^2)^2}\frac{1}{4}\iint_{\boldsymbol{r}_1,\boldsymbol{r}_2}\frac{1}{|\boldsymbol{r}_1-\boldsymbol{r}_2|}\big(&b_{m_q}(\boldsymbol{r}_1,\boldsymbol{r}_2)d_{m_q}(\boldsymbol{r}_2,\boldsymbol{r}_1)\\ &+ b_{m_q}(\boldsymbol{r}_2,\boldsymbol{r}_1)d_{m_q}(\boldsymbol{r}_1,\boldsymbol{r}_2)\big)\end{aligned} \tag{5.19}$$

Taking $b_{m_q}(\boldsymbol{r}_1,\boldsymbol{r}_2)$ from Eq.(4.70) and $d_{m_q}(\boldsymbol{r}_1,\boldsymbol{r}_2)$ from Eq.(4.71) and plugging in above equation,

$$\begin{aligned}\mathcal{I}_2 = \Big(\frac{1}{2}\frac{e^2}{4\pi\varepsilon\ell_c}\Big)\frac{1}{(2\pi\ell_c^2)^2}\frac{1}{32\pi}\iint_{s_1,s_2}&\frac{\mathrm{e}^{-s_1m_q^2}}{\sqrt{s_1}\sinh^2(s_1)}\frac{\mathrm{e}^{-s_2m_q^2}}{\sqrt{s_2}\sinh^2(s_2)}\\ &\iint_{\boldsymbol{r}_1,\boldsymbol{r}_2}|\boldsymbol{r}_1-\boldsymbol{r}_2|\,\mathrm{e}^{-\frac{1}{4}|\boldsymbol{r}_1-\boldsymbol{r}_2|^2(\coth(s_1)+\coth(s_2))}\end{aligned} \tag{5.20}$$

Once again spatial integration done by transforming to center of mass and relative coordinates and done analytically using gamma functions.

$$\mathcal{I}_2 = \Big(\frac{1}{2}\frac{e^2}{4\pi\varepsilon\ell_c}\Big)\frac{\mathrm{V}}{2\pi\ell_c^2}\frac{1}{16\sqrt{\pi}}\iint_{s_1,s_2}\frac{\mathrm{e}^{-s_1m_q^2}}{\sqrt{s_1}\sinh^2(s_1)}\frac{\mathrm{e}^{-s_2m_q^2}}{\sqrt{s_2}\sinh^2(s_2)}\frac{1}{(\coth(s_1)+\coth(s_2))^{\frac{3}{2}}} \tag{5.21}$$

The double integral over s variable is diverging at lower limit and its leading contribution is independent of variational parameter, a situation similar was seen in computation of expectation value of kinetic term.

$$\begin{aligned}\int_{s_1}\int_{s_2}\frac{\mathrm{e}^{-s_1 m_q^2}}{\sqrt{s_1}\sinh^2(s_1)}\frac{\mathrm{e}^{-s_2 m_q^2}}{\sqrt{s_2}\sinh^2(s_2)}\frac{1}{(\coth(s_1)+\coth(s_2))^{\frac{3}{2}}}&\\ =\int_{s_1}\int_{s_2}\frac{1}{\sqrt{s_1}\sqrt{s_2}\sinh^2(s_1)\sinh^2(s_2)}\frac{1}{(\coth(s_1)+\coth(s_2))^{\frac{3}{2}}}&\\ +\int_{s_1}\int_{s_2}\frac{(\mathrm{e}^{-(s_1+s_2)m_q^2}-1)}{\sqrt{s_1}\sqrt{s_2}\sinh^2(s_1)\sinh^2(s_2)}\frac{1}{(\coth(s_1)+\coth(s_2))^{\frac{3}{2}}}&\end{aligned}\tag{5.22}$$

The first term on the right hand side of the above equation is independent of variational parameter, hence we drop it and only retain the second term.

$$\mathcal{I}_2=\Big(\frac{1}{2}\frac{e^2}{4\pi\varepsilon\ell_c}\Big)\frac{\mathrm{V}}{2\pi\ell_c^2}\,\eta_{bd}(m_q)\tag{5.23}$$

The coefficient $\eta_{bd}(m_q)$ is computed numerically by implementing the double integral

$$\eta_{bd}(m_q)=\frac{2\sqrt{2}}{\sqrt{\pi}}\int\limits_{\frac{1}{\sqrt{2N_C}}}^{\infty}\mathrm{d}\xi_1\frac{1}{\sqrt{(1-\mathrm{e}^{2\xi_1^2})}}\int\limits_{\frac{1}{\sqrt{2N_C}}}^{\xi_1}\mathrm{d}\xi_2\frac{(\mathrm{e}^{-(\xi_1^2+\xi_2^2)m_q^2}-1)\mathrm{e}^{-2(\xi_1^2+\xi_2^2)}}{\sqrt{(1-\mathrm{e}^{2\xi_2^2})(1-\mathrm{e}^{-2(\xi_1^2+\xi_2^2)})^3}}\tag{5.24}$$

The coefficients $\eta_{fg}(m_q)$ and $\eta_{bd}(m_q)$ both are function of m_q^2. We club them together,

$$\eta_C(m_q)=\eta_{fg}(m_q)+\eta_{bd}(m_q)\tag{5.25}$$

The net variational parameter dependence of Coulomb term can be expressed as,

$$\langle\mathcal{H}_C\rangle=\frac{\mathrm{V}}{2\pi\ell_c^2}\Big(\frac{1}{2}\frac{1}{4\pi\varepsilon\ell_c}\Big)\sum_{q=1}^{4}\eta_C(m_q)\tag{5.26}$$

5.2 Ground state energy minimization

In this section we compute the ground state energies for Hall conductivity states $\sigma_H = 0$ and $\sigma_H = -1$ for the symmetric model. The general expression from the previous section are applied for each case and minimization is done numerically.

5.2.1 Ground state at $\sigma_H = 0$

The many body ground state has filled Dirac sea and two of four sub-levels of $n = 0$ Landau levels. As we discussed in section 4.3.2, the diagonal mass matrix takes the form $M_D = \{m_o, m_o, -m_u, -m_u\}$, i.e. $m_1 = m_2 = m_o$ the mass for the occupied $n = 0$ Landau levels and $m_3 = m_4 = -m_u$ are for the unoccupied ones.

The mean field energy for the ground state at Hall conductivity $\sigma_H = 0$ for the symmetry model,

$$\mathcal{E} = \langle \mathcal{H}_0 \rangle + \langle \mathcal{H}_C \rangle \tag{5.27}$$

We only retain the terms that depend on the variational parameters for the ground state energy as other terms are inconsequential for the minimization routine. Using Eq.(5.10) for the kinetic energy and Eq.(5.26) Coulomb energy, and denoting

$$\kappa_t = \Big(\frac{\hbar v_F}{\ell_c}\Big) \tag{5.28}$$

$$\kappa_C = \Big(\frac{1}{2}\frac{1}{4\pi\varepsilon\ell_c}\Big) \tag{5.29}$$

$$\mathcal{E} = \frac{\mathrm{V}}{2\pi\ell_c^2} 2\bigg(\kappa_t\big(\eta_t(m_o) + \eta_t(-m_u)\big) - \kappa_C\big(\eta_C(m_o) + \eta_C(-m_u)\big)\bigg) \tag{5.30}$$

The mean field energy is decoupled for variational parameters, m_o and m_u. Hence we can

minimize the two equations separately,

$$\tilde{\mathcal{E}}(m_o) = \kappa_t\, \eta_t(m_o) - \kappa_C \eta_{C_2}(m_o) \tag{5.31}$$

$$\tilde{\mathcal{E}}(-m_u) = \kappa_t\, \eta_t(-m_u) - \kappa_C \eta_{C_2}(-m_u) \tag{5.32}$$

The coefficients $\eta_t(m)$ and $\eta_{C_2}(m)$ are even functions of m. Hence $\tilde{\mathcal{E}}(-m_u) = \tilde{\mathcal{E}}(m_o)$. This implies that if $m_o = \tilde{m}$ results in extreme value for $\tilde{\mathcal{E}}(m_o)$ then $m_u = \tilde{m}$ will be yield same type of extreme value for $\tilde{\mathcal{E}}(-m_u)$, because they are even function of the mass parameter. The diagonal mass matrix for the ground state at Hall conductivity $\sigma_H = 0$ take the form

$$M_D = \{\tilde{m}, \tilde{m}, -\tilde{m}, -\tilde{m}\} \tag{5.33}$$

The angle parameters for the mass matrix M do not get fixed when working with the $SU(4)$ symmetric model for Hall conductivity at $\sigma_H = 0$.

5.2.2 Ground state at $\sigma_H = -1$

In the case for the ground state at $\sigma_H = -1$, there is the filled Dirac sea and one of the sub-levels of the $n = 0$ Landau level is occupied. Following the discussion in section 4.3.1, the diagonal mass matrix takes the form, $M_D = \{m_o, -m_u, -m_u, -m_u\}$, i.e. the occupied sub-level for $n = 0$ Landau level is attributed mass, $m_1 = m_o$ and the unoccupied ones $m_2 = m_3 = m_4 = -m_u$.

The mean field energy is computed by collecting variational parameter dependent of the kinetic, $\langle \mathcal{H}_t \rangle$ using Eq.(5.10) and the Coulomb term, $\langle \mathcal{H}_C \rangle$, using Eq.(5.26). Using the definition of κ_t in Eq.(5.28) and κ_C in Eq.(5.29), the mean field energy can be arranged as decoupled functions of variational parameters, m_o and m_u.

$$\mathcal{E} = \frac{\mathrm{V}}{2\pi\ell_c^2}\Big(\kappa_t\, \eta_t(m_o) - \kappa_C \eta_{C_2}(m_o) + 3\Big(\kappa_t\, \eta_t(m_u) - \kappa_C \eta_{C_2}(m_u)\Big)\Big) \tag{5.34}$$

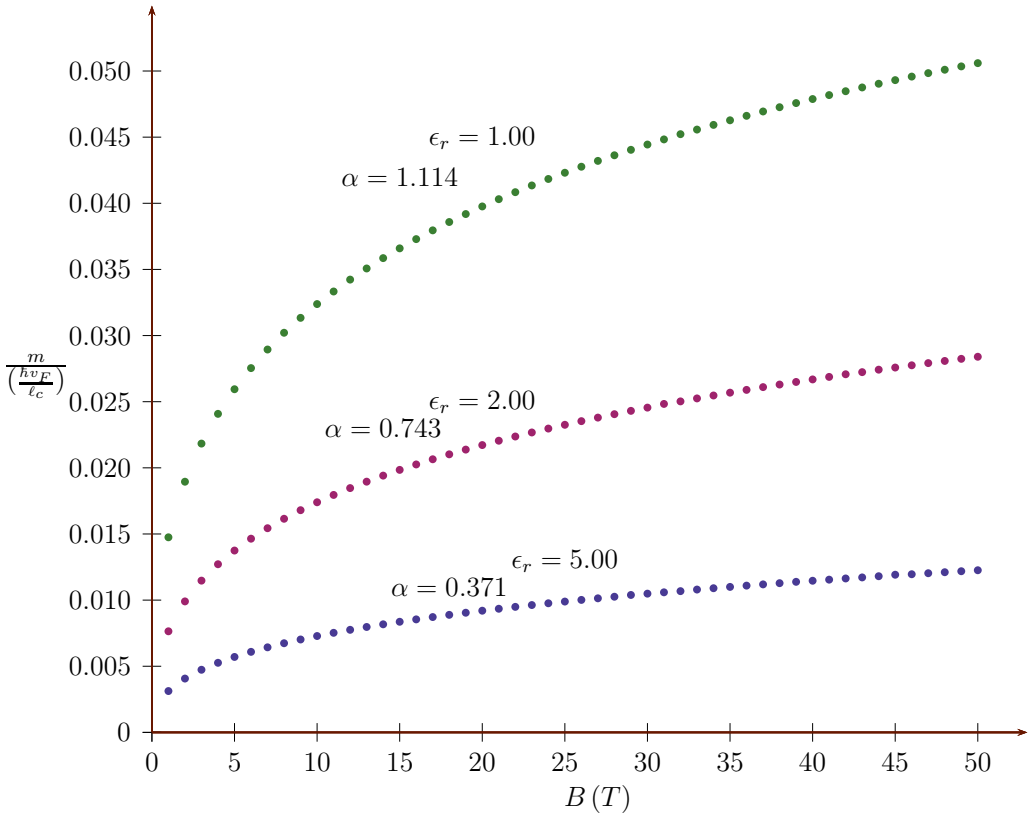

Figure 5.1: This figure shows the variation of dimensionless mass parameter with magnetic field. The mean field energy is minimized by these mass parameter for the particular magnetic field. We have shown the variation of mass parameter with dielectric constant of the substrates. $\epsilon_r = 1$ corresponds for suspended graphene. The mass parameter is in units of $(\hbar\, v_F/l_c)$, so $m \to 0$ as $B \to 0$. Here dimensionless constant α is the ratio κ_C/κ_t.

The decoupling of variables m_o and m_u in the above equation yields us similar situation as we had seen in the case for $\sigma_H = 0$. Once again the decoupled equations that needs to minimized are exactly same as we had seen in Eq.(5.31) for parameter m_o and Eq.(5.32). And same argument holds for the extreme values, i.e. $m_o = \tilde{m} = m_u$. Hence in the case for Hall conductivity $\sigma_H = -1$, the diagonal mass matrix takes the form,

$$M_D = \{\tilde{m}, -\tilde{m}, -\tilde{m}, -\tilde{m}\} \tag{5.35}$$

5.3 Particle-hole gaps

In this section we will compute the particle-hole excitation gaps for the ground states we found for the Hall conductivity states that we found in the previous section. The variational parameters are fixed by the minimization procedure. In the case for the symmetric model, the masses of the Dirac particle get fixed via minimization and the angle parameters are still arbitrary as we saw in the previous section that mean field energy was independent of variational angle parameters. For the particle-hole excitation gaps within the symmetric model, is independent of angle parameters. We will see that the size of the gaps are decided by the symmetric model.

We are considering the particle-hole excitations about the ground state, so in general the excited state can be constructed,

$$|ES\rangle = \psi^{\dagger}_{n_p,l_p,q_p}\psi_{n_h,l_h,q_h}|GS\rangle \tag{5.36}$$

i.e. a hole is created by annihilate a state with quantum numbers (n_h, l_h, q_h), here Landau level index, n_h, of the hole created with l_p its orbital angular momentum and q_h the $SU(4)$ index. And a particle is created by the creation operator with quantum numbers (n_p, l_p, q_p).

The particle-hole activation gap is computed from the expectation value of hamiltonian for excited state and the ground state,

$$\Delta_{gap} = \frac{1}{2}\big(\langle ES|\mathcal{H}|ES\rangle - \langle GS|\mathcal{H}|GS\rangle\big) \tag{5.37}$$

The ground state expectation value of hamiltonian can be expressed in terms of two point correlator, used for mean field energy calculation. In the similar fashion as we did for ground state computations, we can define two point correlator for excited states,

$\Upsilon(\boldsymbol{r}_1, \boldsymbol{r}_2)$, which is excited state expectation value for two field operators, defined as

$$\Upsilon_{r,A;s,B}(\boldsymbol{r}_1, \boldsymbol{r}_2) = \langle ES|\Psi^{\dagger}_{s,B}(\boldsymbol{r}_2)\Psi_{r,A}(\boldsymbol{r}_1)|ES\rangle \tag{5.38}$$

This expectation value can be expressed in terms of the wave functions used to construct the variational state,

$$\Upsilon_{r,A;s,B}(\boldsymbol{r}_1, \boldsymbol{r}_2) = \Phi^{n_p,l_p,q_p}_{r,A}(\boldsymbol{r}_1)\big(\Phi^{n_p,l_p,q_p}_{s,B}(\boldsymbol{r}_2)\big)^* - \Phi^{n_h,l_h,q_h}_{r,A}(\boldsymbol{r}_1)\big(\Phi^{n_h,l_h,q_h}_{s,B}(\boldsymbol{r}_2)\big)^* + \Gamma_{r,A;s,B}(\boldsymbol{r}_1, \boldsymbol{r}_2) \tag{5.39}$$

This correlator is 8×8 matrix and in compact notation we can write,

$$\Upsilon(\boldsymbol{r}_1, \boldsymbol{r}_2) = \Gamma^{(p)}(\boldsymbol{r}_1, \boldsymbol{r}_2) - \Gamma^{(h)}(\boldsymbol{r}_1, \boldsymbol{r}_2) + \Gamma(\boldsymbol{r}_1, \boldsymbol{r}_2) \tag{5.40}$$

Here, the correlator for the particle,

$$\Gamma^{(p)}(\boldsymbol{r}_1, \boldsymbol{r}_2) = \Phi^{n_p,l_p,q_p}(\boldsymbol{r}_1)\Phi^{n_p,l_p,q_p\,\dagger}(\boldsymbol{r}_2) \tag{5.41}$$

and the correlator for the hole,

$$\Gamma^{(h)}(\boldsymbol{r}_1, \boldsymbol{r}_2) = \Phi^{n_h,l_h,q_h}(\boldsymbol{r}_1)\Phi^{n_h,l_h,q_h\,\dagger}(\boldsymbol{r}_2) \tag{5.42}$$

$\Gamma(\boldsymbol{r}_1, \boldsymbol{r}_2)$ is the two point correlator for the ground state.

In our case, the excited state for the ground states at Hall conductivity at $\sigma_H = 0, -1$ has particle and hole state belong to different sub-levels of $n = 0$ Landau level.

$$|ES\rangle = \psi^{\dagger}_{0,l_p,q_p}\psi_{0,l_h,q_h}|GS\rangle \tag{5.43}$$

The wave function for the $n = 0$ Landau level,

$$\Phi_{0,l,q}(\boldsymbol{r}) = \begin{pmatrix} 0 \\ \\ \varphi_{0,l}(\boldsymbol{r}) \end{pmatrix} \chi^q \chi^{q\dagger} \tag{5.44}$$

Here,

$$\varphi_{0,l}(\boldsymbol{r}) = \frac{1}{\sqrt{2\pi\ell_c^2}} \frac{1}{\sqrt{2^l l!}} \mathrm{e}^{-\mathrm{i}\, l\theta} r^l \mathrm{e}^{-\frac{1}{4}r^2} = \frac{1}{\sqrt{2\pi\ell_c^2}} \frac{1}{\sqrt{l!}} \Big(\frac{\bar{z}}{\sqrt{2}}\Big)^l \mathrm{e}^{-\frac{1}{4}|z|^2} \tag{5.45}$$

the wave function expressed in complex variable will be useful for analytic computation of the gaps as we shall see shortly.

The correlator for the particle or hole, ($\mathtt{x} = p, h$)

$$\begin{aligned} \Gamma^{(\mathtt{x})}(\boldsymbol{r}_1, \boldsymbol{r}_2) &= \Phi^{0,l_\mathtt{x},q_\mathtt{x}}(\boldsymbol{r}_1) {\Phi^{0,l_\mathtt{x},q_\mathtt{x}}}^\dagger(\boldsymbol{r}_2) \\ &= \frac{1}{2\pi\ell_c^2} \frac{1}{2} (\mathbb{1}_2 - \beta) \frac{1}{l_\mathtt{x}!} \Big(\frac{\bar{z}_1 z_2}{2}\Big)^{l_\mathtt{x}} \mathrm{e}^{-\frac{1}{4}(|z_1|^2 + |z_2|^2)} P_{q_\mathtt{x}} \end{aligned}$$

It is useful for computations to express the above expression in relative coordinates and this achieved by using following relations,

$$|\boldsymbol{r}_1 - \boldsymbol{r}_2|^2 = |z_1 - z_2|^2 = |z_1|^2 + |z_2|^2 - (\bar{z}_1 z_2 + z_1 \bar{z}_2) \tag{5.46}$$

$$\Gamma^{(\mathtt{x})}(\boldsymbol{r}_1, \boldsymbol{r}_2) = \Big(\frac{1}{2\pi\ell_c^2}\Big) \frac{1}{2} (\mathbb{1}_2 - \beta) \frac{1}{l_\mathtt{x}!} \Big(\frac{\bar{z}_1 z_2}{2}\Big)^{l_\mathtt{x}} \mathrm{e}^{-\frac{1}{4}(\bar{z}_1 z_2 + z_1 \bar{z}_2)} \mathrm{e}^{-\frac{1}{4}|z_1 - z_2|^2} P_{q_\mathtt{x}} \tag{5.47}$$

Note that we have not mentioned anything about the angle parameters for the hole and particle states. Within symmetric model we will show that $SU(4)$ component of the correlator gets traced out leaving no angle dependence for the activation gaps.

5.3.1 Kinetic term

To compute the contribution to the activation gap from the kinetic terms we need to evaluate

$$\Delta_t = \frac{1}{2}\Big(\langle ES|\mathcal{H}_0|ES\rangle - \langle GS|\mathcal{H}_0|GS\rangle\Big) \tag{5.48}$$

We can express the left hand side of the above equation in terms of the correlator, following the discussion of section 5.1.1.

$$\Delta_t = \frac{1}{2}\Big(\frac{\hbar v_F}{\ell_c}\Big)\Big(\int_{\boldsymbol{r}} \lim_{\boldsymbol{r}_0\to\boldsymbol{r}} \mathrm{Tr}[\mathrm{h}\,\Upsilon(\boldsymbol{r},\boldsymbol{r}_0)] - \int_{\boldsymbol{r}} \lim_{\boldsymbol{r}_0\to\boldsymbol{r}} \mathrm{Tr}[\mathrm{h}\,\Gamma(\boldsymbol{r},\boldsymbol{r}_0)]\Big) \tag{5.49}$$

Using the definition of two point correlator for excited state, Eq.(5.40), we find evaluation of correlator for the particle and hole, $\mathrm{Tr}[\mathrm{h}\Gamma^{(p)}(\boldsymbol{r},\boldsymbol{r}_0)] = 0$ and $\mathrm{Tr}[\mathrm{h}\Gamma^{(h)}(\boldsymbol{r},\boldsymbol{r}_0)] = 0$. And the $\mathrm{Tr}[\mathrm{h}\Gamma(\boldsymbol{r},\boldsymbol{r}_0)]$ cancels and hence this leads to conclusion that there is no contribution to activation gap from the kinetic term. This is has to do with the fact that both particle and hole states which are $n = 0$ Landau levels are same for both massless and massive cases. And here the hamiltonian h is for massless Dirac particle which have zero eigenvalue for $n = 0$ Landau level.

5.3.2 Coulomb term

The contribution to the activation gap from the Coulomb term is computed by evaluating,

$$\Delta_C = \frac{1}{2}\Big(\langle ES|\mathcal{H}_C|ES\rangle - \langle GS|\mathcal{H}_C|GS\rangle\Big) \tag{5.50}$$

Here $\mathcal{H}_C$ is taken from Eq.(5.3). And use two point correlator to evaluate the above expression in a similar fashion as we accomplished for mean field energy computation in section 5.1.2

The direct term contributions for Δ_C

$$\frac{1}{2}\Big(\frac{1}{2}\frac{e^2}{4\pi\varepsilon}\Big)\iint_{\boldsymbol{r}_1,\boldsymbol{r}_2}\frac{1}{|\boldsymbol{r}_1-\boldsymbol{r}_2|}\left(\mathrm{Tr}[\Gamma^{(p)}(\boldsymbol{r}_1,\boldsymbol{r}_1)-\Gamma^{(h)}(\boldsymbol{r}_1,\boldsymbol{r}_1)]\right)$$
$$\left(\mathrm{Tr}[\Gamma^{(p)}(\boldsymbol{r}_2,\boldsymbol{r}_2)-\Gamma^{(h)}(\boldsymbol{r}_2,\boldsymbol{r}_2)]\right) \quad (5.51)$$

The exchange contributions

$$\begin{aligned}\frac{1}{2}\Big(\frac{1}{2}\frac{e^2}{4\pi\varepsilon}\Big)\iint_{\boldsymbol{r}_1,\boldsymbol{r}_2}\frac{1}{|\boldsymbol{r}_1-\boldsymbol{r}_2|}\Bigg(&\mathrm{Tr}\big[\big(\Gamma^{(p)}(\boldsymbol{r}_1,\boldsymbol{r}_2)-\Gamma^{(h)}(\boldsymbol{r}_1,\boldsymbol{r}_2)\big)\Gamma(\boldsymbol{r}_2,\boldsymbol{r}_1)\big]\\&+\mathrm{Tr}\big[\big(\Gamma^{(p)}(\boldsymbol{r}_2,\boldsymbol{r}_1)-\Gamma^{(h)}(\boldsymbol{r}_2,\boldsymbol{r}_1)\big)\Gamma(\boldsymbol{r}_1,\boldsymbol{r}_2)\big]\\&+\mathrm{Tr}\Big[\big(\Gamma^{(p)}(\boldsymbol{r}_1,\boldsymbol{r}_2)-\Gamma^{(h)}(\boldsymbol{r}_1,\boldsymbol{r}_2)\big)\big(\Gamma^{(p)}(\boldsymbol{r}_2,\boldsymbol{r}_2)-\Gamma^{(h)}(\boldsymbol{r}_2,\boldsymbol{r}_2)\big)\Big]\Bigg)\end{aligned} \quad (5.52)$$

On collecting the direct and exchange contributions together to find the final expression for excitation gap, we find terms

$$\mathrm{Tr}[\Gamma^{(p)}(\boldsymbol{r}_1,\boldsymbol{r}_1)]\mathrm{Tr}[\Gamma^{(p)}(\boldsymbol{r}_2,\boldsymbol{r}_2)]-\mathrm{Tr}\big[\Gamma^{(p)}(\boldsymbol{r}_1,\boldsymbol{r}_2)\Gamma^{(p)}(\boldsymbol{r}_2,\boldsymbol{r}_1)\big]$$

and

$$\mathrm{Tr}[\Gamma^{(h)}(\boldsymbol{r}_1,\boldsymbol{r}_1)]\mathrm{Tr}[\Gamma^{(h)}(\boldsymbol{r}_2,\boldsymbol{r}_2)]-\mathrm{Tr}\big[\Gamma^{(h)}(\boldsymbol{r}_1,\boldsymbol{r}_2)\Gamma^{(h)}(\boldsymbol{r}_2,\boldsymbol{r}_1)\big]$$

on spatial integration have no contribution as the direct and exchange terms cancel each other. The terms

$$\mathrm{Tr}\big[\Gamma^{(p)}(\boldsymbol{r}_1,\boldsymbol{r}_2)\Gamma^{(h)}(\boldsymbol{r}_2,\boldsymbol{r}_1)\big]=0$$

by virtue of orthonormal $SU(4)$ components of the particle and hole wave functions.

In our simplified picture of activation process we are assuming that the hole is created at one end of the sample and the particle is created on the other end. The overlap of particle and hole wave functions, whose centers are separated by large distances can neglected.

And the term

$$\iint_{\boldsymbol{r}_1,\boldsymbol{r}_2} \frac{1}{|\boldsymbol{r}_1-\boldsymbol{r}_2|}\,\mathrm{Tr}[\Gamma^{(p)}(\boldsymbol{r}_1,\boldsymbol{r}_1)]\mathrm{Tr}[\Gamma^{(h)}(\boldsymbol{r}_2,\boldsymbol{r}_2)]$$

which is essentially overlap of particle and hole wave functions with a weight factor of inverse of distance between them, i.e. we are not considering the possibility that particle and hole states can form a bound state. Hence we can neglect this integral.

The activation gap in $SU(4)$ symmetric model comes from the exchange terms only,

$$\frac{1}{2}\Big(\frac{1}{2}\frac{e^2}{4\pi\varepsilon}\Big)\iint_{\boldsymbol{r}_1,\boldsymbol{r}_2}\frac{1}{|\boldsymbol{r}_1-\boldsymbol{r}_2|}\Big(\mathrm{Tr}\big[\big(\Gamma^{(p)}(\boldsymbol{r}_1,\boldsymbol{r}_2)-\Gamma^{(h)}(\boldsymbol{r}_1,\boldsymbol{r}_2)\big)\Gamma(\boldsymbol{r}_2,\boldsymbol{r}_1)\big] + \mathrm{Tr}\big[\big(\Gamma^{(p)}(\boldsymbol{r}_2,\boldsymbol{r}_1)-\Gamma^{(h)}(\boldsymbol{r}_2,\boldsymbol{r}_1)\big)\Gamma(\boldsymbol{r}_1,\boldsymbol{r}_2)\big] \quad (5.53)$$

The activation gap from the Coulomb term,

$$\Delta_C = \frac{1}{2}\Big(\frac{1}{2}\frac{e^2}{4\pi\varepsilon}\Big)2\iint_{\boldsymbol{r}_1,\boldsymbol{r}_2}\frac{1}{|\boldsymbol{r}_1-\boldsymbol{r}_2|}\Big(\mathrm{Tr}[\Gamma^{(h)}(\boldsymbol{r}_1,\boldsymbol{r}_2)\Gamma(\boldsymbol{r}_2,\boldsymbol{r}_1)] - \mathrm{Tr}[\Gamma^{(p)}(\boldsymbol{r}_1,\boldsymbol{r}_2)\Gamma(\boldsymbol{r}_2,\boldsymbol{r}_1)]\Big) \quad (5.54)$$

Using the particle and hole correlator from Eq.(5.47) and the correlator for filled Dirac sea from Eq.(4.67). And we convert the integrals to complex coordinates as we did earlier.

$$\Delta_C = \Big(\frac{1}{2}\frac{e^2}{4\pi\varepsilon\ell_c}\Big)\Big(\frac{1}{2\pi\ell_c^2}\Big)^2\frac{1}{2}\sum_{i=q}^{4}\mathrm{Tr}[(P_h-P_p)P_q] \iint_{z_1,z_2}\frac{1}{|z_1-z_2|}\frac{1}{l!}\Big(\frac{\bar{z}_1 z_2}{2}\Big)^l \mathrm{e}^{-\frac{1}{4}(\bar{z}_1 z_2+z_1\bar{z}_2)}\mathrm{e}^{-\frac{1}{4}|z_1-z_2|^2} g_{m_q}(z_2,z_1) \quad (5.55)$$

After plugging in $g_{m_q}(z_2,z_1)$

$$\Delta_C = \Big(\frac{1}{2}\frac{e^2}{4\pi\varepsilon\ell_c}\Big)\Big(\frac{1}{2}\sum_{q=1}^{4}\mathrm{Tr}[P_hP_q-P_pP_q]\frac{m_q}{2\sqrt{\pi}}\int_s\frac{\mathrm{e}^{-s(m_q^2-1)}}{\sqrt{s}\sinh(s)} \frac{1}{(2\pi)^2}\iint_{z_1,z_2}\frac{1}{|z_1-z_2|}\frac{1}{l!}\Big(\frac{\bar{z}_1 z_2}{2}\Big)^l \mathrm{e}^{-\frac{1}{2}\bar{z}_1 z_2}\mathrm{e}^{-\frac{1}{4}|z_1-z_2|^2(1+\coth(s))}\Big) \quad (5.56)$$

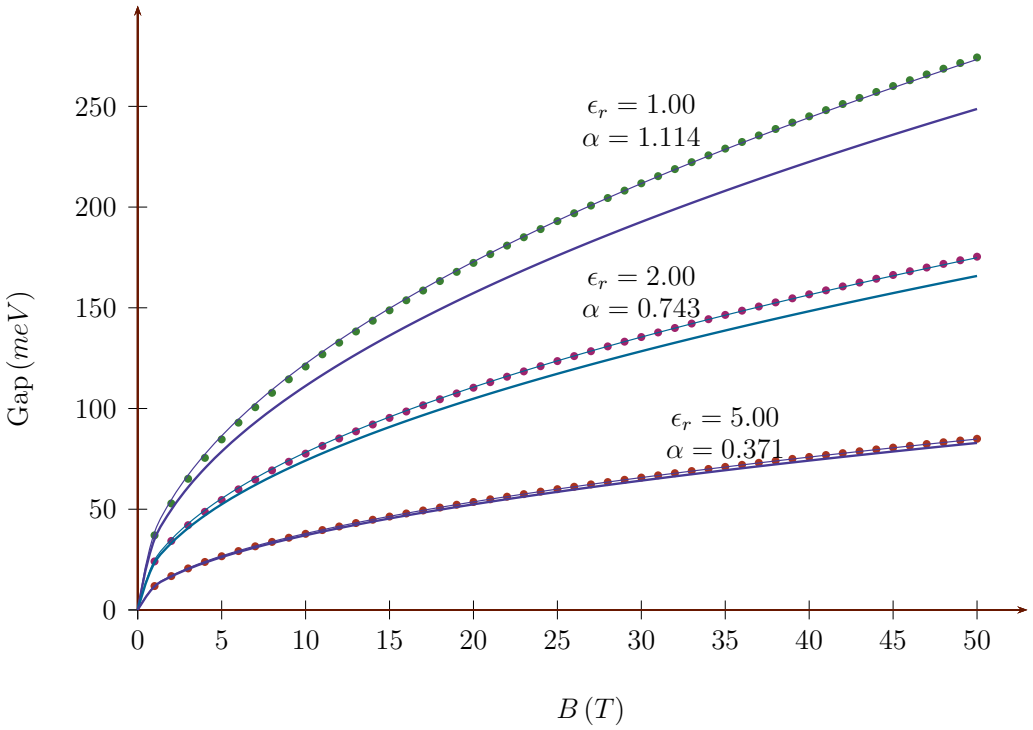

Figure 5.2: This figure shows the variation of activation gap with applied magnetic field. The gaps in meV and magnetic field in Tesla. The gaps for the Hall conductivity at $\sigma_H = 0$ and $\sigma_H = -1$ are same. The points are values for the gap obtained from our calculations where filled Dirac sea is taken into account and solid line curve is obtained when lowest Landau level projection is considered. The thin solid line with the points show the best fit. The best fit is function of magnetic field of the form $a\sqrt{B} + b\,B + c$, with a, b and c are best fit parameters. We have shown the variation of gaps with change in the dielectric constant of the substrate. The dielectric constant $\epsilon_r = 1$ corresponds to the suspended graphene. The best fit showed the dominant $\sqrt{B}$ contribution and linear B decreases as the dielectric constant of substrate increased. The constant term in the best fit was negligible. Along with dielectric constant we have presented the value $\alpha = \kappa_C/\kappa_t$.

The spatial integrals are solved analytically using the general solution from Appendix G.

$$\Delta_C = \Big(\frac{1}{2}\frac{e^2}{4\pi\varepsilon\ell_c}\Big)\frac{1}{2}\sum_{q=1}^{4}\mathrm{Tr}[P_hP_q - P_pP_q]\frac{m_q}{2\sqrt{\pi}}\int_s \frac{\mathrm{e}^{-s(m_q^2-1)}}{\sqrt{s}\sinh(s)}\sqrt{\frac{\pi}{(1+\coth(s))}} \tag{5.57}$$

Using the fact from the energy minimization $m_h = \tilde{m}$ and $m_p = -\tilde{m}$, the contribution to gap from filled Dirac sea,

$$\Delta_C = \Big(\frac{1}{2}\frac{e^2}{4\pi\varepsilon\ell_c}\Big)\frac{\tilde{m}}{2}\int_s \frac{\mathrm{e}^{-s\tilde{m}^2}}{\sqrt{s}}\frac{\mathrm{e}^{\frac{s}{2}}}{\sqrt{\sinh(s)}} = \Big(\frac{1}{2}\frac{e^2}{4\pi\varepsilon\ell_c}\Big)\,\eta_{C_1}(\tilde{m}) \tag{5.58}$$

The coefficient η_{C_1} in numerically implemented as following

$$\eta_{C_1} = \tilde{m}\sqrt{2} \int\limits_{\frac{1}{\sqrt{2N_C}}}^{\infty} \mathrm{d}\xi \frac{\mathrm{e}^{-m^2\xi^2}}{\sqrt{1-\mathrm{e}^{-2\xi^2}}} \tag{5.59}$$

The activation gap for the symmetric model for the Hall conductivity at $\sigma_H = 0$ and $\sigma_H = -1$,

$$\Delta_{gap} = \Delta_C \tag{5.60}$$

The variation of particle-hole gap with magnetic field is shown in Fig.5.2. The values of gap were computed numerically and the result was best fitted to a curve of the form $a\sqrt{B} + b\,B + c$. Here a, b, c are the best fit coefficients. We observe that dominant contribution comes from the $\sqrt{B}$ contribution and few percent contribution from the linear term and the constant term was very small compared to $\sqrt{B}$ contribution. We have compared results of our calculations where filled Dirac sea is taken into account with that of lowest Landau level projection. In Fig.5.2, we have also presented the variation of gaps with dielectric constant of the substrate. It clearly shows decrease in gaps as dielectric constant increases and also the linear magnetic field dependence of our best fit of the gaps. The magnitude of gaps that we obtained from our computations is approximately double of what is seen in the gap measurements for the suspended graphene [1].

5.4 Summary

We here summarize the results of our symmetric model calculations,

1. We have showed that the Coulomb interaction breaks the $SU(4)$ symmetry spontaneously for the ground states for Hall conductivity at $\sigma_H = 0$ and $\sigma_H = -1$.

2. The order parameter for spontaneous symmetry breaking is the mass of the Dirac particle which is proportional to a dimensionless $\alpha = \kappa_C/\kappa_t$, which depends on

dielectric constant.

3. The order parameter is proportional to magnetic field and tends to zero as magnetic field goes to zero which indicates spontaneous symmetry breaking of $SU(4)$ symmetry by Coulomb interaction in presence of magnetic field.

4. The particle-hole gaps from symmetric model showed a square root dependence on the applied magnetic field. Our symmetric model without disorder taken into account over estimates the gaps when compared with experimental values.

Chapter 6

Symmetry breaking terms

In the previous chapter, we saw the spontaneous symmetry breaking of $SU(4)$ symmetry of the non-interacting model by considering the $SU(4)$ symmetric long ranged Coulomb interaction. Though the $SU(4)$ symmetry is broken, the $SU(4)$ polarization of the ground state is ambiguous within the $SU(4)$ symmetric model. In this chapter, we consider the $SU(4)$ symmetry breaking terms of the model adopted in this thesis. We obtain the mean field energy of the interacting model in term of the variational angle parameters and minimize the energy with respect to these angle parameters to obtain the $SU(4)$ polarization for the ground states for the Hall conductivity $\sigma_H = 0$ and $\sigma_H = -1$. We obtain all possible ground states by conducting a complete search of the variational parameter space for the coupling parameters used for short ranged interactions, V, nearest neighbour interaction and U, Hubbard interaction. We have presented this in the phase diagram in U-V space. The $SU(4)$ polarization of the excitations from the ground states was also ambiguous within the symmetric model as we had seen in the previous chapter. Incorporating the symmetry breaking term in the calculations for the particle-hole excitations reveal possible excitations in the U-V parameter space for the ground states obtained in this chapter. Although contributions of short ranged interactions to the particle-hole excitations is considerably small compared long ranged Coulomb interaction but they decide

the $SU(4)$ polarization of the excitations. We also compared results from our calculations with that of obtained from the experiments and present a detailed discussion.

6.1 Symmetry breaking terms

In this section we consider the all the symmetry breaking term of our interacting model and express their expectation value for the variational ground states of $\sigma_H = 0$ and $\sigma_H = -1$. This is expressed in terms of the coincident correlator, which contains all the variational parameters. These general expressions will be used to find the explicit dependence on the variational parameters ground states at Hall conductivity at $\sigma_H = 0, -1$ discussed in section 4.3. Unlike the computation of expectation value for Coulomb term, the evaluation of expectation value for symmetry breaking terms involves coincident correlator which have no spatial dependence. Hence the spatial integration is trivial and results in a factor of volume of the system, V.

6.1.1 Nearest Neighbour term

The nearest neighbour interaction term was introduced into our interacting model to take into account the sub-leading resulting after the continuum approximation of Coulomb interaction and finite size wave function effects of the short ranged interaction. We had approximated this sub-leading term was approximated with nearest neighbour interaction because both break the $SU(4)$ in similar fashion. At the lattice level, the nearest neighbour interaction takes into account electron-electron interaction between a sub-lattice point and its three nearest neighbour which belong to the second sub-lattice point. The bare strength of this interaction is that of Coulomb interaction between two electron separated by bond length, $a/\sqrt{3}$, a is lattice constant. In reality the electron are not point objects, instead described by the wave functions. This interaction gets modified due to spread of the wave function. We are going to treat this interaction strength, V, as a parameter. Moreover

nearest neighbour is simplified form of much more complicated interaction term that resulted from the continuum approximation of lattice Coulomb interaction. Treating V as parameter allows us to explore the change in the ground state for a range of values. The continuum approximation derivation of nearest neighbour interaction term is provided in Appendix D. In the lattice model we also take into account the background charge from positive ions. The nearest neighbour interaction at continuum level is given by,

$$\mathcal{H}_V = \frac{3}{4} V a^2 \int_{\boldsymbol{x}} \Big(\big(\Psi^\dagger(\boldsymbol{x})\Psi(\boldsymbol{x})\big)^2 - \big(\Psi^\dagger(\boldsymbol{x})\beta\,\tau^z\Psi(\boldsymbol{x})\big)^2 - 2\bar{\rho}\,\Psi^\dagger(\boldsymbol{x})\Psi(\boldsymbol{x}) + \bar{\rho}^2 \Big) \quad (6.1)$$

Here $\bar{\rho}$ is the average charge density and is related to the coincident correlator, Γ

$$\bar{\rho} = \mathrm{Tr}[\Gamma] \quad (6.2)$$

The expectation value of nearest neighbour term,

$$\langle \mathcal{H}_V \rangle = \langle GS|\mathcal{H}_V|GS\rangle$$

$|GS\rangle$ is the ground state under consideration. This expectation value can be expressed in terms expectation value of pair of creation and annihilation field operators via Wick's decomposition as performed in section 5.1.2. A similar process to that we has seen in the case of Coulomb interaction term, write the expectation value of nearest neighbour interaction, Eq.(6.1), in terms of two point coincident correlator.

$$\langle \mathcal{H} \rangle = \frac{\mathrm{V}}{2\pi\ell_c^2}\kappa_V \Big(- \mathrm{Tr}[\tilde{\Gamma}\,\tilde{\Gamma}] - \big(\mathrm{Tr}[\beta\,\tau^z\,\tilde{\Gamma}]\big)^2 + \mathrm{Tr}[\beta\,\tau^z\,\tilde{\Gamma}\,\beta\,\tau^z\,\tilde{\Gamma}] \Big) \quad (6.3)$$

Here, $\Gamma = \tilde{\Gamma}/(2\pi\ell_c^2)$ and κ_V is function of coupling parameter, V,

$$\kappa_V = \frac{3Va^2}{8\pi\ell_c^2} \quad (6.4)$$

The factor, a^2/ℓ_c^2 symbolizes the leading lattice order correction to the continuum energy. The value of $a^2/\ell_c^2 \approx 9.2 \times 10^{-5}\, B$, varies linearly with magnetic field, B and magnetic field is expressed in Tesla. The value of $\kappa_V \approx 10^{-2} B\, meV$ for V is order of few electron volts. On comparison with the κ_t and κ_C which have square root magnetic field dependence, κ_V is at least two order of magnitude smaller for the magnetic fields achieved in laboratory.

6.1.2 Hubbard term

The second short ranged of interaction at lattice level is the Hubbard on-site interaction. This takes into account the interaction between two electron wave function with spins pointing in opposite direction interacting at same lattice point. The continuum derivation of on-site Hubbard term is provided in Appendix E. Here also we have taken into account the charge due to background positive ions, like the way did for nearest neighbour and Coulomb interaction terms. The continuum approximation for Hubbard term results in,

$$\mathcal{H}_U = \frac{1}{4} U a^2 \int_{\boldsymbol{x}} \Big(\big(\Psi^\dagger(\boldsymbol{x})\Psi(\boldsymbol{x})\big)^2 + \big(\Psi^\dagger(\boldsymbol{x})\beta\,\tau^z\Psi(\boldsymbol{x})\big)^2 + \frac{1}{2}\sum_{j,k=x,y} \big(\Psi^\dagger(\boldsymbol{x})\alpha^j\,\tau^k\Psi(\boldsymbol{x})\big)^2 - 2\bar{\rho}\,\Psi^\dagger(\boldsymbol{x})\Psi(\boldsymbol{x}) + \bar{\rho}^2 \Big) \quad (6.5)$$

For the mean field computation we are interested in evaluation of the expectation value of the Hubbard term for the ground state under consideration,

$$\langle \mathcal{H}_U \rangle = \langle GS|\mathcal{H}_U|GS\rangle$$

Once again we make use of Wick's decomposition to express this into expectation value of pair of creation and annihilation field operators and to express in terms of the two point

coincident correlator.

$$\langle \mathcal{H}_U \rangle = \frac{\mathrm{V}}{2\pi\ell_c^2}\kappa_U \Bigg(-\mathrm{Tr}[\tilde{\Gamma}\,\tilde{\Gamma}] + \big(\mathrm{Tr}[\beta\,\tau^z\,\tilde{\Gamma}]\big)^2 - \mathrm{Tr}[\beta\,\tau^z\,\tilde{\Gamma}\,\beta\,\tau^z\,\tilde{\Gamma}] + \frac{1}{2}\sum_{j,k=x,y}\Big(\big(\mathrm{Tr}[\alpha^j\,\tau^k\,\tilde{\Gamma}]\big)^2 - \mathrm{Tr}[\alpha^j\,\tau^k\,\tilde{\Gamma}\,\alpha^j\,\tau^k\,\tilde{\Gamma}]\Big)\Bigg) \quad (6.6)$$

Here κ_U is function of coupling parameter, U,

$$\kappa_U = \frac{Ua^2}{8\pi\ell_c^2} \quad (6.7)$$

Similar to that we had seen in the case of nearest neighbour interaction, the coupling parameter, κ_U varies linearly with magnetic field and is also at least two order smaller in magnitude when compared to κ_C and κ_t for magnetic fields used in the quantum Hall experiments.

Both coupling parameters κ_V and κ_U has linear dependence on the perpendicular component of the applied magnetic field and are of same order of magnitude.

6.1.3 Zeeman term

The Zeeman term is one-particle term that becomes relevant in presence of magnetic field. This term lifts the spin degeneracy takes by the splitting in energy level of spins pointing in direction of the magnetic field and in the opposite direction. The continuum approximation of Zeeman term,

$$\mathcal{H}_Z = -\frac{1}{2}g\mu_B \int_{\boldsymbol{x}} \Psi^\dagger(\boldsymbol{x})\,\boldsymbol{\sigma}\cdot\boldsymbol{B}\,\Psi(\boldsymbol{x}) \quad (6.8)$$

The expectation value of Zeeman term can be expressed in terms of coincident correlator,

$$\langle \mathcal{H}_Z \rangle = -\frac{\mathrm{V}}{2\pi\ell_c^2}\kappa_Z\,\mathrm{Tr}[\sigma^z\,\tilde{\Gamma}] \quad (6.9)$$

Here κ_Z give the measure of strength of the Zeeman term,

$$\kappa_Z = \frac{1}{2} g \mu_B B \tag{6.10}$$

$g \approx 2$ is the Lande's g-factor. $\mu_B = 9.274 \times 10^{-24} JT$ is Bohr magneton. This term also varies linearly with magnetic field like the other $SU(4)$ symmetry breaking terms. $\kappa_Z = 5.78 \times 10^{-2} B_T \, meV$, here B_T is total applied magnetic field. Whereas the orbital motion of the electron only see the perpendicular component of the magnetic field to the plane, $B_\perp = B_T \cos(\theta)$. θ here is the angle between applied magnetic field and the line perpendicular to plane of graphene. In the case when $B_T = B_\perp$, the Zeeman term also contribute energies of same order of magnitude as the nearest neighbour and Hubbard terms. The linear dependence on B_T of Zeeman coupling enables to distinguish the gaps that are caused by the spin splitting.

6.1.4 Kinetic - Sub-leading term

Last $SU(4)$ symmetry breaking term comes from the leading order lattice correction to the continuum kinetic term which we had described in section 3.1. Taking the leading order correction term to kinetic term of the lattice model from Eq.(3.12) and changing the momenta operator to conjugate momenta to account for the presence of magnetic field,

$$\mathcal{H}_1 = \frac{t}{8} \frac{a^2}{\ell_c^2} \int_{\boldsymbol{x}} \Psi^\dagger(\boldsymbol{x}) \left(\left(\alpha^x (\pi_x^2 + 3\pi_y^2) - \alpha^y 3(\pi_x \pi_y + \pi_y \pi_x) \right) \otimes \tau^z \right) \Psi(\boldsymbol{x}) \tag{6.11}$$

The expectation value of sub-leading correction to the kinetic term is obtained in the similar fashion as we discussed in section 5.1.1 for the kinetic term.

$$\langle \mathcal{H}_1 \rangle = \kappa_{t_1} \int_{\boldsymbol{r}} \lim_{\boldsymbol{r} \to \boldsymbol{r}_0} \mathrm{Tr}[\mathrm{h}_1 \, \Gamma(\boldsymbol{r}, \boldsymbol{r}_0)] \tag{6.12}$$

Here

$$\kappa_{t_1} = \frac{t}{8}\frac{a^2}{\ell_c^2} \tag{6.13}$$

The value $\kappa_{t_1} \approx 3.485 \times 10^{-2} B\, meV$ for $t = 3.03\, eV$, has linear dependence on the magnetic field and is of same order of magnitude like the other $SU(4)$ symmetry breaking terms.

We shall show later that this term does not contribute to the mean field energy for the Hall conductivity $\sigma_H = 0$ and $\sigma_H = -1$.

6.2 Mean field energy minimization and phase diagrams

In the previous section we had demonstrated that energy contribution from the $SU(4)$ symmetry breaking interaction terms are all proportional to $B_\perp$, perpendicular magnetic field (via a^2/ℓ_c^2) and they are at least two order of magnitude smaller when compared to terms from the $SU(4)$ symmetric terms. The single particle Zeeman term has got linear dependence on B_T, total applied magnetic field. In this section we compute the expectation value of symmetry breaking terms for the Hall conductivity states of $\sigma_H = 0$ and $\sigma_H = -1$. The mean field energy is expressed as a function of mass parameters and $SU(4)$ angle parameters. The angle parameters dependence solely comes from the symmetry breaking terms considered in this chapter and independent of contributions from the symmetric model. Whereas the variational mass parameter dependence comes from both symmetric and breaking terms of our model. In principle we should consider both symmetric and symmetry breaking terms in order to evaluate the mass parameter that minimizes the mean field energy. We had shown in the previous section that energy contributions to the mean field energy from the symmetry breaking terms are at least two order smaller when compared to the symmetric terms for magnetic field employed in quantum Hall experiments. As a consequence the values of mass parameter that minimizes the mean field energy gets only few percent correction from the symmetry breaking terms.

And subsequently the effect of the few percent change in mass parameter has negligible effect on the mean field energy. Hence we use the minimum values of mass parameter obtained from the symmetric model calculations. This amounts to treating the symmetry breaking terms as perturbations about the symmetric model.

The computation of mean field energy from the symmetry breaking terms requires the information of two point coincident correlator for the Hall conductivity $\sigma_H = 0, -1$. These correlator requires the information of mass matrix for specific Hall conductivity. The angle parameterization of the mass matrix is described in section 4.3 and the diagonal mass matrix form is taken from the solutions obtained from symmetric model computations for respective Hall conductivity obtained in the previous chapter, which is

$$\sigma_H = 0 : \qquad M_D = \{m, m, -m, -m\} \tag{6.14}$$

$$\sigma_H = -1 : \qquad M_D = \{m, -m, -m, -m\} \tag{6.15}$$

First we show that the contributions from the sub-leading kinetic term Eq.(6.12) vanishes for the Hall conductivity $\sigma_H = 0$ and -1. The action of h_1 on two point correlator and traced over requires evaluation

$$\mathrm{Tr}[\mathrm{h}_1 \Gamma(\boldsymbol{r}, \boldsymbol{r}_0)] = f_1(m^2)\mathrm{Tr}[\tau^z] \tag{6.16}$$

Here $f_1(m^2)$ is evaluated by using $b_m(\boldsymbol{r}, \boldsymbol{r}_0)$ from Eq.(4.70) and $d_m(\boldsymbol{r}, \boldsymbol{r}_0)$ from Eq.(4.71) which are functions of square of mass parameter,

$$\begin{aligned}\big(\pi_x^2 + 3\pi_y^2 + \mathrm{i}\,3(\pi_x\pi_y + \pi_y\pi_x)\big) b_m(\boldsymbol{r}, \boldsymbol{r}_0) \\ + \big(\pi_x^2 + 3\pi_y^2 - \mathrm{i}\,3(\pi_x\pi_y + \pi_y\pi_x)\big) d_m(\boldsymbol{r}, \boldsymbol{r}_0) = f_1(m^2)\end{aligned} \tag{6.17}$$

We do not need to this explicitly as the trace over the $SU(4)$ indices vanishes, hence

$$\langle \mathcal{H}_1 \rangle = 0 \tag{6.18}$$

Hence we drop the kinetic sub-leading term completely and compute the mean field energy for Hall conductivity at $\sigma_H = 0$ and $\sigma_H = -1$ using nearest neighbour, Hubbard and Zeeman terms.

6.2.1 Ground state at $\sigma_H = 0$

The mass matrix for the $\sigma_H = 0$ obtained from the symmetric model calculations,

$$M_D = \{m, m, -m, -m\}$$

and the two point coincident correlator takes the form after this choice of diagonal mass matrix,

$$\tilde{\Gamma} = (2\pi\ell_c^2)\Gamma = (u_m \mathbb{1}_2 - v_m \beta) \otimes \Big(\sum_{j=1,2} P_i - \frac{1}{2}\mathbb{1}_4 \Big) \tag{6.19}$$

Here $P_1 = |1\rangle\langle 1|$ and $P_2 = |2\rangle\langle 2|$ are projection operators constructed from the vectors of $SU(4)$ component of occupied $n = 0$ Landau levels from parameterization scheme discussed in section 4.3.2,

$$|1\rangle = \cos(\frac{\gamma_1}{2})|+\rangle|\boldsymbol{n}_1\rangle + \mathrm{e}^{\mathrm{i}\,\Omega_1} \sin(\frac{\gamma_1}{2})|-\rangle|-\boldsymbol{n}_2\rangle \tag{6.20}$$

$$|2\rangle = \cos(\frac{\gamma_2}{2})|+\rangle|-\boldsymbol{n}_1\rangle + \mathrm{e}^{\mathrm{i}\,\Omega_2} \sin(\frac{\gamma_2}{2})|-\rangle|\boldsymbol{n}_2\rangle \tag{6.21}$$

The expectation values of the symmetry breaking terms i.e the nearest neighbour interaction, Hubbard and Zeeman terms by evaluating the various traces involved with two point coincident correlator. The resulting mean field energy contributions from these terms is expressed as function of the variational parameters. The details of the calculation is provided in Appendix. I and here we present the final results obtained for each symmetry breaking term showing explicit the $SU(4)$ angle dependence.

Nearest neighbour interaction

The expectation value of nearest neighbour interaction, Eq(I.15),

$$\langle \mathcal{H}_V \rangle = -\frac{\mathrm{V}}{2\pi\ell_c^2}\kappa_V \Big(8v_m^2 \cos(\gamma_1)\cos(\gamma_2) + 2\big(v_m^2 - u_m^2\big)\big(\cos^2(\gamma_1) + \cos^2(\gamma_2)\big) + 4\big(v_m^2 + u_m^2\big)\Big) \quad (6.22)$$

The nearest neighbour energy is function of only two angle parameters γ_1 or γ_2. Since $v_m > u_m$ the nearest neighbour energy minimization is solely decided by the first term in Eq.(6.22). It minimizes for the values $\gamma_1 = \gamma_2 = 0$ or π. Substituting these values in Eq.(6.20) and Eq.(6.21), we obtain a charge ordering for the $n = 0$ Landau level.

Hubbard term

The expectation value for the Hubbard term, Eq.I.16

$$\langle \mathcal{H}_U \rangle = \frac{\mathrm{V}}{2\pi\ell_c^2}\kappa_U \Big(8v_m^2 \cos(\gamma_1)\cos(\gamma_2) + 2\big(v_m^2 - u_m^2\big)\big(\cos(\gamma_1) - \cos(\gamma_2)\big)^2 |\langle \boldsymbol{n}_1 | \boldsymbol{n}_2 \rangle|^2 \Big) \quad (6.23)$$

Here the mean field energy is function of $\gamma_1, \gamma_2, \theta_1, \theta_2, \phi_1$ and ϕ_2. The Hubbard term minimizes for the values $\gamma_1 = 0$ or π, $\gamma_2 = \pi - \gamma_1$ and $|\langle \boldsymbol{n}_1 | \boldsymbol{n}_2 \rangle|^2 = 0$. These values indicate that Hubbard term prefers an anti-ferromagnetic ordering for $n = 0$ Landau levels.

Zeeman term

The Zeeman energy contributions to the mean field energy, Eq.(I.17),

$$\langle \mathcal{H}_Z \rangle = -\frac{\mathrm{V}}{2\pi\ell_c^2}\kappa_Z\, u_m \big(\cos(\gamma_1) - \cos(\gamma_2)\big)\big(\cos(\theta_1) + \cos(\theta_2)\big) \quad (6.24)$$

Here the values of angle parameter that minimizes the Zeeman energy correspond to a ferromagnetic ordering for $n = 0$ Landau level, for example $\gamma_1 = 0$, $\gamma_2 = \pi$, $\theta_1 = 0$ and $\theta_2 = 0$.

Minimization

To obtain the $SU(4)$ polarization of the ground state, we need to obtain the values of the angle parameters that minimizes the mean field energy of the symmetry breaking terms. For this we collect the angle dependent contributions from the nearest neighbour, Hubbard and Zeeman terms.

$$\begin{aligned}\mathcal{E} = 2\big(v_m^2 - u_m^2\big)\Bigg(&- \frac{4v_m^2}{v_m^2 - u_m^2}(\kappa_V - \kappa_U)\cos(\gamma_1)\cos(\gamma_2) - \kappa_V\big(\cos^2(\gamma_1) + \cos^2(\gamma_2)\big) \\ &+ \frac{1}{2}\kappa_U\big(\cos(\gamma_1) - \cos(\gamma_2)\big)^2\big(1 + \cos(\theta_1)\cos(\theta_2) + \cos(\varphi_1 - \varphi_2)\sin(\theta_1)\sin(\theta_2)\big) \\ &- \kappa_Z\frac{u_m}{2(v_m^2 - u_m^2)}\big(\cos(\gamma_1) - \cos(\gamma_2)\big)\big(\cos(\theta_1) + \cos(\theta_2)\big) \quad (6.25)\end{aligned}$$

The minimization with respect to angle variables was achieved numerically and details are provided in section. I.1. These are three types of solutions corresponding to three phases seen in the U-V parameter space.

1. Charge ordered state:

$$\gamma_1 = \gamma_2 = 0 \text{ or } \pi$$

The corresponding energy

$$\mathcal{E}_{CDW} = -8v_m^2(\kappa_V - \kappa_U) - 4(v_m^2 - u_m^2)\kappa_V \quad (6.26)$$

2. Ferromagnetic ordered state:

$$\gamma_1 = 0(\pi),\ \gamma_2 = 0(\pi),\ \varphi_1 - \varphi_2 = 0,\ \theta_1 = 0(\pi) \text{ and } \theta_2 = 0(\pi)$$

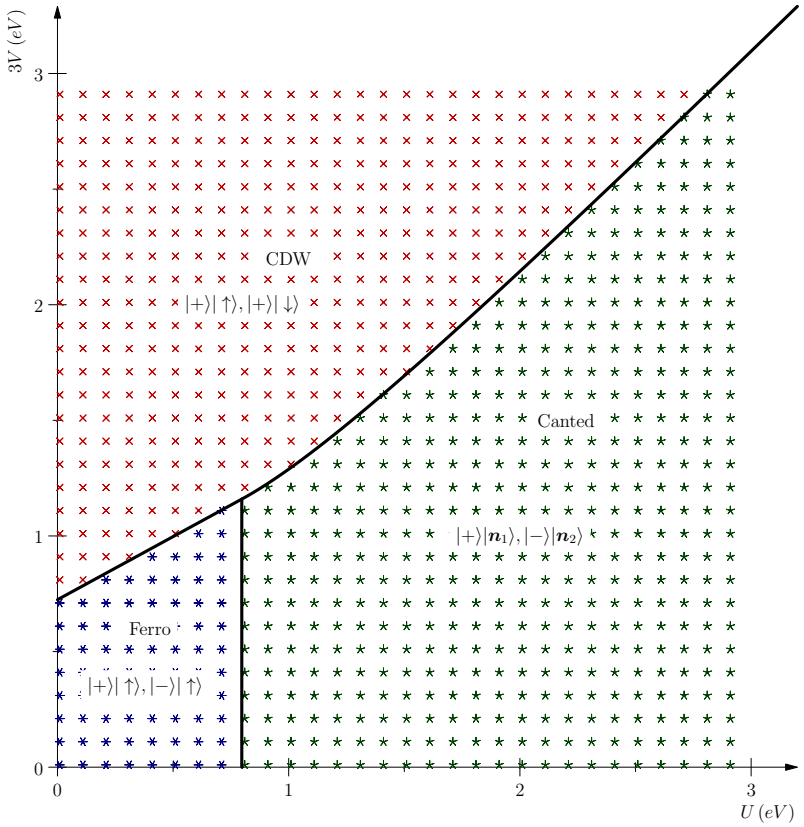

Figure 6.1: The figure shows the phase diagram for possible ground states for Hall conductivity $\sigma_H = 0$ in U-V parameter space. Both parameters are expressed in electron volts. This phase diagram is for magnetic field $B = 40\,T$. The region marked with dots in the phase space where ferromagnetic spin ordering preferred. The region marked with plus sign, '+', corresponds to the charge ordered state. This region is doubly degenerate the other possible ground will have $|-\rangle|\uparrow\rangle, |-\rangle|\downarrow\rangle$ $SU(4)$ components for $n = 0$ Landau level. The region marked with asterisk, $*$, is for the canted spin ordered state. The bold line separating the three phases were obtained analytically after equating pair of the analytical expression for the mean field energies in Eq.(6.26), Eq.(6.27) and Eq.(6.28), which are function of parameters U and V. Equations for these lines are shown in Eq.(6.29), Eq.(6.31) and Eq.(6.32). Phase transition across these lines is first order.

Ferromagnetic state energy

$$\mathcal{E}_{Ferro} = 8v_m^2(\kappa_V - \kappa_U) - 4(v_m^2 - u_m^2)\kappa_V + 8(v_m^2 - u_m^2)\kappa_U - 4u_m\kappa_Z \quad (6.27)$$

3. Canted spin ordered state:

$$\gamma_1 = 0(\pi),\ \gamma_2 = \pi(0),$$

$$\varphi_1 - \varphi_2 = \pi,\ \theta_1 - \theta_2 = 0 \text{ and } \cos(\frac{\theta_1 + \theta_2}{2}) = +(-)\frac{1}{4}\frac{u_m}{v_m^2 - u_m^2}\frac{\kappa_Z}{\kappa_U}$$

Energy for canted state,

$$\mathcal{E}_{Canted} = 8v_m^2(\kappa_V - \kappa_U) - 4(v_m^2 - u_m^2)\kappa_V - \frac{1}{2}\frac{u_m^2}{v_m^2 - u_m^2}\frac{\kappa_Z^2}{\kappa_U} \quad (6.28)$$

The Fig.6.1 shows results of minimization of mean field energy obtained numerically. These phases show first order phase transition with change in the parameters U and V. The lines separating the three phases can be obtained by comparing the energies for the corresponding phases. The equation of line separating the ferromagnetic and charge ordered phases is given by

$$3V = \frac{1}{2}\Big(1 + \frac{u_m^2}{v_m^2}\Big)U + \frac{1}{4}\frac{u_m}{v_m^2}\tilde{Z} \quad (6.29)$$

Here,

$$\tilde{Z} = \frac{\kappa_Z}{e}\frac{8\pi\ell_c^2}{a^2} = \frac{4\pi g\mu_B\hbar}{a^2e^2} \quad (6.30)$$

is constant parameter independent of magnetic field and expressed in electron volts.The equation of line separating ferromagnetic and canted spin ordered state is line parallel to the V axis.

$$U = \frac{1}{4}\frac{u_m}{v_m^2 - u_m^2}\tilde{Z} \quad (6.31)$$

The line separating the charge ordered and canted spin ordered state is straight line, $3V = U$, for large U and V limit. It has a singular nature in the limit $U \to 0$.

$$3V = U + \frac{1}{32}\frac{u_m^2}{v_m^2(v_m^2 - u_m^2)}\frac{\tilde{Z}^2}{U} \tag{6.32}$$

We can notice the deviation from the straight line near the point where three phases meet in the phase diagram.

6.2.2 Ground state at $\sigma_H = -1$

The mass matrix for the $\sigma_H = -1$ obtained from the symmetric model calculations like we did in the case for $\sigma_H = 0$,

$$M_D = \{m, -m, -m, -m\}$$

and the two point coincident correlator is constructed incorporating the diagonal mass matrix structure

$$\tilde{\Gamma} = (2\pi\ell_c^2)\Gamma = (u_m \mathbb{1}_2 - v_m\beta) \otimes \left(P_1 - \frac{1}{2}\mathbb{1}_4\right) \tag{6.33}$$

Here $P_1 = |1\rangle\langle 1|$ is projection operators constructed from the vectors of $SU(4)$ component of occupied $n = 0$ Landau levels as we discussed in section 4.3.1

$$|1\rangle = \cos(\frac{\gamma_1}{2})|+\rangle|\boldsymbol{n}_1\rangle + \mathrm{e}^{\mathrm{i}\,\Omega_1}\sin(\frac{\gamma_1}{2})|-\rangle|-\boldsymbol{n}_2\rangle \tag{6.34}$$

The expectation values of the symmetry breaking terms i.e the nearest neighbour interaction, Hubbard and Zeeman terms by evaluating the various traces involved with two point coincident correlator. The resulting mean field energy contributions from these terms is expressed as function of the variational parameters. The details of the calculation is provided in Appendix. J.

Nearest neighbour interaction

The nearest neighbour interaction is function of only one angle parameter,

$$\langle \mathcal{H}_V \rangle = -\frac{\mathrm{V}}{2\pi\ell_c^2}\kappa_V \bigg(2\big(v_m^2 - u_m^2\big)\cos^2(\gamma_1) + 2(v_m^2 + u_m^2) \bigg) \tag{6.35}$$

and this terms individually minimizes for $\gamma_1 = 0$ or π, which implies that $n = 0$ Landau level will be localized on one of the sub-lattice point

Hubbard term

The expectation value for Hubbard term,

$$\langle \mathcal{H}_U \rangle = \frac{\mathrm{V}}{2\pi\ell_c^2}\kappa_U \bigg(-2\big(v_m^2 - u_m^2\big)\sin^2(\gamma_1)|\langle \boldsymbol{n}_1|\boldsymbol{n}_2\rangle|^2 - 4u_m^2 \bigg) \tag{6.36}$$

minimizes for value $\gamma_1 = \pi/2$, provided that $|\langle \boldsymbol{n}_1|\boldsymbol{n}_2\rangle|^2 = 1$. This indicates that occupied $n = 0$ Landau level has equal weights on two sub-lattice points and spins are polarized in opposite direction.

Zeeman term

The Zeeman term depends on three angle variables,

$$\langle \mathcal{H}_Z \rangle = -\frac{\mathrm{V}}{2\pi\ell_c^2}\kappa_Z \bigg(u_m \Big(\big(\cos(\theta_1) - \cos(\theta_2)\big) + \cos(\gamma_1)\big(\cos(\theta_1) + \cos(\theta_2)\big)\Big)\bigg) \tag{6.37}$$

and it minimizes for either $\theta_1 = 0, \theta_2 = \pi, \gamma_1 = \pi/2$ implying that equal weights on two sub-lattice points with spins pointing in same direction that of magnetic field, or $\gamma_1 = 0(\pi), \theta_1 = 0(\theta_2 = \pi)$, indicating that $n = 0$ Landau level is localized on one sub-lattice with spin pointing in same direction of magnetic field.

Minimization

We collect the angle parameter dependent terms for symmetry breaking terms

$$\begin{aligned}\mathcal{E} = &-2(v_m^2 - u_m^2)\kappa_V \cos^2(\gamma_1) \\ &- (v_m^2 - u_m^2)\kappa_U \sin^2(\gamma_1)\Big(1 + \cos(\theta_1)\cos(\theta_2) + \cos(\varphi_1 - \varphi_2)\sin(\theta_1)\sin(\theta_2)\Big) \\ &- u_m\kappa_Z\Big(\big(\cos(\theta_1) - \cos(\theta_2)\big) + \cos(\gamma_1)\big(\cos(\theta_1) + \cos(\theta_2)\big)\Big) \quad (6.38)\end{aligned}$$

to evaluate the angle parameters that minimizes the energy numerically.

The results of numerical minimization resulted in two types of solutions corresponding to two phases which we have enumerated below.

1. Valley-spin polarized state:

$$\gamma_1 = 0, \theta_1 = 0 \qquad \text{or} \qquad \gamma_1 = \pi, \theta_2 = \pi$$

   This ground state is doubly degenerate and at $n = 0$ Landau level, the wave function is localized on either sub-lattice point with spin pointing is same direction that of magnetic field. The energy in terms of coupling parameter for this ground state is,

$$\mathcal{E}_1 = -2(v_m^2 - u_m^2)\kappa_V - 2u_m\kappa_Z \quad (6.39)$$

2. Canted valley ordered state:

$$\theta_1 = \theta_2 = 0(\pi)$$

$$\cos(\gamma_1) = +(-)\frac{1}{2}\frac{u_m}{v_m^2 - u_m^2}\frac{\kappa_Z}{\kappa_U - \kappa_V}$$

   The $SU(4)$ component of the occupied $n = 0$ Landau level,

$$|1\rangle = \cos(\frac{\gamma_1}{2})|+\rangle|\uparrow\rangle + \mathrm{e}^{\mathrm{i}\,\Omega_0}\sin(\frac{\gamma_1}{2})|-\rangle|\downarrow\rangle \quad (6.40)$$

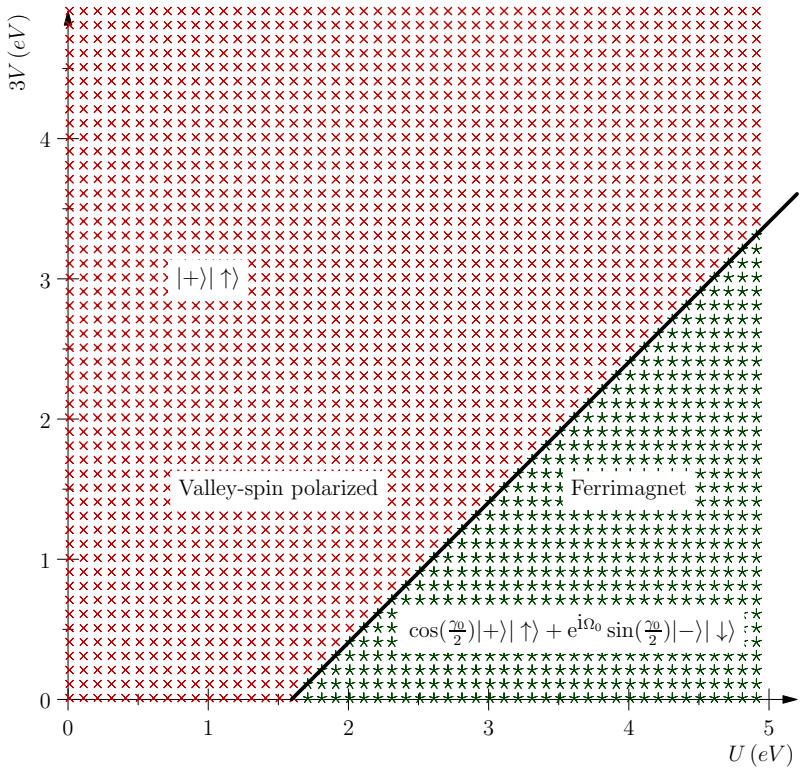

Figure 6.2: The figure shows the phase diagram for possible ground states for Hall conductivity at $\sigma_H = -1$ in U-V parameter space. Both parameters are expressed in electron volts. This phase diagram is for magnetic field $B = 40\,T$ The region marked with plus sign, '$+$', corresponds to the valley-spin polarized state for $n = 0$ Landau level. This state is doubly degenerate, we have shown one of the degenerate state in the figure and the other is $|-\rangle|\uparrow\rangle$. green. The region marked with asterisk, '$*$', corresponds to ferrimagnetic state. The $SU(4)$ components shown in the figure has extra charge density for $|+\rangle$ valley. This phase also doubly degenerate, where the second degenerate state has extra charge density for $|-\rangle$ valley. The bold line separating the two phases is obtained by equating the energies of these two phases give in Eq.(6.39) and Eq.(6.41). The equation for this line is given in Eq.(6.42) and the order transition across this line is continuous.

For $n = 0$ Landau level, these angle parameter values indicate that the wave function has anti-parallel spins residing on the two sub-lattice points. And the weight on the wave function is more on the sub-lattice point which carries the spin pointing in the direction of the magnetic field. The energy for this ground state as a function of U and V parameters,

$$\mathcal{E}_2 = -2(v_m^2 - u_m^2)\kappa_U - \frac{1}{2}\frac{u_m^2}{v_m^2 - u_m^2}\frac{\kappa_Z^2}{\kappa_U - \kappa_V} \tag{6.41}$$

Phase boundary is computed by comparing the energies and we obtain the straight line,

$$3V = U - \frac{1}{2}\frac{u_m}{v_m^2 - u_m^2}\tilde{Z} \tag{6.42}$$

separating the two phases. Unlike $\sigma_H = 0$ where the phase transition in U-V space was first order, here we find a continuous phase transition.

6.3 Excitations for ground states

The particle-hole excitations from the symmetric model was only able to describe the magnitude of the gaps. The exact nature of these excitation, i.e. polarization in $SU(4)$ space of the excitations was ambiguous. In this section we compute the contributions to particle-hole excitations from the $SU(4)$ symmetry breaking terms of our model. The ground states has been fixed in the U-V phase space by the local terms as we had seen in the previous section. The gaps from the local interaction terms is going to be two orders smaller when compared with that resulting from long ranged Coulomb interaction. But the angle parameter dependence that results from symmetry breaking terms decides the $SU(4)$ polarization of the excitations.

A general particle-hole excitations for the ground states at Hall conductivity $\sigma_H = 0$ and

$\sigma_H = -1$ obtained in previous section can be constructed in the following way,

$$|ES\rangle = \psi^\dagger_{0,l_p,q_p}\psi_{0,l_h,q_h}|GS\rangle \tag{6.43}$$

i.e. a hole is created by annihilating a state with quantum numbers $(0, l_h, q_h)$, for the $n = 0$ Landau level with quantum numbers, l_p, for orbital angular momentum and q_h for the $SU(4)$ index. And a particle is created by the creation operator for $n = 0$ Landau level with quantum numbers $(0, l_p, q_p)$.

To compute the contribution to particle-hole gap from the short ranged interaction terms, we need to compute

$$\langle ES|\big(\Psi^\dagger(\boldsymbol{r})\,\mathbb{G}\,\Psi(\boldsymbol{r})\big)^2|ES\rangle - \langle GS|\big(\Psi^\dagger(\boldsymbol{r})\,\mathbb{G}\,\Psi(\boldsymbol{r})\big)^2|GS\rangle \tag{6.44}$$

where the matrix $\mathbb{G} = \mathbb{1}_4, \beta\tau^z, \alpha^j\tau^k$ and $j, k = x, y$. Similar procdure that we followed for particle-hole excitations for symmetric model in section 5.3, we define two point coincident correlator for the excited state,

$$\Upsilon(\boldsymbol{r}, \boldsymbol{r}) = \Gamma^{(p)}(\boldsymbol{r}, \boldsymbol{r}) - \Gamma^{(h)}(\boldsymbol{r}, \boldsymbol{r}) + \Gamma(\boldsymbol{r}, \boldsymbol{r}) \tag{6.45}$$

$\Gamma^{(p)}$ and $\Gamma^{(h)}$ are correlator for particle and hole state. $\Gamma(\boldsymbol{r}, \boldsymbol{r})$ is the coincident correlator for the ground state.

The contribution to particle-hole excitation from short ranged interaction terms can be

written in general form,

$$\begin{aligned}
&\langle ES|\big(\Psi^\dagger(\boldsymbol{r})\,\mathbb{G}\,\Psi(\boldsymbol{r})\big)^2|ES\rangle - \langle GS|\big(\Psi^\dagger(\boldsymbol{r})\,\mathbb{G}\,\Psi(\boldsymbol{r})\big)^2|GS\rangle \\
&\qquad = \int_{\boldsymbol{r}} \Big((\mathrm{Tr}[\mathbb{G}\,\Phi^{(p)}(\boldsymbol{r})\,\Phi^{(p)\dagger}(\boldsymbol{r})])^2 + (\mathrm{Tr}[\mathbb{G}\,\Phi^{(h)}(\boldsymbol{r})\,\Phi^{(h)\dagger}(\boldsymbol{r})])^2 \\
&\qquad\qquad - 2\,\mathrm{Tr}[\mathbb{G}\,\Phi^{(p)}(\boldsymbol{r})\,\Phi^{(p)\dagger}(\boldsymbol{r})]\,\mathrm{Tr}[\mathbb{G}\,\Phi^{(h)}(\boldsymbol{r})\,\Phi^{(h)\dagger}(\boldsymbol{r})] \\
&\qquad\qquad - \mathrm{Tr}[\mathbb{G}\,\Phi^{(p)}(\boldsymbol{r})\,\Phi^{(p)\dagger}(\boldsymbol{r})\,\mathbb{G}\,\Phi^{(p)}(\boldsymbol{r})\,\Phi^{(p)\dagger}(\boldsymbol{r})] \\
&\qquad\qquad - \mathrm{Tr}[\mathbb{G}\,\Phi^{(h)}(\boldsymbol{r})\,\Phi^{(h)\dagger}(\boldsymbol{r})\,\mathbb{G}\,\Phi^{(h)}(\boldsymbol{r})\,\Phi^{(h)\dagger}(\boldsymbol{r})] \\
&\qquad\qquad + 2\,\mathrm{Tr}[\mathbb{G}\,\Phi^{(p)}(\boldsymbol{r})\,\Phi^{(p)\dagger}(\boldsymbol{r})\,\mathbb{G}\,\Phi^{(h)}(\boldsymbol{r})\,\Phi^{(h)\dagger}(\boldsymbol{r})] \\
&\qquad + 2\,\big(\mathrm{Tr}[\mathbb{G}\,\Phi^{(p)}(\boldsymbol{r})\,\Phi^{(p)\dagger}(\boldsymbol{r})] - \mathrm{Tr}[\mathbb{G}\,\Phi^{(h)}(\boldsymbol{r})\,\Phi^{(h)\dagger}(\boldsymbol{r})]\big)\mathrm{Tr}[\mathbb{G}\,\Gamma(\boldsymbol{r},\boldsymbol{r})] \\
&\qquad\qquad - 2\,\mathrm{Tr}[\mathbb{G}\,\Phi^{(p)}(\boldsymbol{r})\,\Phi^{(p)\dagger}(\boldsymbol{r})\,\mathbb{G}\,\Gamma(\boldsymbol{r},\boldsymbol{r})] \\
&\qquad\qquad\qquad + 2\,\mathrm{Tr}[\mathbb{G}\,\Phi^{(h)}(\boldsymbol{r})\,\Phi^{(h)\dagger}(\boldsymbol{r})\,\mathbb{G}\,\Gamma(\boldsymbol{r},\boldsymbol{r})]\Big) \qquad (6.46)
\end{aligned}$$

Similar arguments as we had seen in the case for symmetric model particle-hole excitations computation in section 5.3, various terms cancel and the assumption that large separation between particle and hole wave functions results

$$\begin{aligned}
&\langle ES|(\Psi^\dagger(\boldsymbol{r})\,\mathbb{G}\,\Psi(\boldsymbol{r}))^2|ES\rangle - \langle GS|(\Psi^\dagger(\boldsymbol{r})\,\mathbb{G}\,\Psi(\boldsymbol{r}))^2|GS\rangle \\
&\qquad = 2\int_{\boldsymbol{r}} \Big(\big(\mathrm{Tr}[\mathbb{G}\,\Gamma^{(p)}(\boldsymbol{r},\boldsymbol{r})] - \mathrm{Tr}[\mathbb{G}\,\Gamma^{(h)}(\boldsymbol{r},\boldsymbol{r})]\big)\mathrm{Tr}[\mathbb{G}\,\Gamma(\boldsymbol{r},\boldsymbol{r})] \\
&\qquad\qquad - \mathrm{Tr}[\mathbb{G}\,\Gamma^{(p)}(\boldsymbol{r},\boldsymbol{r})\,\mathbb{G}\,\Gamma(\boldsymbol{r},\boldsymbol{r})] + \mathrm{Tr}[\mathbb{G}\,\Gamma^{(h)}(\boldsymbol{r},\boldsymbol{r})\,\mathbb{G}\,\Gamma(\boldsymbol{r},\boldsymbol{r})]\Big) \qquad (6.47)
\end{aligned}$$

The two-point coincident correlator has no coordinate dependence and the position dependence comes from the correlator for particle and hole. Expressing the correlator for particle and hole in terms of complex variables, Eq.(5.47), the coordinate integration is

accomplished using gamma functions,

$$\Gamma^{(q)} = \int_{\boldsymbol{r}} \Gamma^{(q)}(\boldsymbol{r}) = \Big(\frac{1}{2\pi\ell_c^2}\Big)\frac{1}{2}(\mathbb{1}_2 - \beta)P_q \int_{\boldsymbol{r}} \frac{1}{l!}\Big(\frac{r^2}{2}\Big)^l \mathrm{e}^{-\frac{1}{2}r^2} \tag{6.48}$$

$$= \frac{1}{2}(\mathbb{1}_2 - \beta)P_q \tag{6.49}$$

In the above equation we made use of relation,

$$\Big(\frac{1}{2\pi\ell_c^2}\Big) \int_{\boldsymbol{r}} \frac{1}{l!}\Big(\frac{r^2}{2}\Big)^l \mathrm{e}^{-\frac{1}{2}r^2} = 1 \tag{6.50}$$

As the result we are only left with computation of various traces for the excitation calculation,

$$\begin{aligned}&\langle ES|(\Psi^\dagger(\boldsymbol{r})\,\mathbb{G}\,\Psi(\boldsymbol{r}))^2|ES\rangle - \langle GS|(\Psi^\dagger(\boldsymbol{r})\,\mathbb{G}\,\Psi(\boldsymbol{r}))^2|GS\rangle \\ &\quad = 2\Big(\big(\mathrm{Tr}[\mathbb{G}\,\Gamma^{(p)}] - \mathrm{Tr}[\mathbb{G}\,\Gamma^{(h)}]\big)\mathrm{Tr}[\mathbb{G}\,\Gamma] - \mathrm{Tr}[\mathbb{G}\,\Gamma^{(p)}\,\mathbb{G}\,\Gamma] + \mathrm{Tr}[\mathbb{G}\,\Gamma^{(h)}\,\mathbb{G}\,\Gamma]\Big)\end{aligned} \tag{6.51}$$

The particle-hole gap contribution from each term is given by

$$\Delta_{\mathbb{G}} = \frac{1}{2}\big(\langle ES|(\Psi^\dagger(\boldsymbol{r})\,\mathbb{G}\,\Psi(\boldsymbol{r}))^2|ES\rangle - \langle GS|(\Psi^\dagger(\boldsymbol{r})\,\mathbb{G}\,\Psi(\boldsymbol{r}))^2|GS\rangle\big) \tag{6.52}$$

The nearest neighbour interaction term contribution to gap is accounted by considering the terms given Eq.(6.1),

$$\begin{aligned}\Delta_V = \frac{1}{2}\Big(\frac{3}{4}Va^2\Big)\Big(\; &-\Big(\mathrm{Tr}[\Gamma^{(p)}\,\Gamma] - \mathrm{Tr}[\Gamma^{(h)}\,\Gamma]\Big) \\ &- \Big(\mathrm{Tr}[\beta\tau^z\,\Gamma^{(p)}] - \mathrm{Tr}[\beta\tau^z\,\Gamma^{(h)}]\Big)\mathrm{Tr}[\beta\tau^z\,\Gamma] \\ &+ \Big(\mathrm{Tr}[\beta\tau^z\,\Gamma^{(p)}\,\beta\tau^z\Gamma] - \mathrm{Tr}[\beta\tau^z\,\Gamma^{(h)}\,\beta\tau^z\Gamma]\Big)\;\Big)\end{aligned} \tag{6.53}$$

Similarly gap contributions from Hubbard interaction by taking into account the terms in

Eq.(6.6),

$$\Delta_U = \frac{1}{2}\Big(\frac{1}{4}Ua^2\Big)\Bigg(-\Big(\text{Tr}[\Gamma^{(p)}\,\Gamma] - \text{Tr}[\Gamma^{(h)}\,\Gamma]\Big) + \Big(\text{Tr}[\beta\tau^z\,\Gamma^{(p)}] - \text{Tr}[\beta\tau^z\,\Gamma^{(h)}]\Big)\text{Tr}[\beta\tau^z\,\Gamma] - \Big(\text{Tr}[\beta\tau^z\,\Gamma^{(p)}\,\beta\tau^z\Gamma] - \text{Tr}[\beta\tau^z\,\Gamma^{(h)}\,\beta\tau^z\Gamma]\Big) + \frac{1}{2}\sum_{j,k=x,y}\Big(\big(\text{Tr}[\alpha^j\tau^k\,\Gamma^{(p)}] - \text{Tr}[\alpha^j\tau^k\,\Gamma^{(h)}]\big)\text{Tr}[\alpha^j\tau^k\,\Gamma] - \Big(\text{Tr}[\alpha^j\tau^k\,\Gamma^{(p)}\alpha^j\tau^k\Gamma] - \text{Tr}[\alpha^j\tau^k\,\Gamma^{(h)}\,\alpha^j\tau^k\Gamma]\Big)\Big)\Bigg) \quad (6.54)$$

Finally the Zeeman term contribution is given by,

$$\Delta_Z = \frac{1}{2}\Big(-\frac{1}{2}g\mu_B\,B\Big)\frac{1}{2}\big(\text{Tr}[\sigma^z\Gamma^{(p)}] - \text{Tr}[\sigma^z\Gamma^{(h)}]\big) \quad (6.55)$$

We now evaluate the gap contributions given in Eq.(6.53), Eq.(6.54) and Eq.(6.55) for each phase obtained for the Hall conductivity $\sigma_H = 0$ and $\sigma_H = -1$ in the U-V parameter space.

6.3.1 Excitations for ground states at $\sigma_H = 0$

In this section we compute the nature of excitations for the ground states for the Hall conductivity at $\sigma_H = 0$ in the U-V phase space. We consider excitations from all three possible ground states in the U-V phase space, i.e. ferromagnetic ordered ground state, charge ordered state and canted spin ordered state. The details of the calculations for exctiations for ground states at $\sigma_H = 0$ is shown in Appendix K. The ground state is specfied by the specifying the two-point coincident correlator, which in turn requires the mass parameter to be specified obtained from the symmetric model computations and the

$SU(4)$ component of occupied $n = 0$ Landau levels. The correlator for the ground state,

$$\Gamma = \frac{1}{2\pi\ell_c^2}\big(u_m \mathbb{1}_2 - v_m\beta\big)\big(P_1 + P_2 - \frac{1}{2}\,\mathbb{1}_4\big) \tag{6.56}$$

Here P_1 and P_2 are the projection operators contructed from the $SU(4)$ components of occupied $n = 0$ Landau levels. The correlators for the hole and particle,

$$\begin{aligned} \Gamma^h &= \frac{1}{2}(\mathbb{1}_2 - \beta)P_h \\ \Gamma^p &= \frac{1}{2}(\mathbb{1}_2 - \beta)P_p \end{aligned} \tag{6.57}$$

Here P_h and P_p are the projections operator constructed from the $SU(4)$ components of hole and particle states of excitations. We use these coincident correlators to compute the contributions from the symmetry breaking terms in rest of this section.

At the end of this section we discuss variation of the gaps with the tilted magnetic field and compare the results with that seen in the quantum Hall experiments in tilted magnetic fields.

Excitations for ferromagnetic ordered state

The $SU(4)$ component of occupied $n = 0$ Landau levels for ferromagetic ordered state are,

$$\begin{aligned} |1\rangle &= |+\rangle|\uparrow\rangle \\ |2\rangle &= |-\rangle|\uparrow\rangle \end{aligned} \tag{6.58}$$

A general hole state is linear combination occupied $n = 0$ Landau level. The $SU(4)$ component such a linear combination can be constructed as following,

$$|h\rangle = \cos(\frac{\gamma_h}{2})|+\rangle|\uparrow\rangle + \mathrm{e}^{\mathrm{i}\,\Omega_h}\sin(\frac{\gamma_h}{2})|-\rangle|\uparrow\rangle \tag{6.59}$$

In a similar fashion, a particle state state is constructed from the unoccupied levels of $n = 0$ Landau levels. $SU(4)$ components of such a particle state can be constructed as following,

$$|p\rangle = \cos(\frac{\gamma_p}{2})|+\rangle|\downarrow\rangle + \mathrm{e}^{\mathrm{i}\,\Omega_p}\sin(\frac{\gamma_p}{2})|-\rangle|\downarrow\rangle \tag{6.60}$$

The contributions to the gaps from the symmetry breaking terms are

$$\begin{aligned}\Delta_V &= 0\\ \Delta_U &= 2\kappa_U v_m\\ \Delta_Z &= \kappa_Z\end{aligned} \tag{6.61}$$

The net gap from the symmetry breaking terms comes from the Zeeman term and angle independence implies that both particle and holes states can be in any linear combination of unoccupied and occupied levels of $n = 0$ Landau level respectively. Since the ferromagnetic ordered states is fully spin polarized hence the excitations will involve a spin flip, which costs Zeeman energy.

Excitations for charge ordered state

The charge ordered state is doubly degenerate as it can be localized on either valley. Here we choose one of the $SU(4)$ component of occupied $n = 0$ Landau levels for charge ordered state,

$$\begin{aligned}|1\rangle &= |+\rangle|\boldsymbol{n}_1\rangle\\ |2\rangle &= |+\rangle|-\boldsymbol{n}_1\rangle\end{aligned} \tag{6.62}$$

The hole state is constructed by choosing a spin in arbitrary direction localized in $|+\rangle$ for valley,

$$|h\rangle = |+\rangle|\boldsymbol{n}_h\rangle \tag{6.63}$$

The particle state has spin pointing in arbitrary direction sitting in $|-\rangle$ state for valley.

$$|p\rangle = |-\rangle|\boldsymbol{n}_p\rangle \tag{6.64}$$

The contribution to gaps from the symmetry breaking terms,

$$\begin{aligned}\Delta_V &= -4\kappa_V v_m \\ \Delta_U &= 2\kappa_U v_m \\ \Delta_Z &= -\frac{1}{2}\kappa_Z(\cos(\theta_p) - \cos(\theta_h))\end{aligned} \tag{6.65}$$

The angle dependence comes only for Zeeman term and the net gap will minimize for $\theta_p = 0$ and $\theta_h = \pi$. $SU(4)$ components of particle and hole states

$$|p\rangle = |-\rangle|\uparrow\rangle, \qquad\qquad |h\rangle = |+\rangle|\downarrow\rangle \tag{6.66}$$

and resulting net gap will be

$$\Delta = -4\kappa_V v_m + 2\kappa_U v_m - \kappa_Z \tag{6.67}$$

The hole is created by removing a down spin from the occupied sub-lattice and particle is created by placing it unoccupied sub-lattice point and this results in lowering Zeeman energy.

Excitations for canted spin state

The canted spin state has both the sub-lattice points are occupied

$$\begin{aligned}|1\rangle &= |+\rangle|\boldsymbol{n}_1\rangle \\ |2\rangle &= |-\rangle|\boldsymbol{n}_2\rangle\end{aligned} \tag{6.68}$$

and the spins on each of the sub-lattice points satisfy

$$\theta_1 - \theta_2 = 0, \qquad \cos(\theta_+) = \frac{1}{4}\frac{u_m}{v_m^2 - u_m^2}\frac{\kappa_Z}{\kappa_U} \tag{6.69}$$

here $\theta_+ = (\theta_1 + \theta_2)/2$. The hole state is constructed by taking a linear superposition of these states,

$$|h\rangle = \cos(\frac{\theta_h}{2})|+\rangle|\boldsymbol{n}_1\rangle + \mathrm{e}^{\mathrm{i}\,\varphi_h}\sin(\frac{\theta_h}{2})|-\rangle|\boldsymbol{n}_2\rangle \tag{6.70}$$

And the particle state is constructed by taking the linear superpostion of unoccupied states of $n = 0$ Landau level,

$$|p\rangle = \cos(\frac{\theta_p}{2})|+\rangle|-\boldsymbol{n}_1\rangle + \mathrm{e}^{\mathrm{i}\,\varphi_p}\sin(\frac{\theta_p}{2})|-\rangle|-\boldsymbol{n}_2\rangle \tag{6.71}$$

The contributions from the symmetry breaking terms,

$$\begin{aligned}
\Delta_V &= 0 \\
\Delta_U &= 2\kappa_U v_m - 2\kappa_U(v_m - u_m)\cos^2(\theta_+) \\
\Delta_Z &= \kappa_Z \cos(\theta_+)
\end{aligned} \tag{6.72}$$

Here also like in the case of ferromagetic ordered state, the gap in independent of the angle parameters of particle and hole states.

The titled magnetic field measurements for the activation gaps in quantum Hall experiments is a good indicator to decipher the spin for the excitations. In tilted field experiment, $B_\perp$, the perpendicular component of the magnetic field is kept fixed and B_T, the total magnetic field is varied by rotation the sample. In Zeeman term, the spin sees only the total magnetic field. Whereas for the interaction terms, the magnetic field comes from the orbital motion of electron, which depends on the magnetic field perpendicular the plane. The contributions to the total particle-hole excitations from the interaction terms has a dominant contribution from the long ranged Coulomb term. The contribution from the short ranged interactions is two orders smaller, hence we ignore them in the following

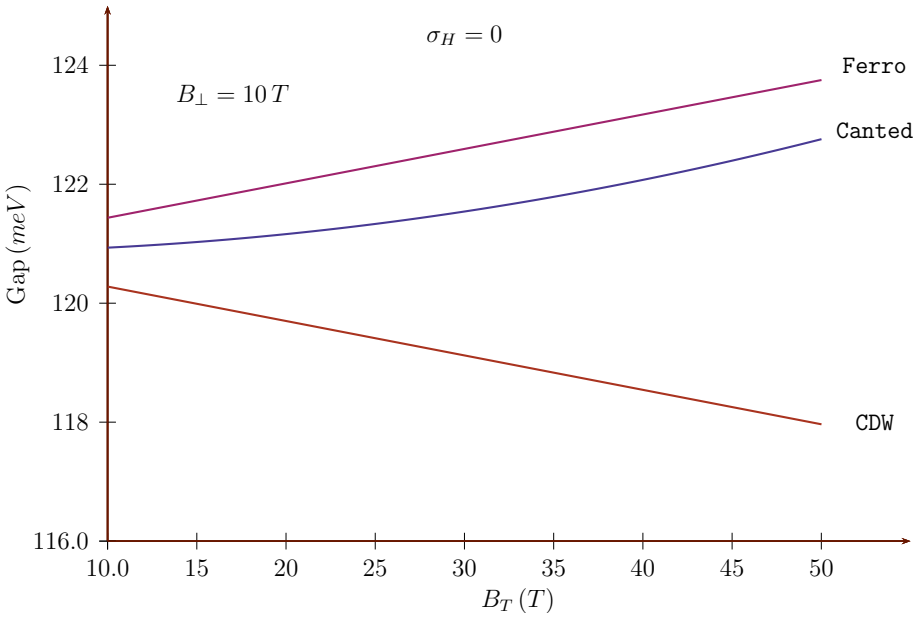

Figure 6.3: The figure shows the variation of particle-hole gap with respect to B_T for all the three phases for quantum Hall state at $\sigma_H = 0$. The tilted field gap for ferromagnetic spin ordered state increases linearly with B_T, whereas the charge ordered state gap decreases linearly. The gap for canted spin phase shows an increase with B_T with a quadratic dependence. Moreover the in the canted phase, gap is inversely proportional to Hubbard interaction strength U. In the figure we have choosen $U = 4\,eV$ for the shown curve. The tilted field activation gap measurement for graphene on boron nitrite [21] has been reported to decrease with tilt angle. This is consistent with behaviour that we find for charge ordered phase.

analysis. The dependence of total gap can be written as

$$\Delta = \Delta_C(B_\perp) + \Delta_Z(B_T) \tag{6.73}$$

For the fixed $B_\perp$, the Coulomb contribution is constant, whereas the Zeeman contribution vary with the B_T. The ferromagnetic ordered is fully spin polarized state and excitations will involve a flipping of spin and this will cost Zeeman energy, hence the dependence on B_T is linear and increasing as we have shown in the Fig.6.3. The charge ordered state is spin unpolarized state and we find that it decreases linearly with the B_T. The canted spin ordered state is not fully spin polarized and gaps show an increasing quadratic dependence

on B_T. It also inversely proportional to the Hubbard interaction strength, U.

In the reference [21], activation gaps are measured in tilted field for graphene on boron nitrite substrate. The authors have reported a decrease in gaps with increase in B_T. This variation of tilted field gap with B_T is consistent with particle-hole excitations for charge ordered ground state of our mean field calculations.

6.3.2 Excitations for ground states at $\sigma_H = -1$

In this section we compute the nature of all the possible excitations for both the ground states for the Hall conductivity at $\sigma_H = -1$ in the U-V phase space. There are two possible ground states in the U-V phase space, valley-spin polarized state and the ferri-magnetic ordered state. The details of the calculations for excoriations for ground states at $\sigma_H = 0$ is shown in Appendix L. The ground state is specified by the specifying the two-point coincident correlator, which in turn requires the mass parameter to be specified obtained from the symmetric model computations and the $SU(4)$ component of occupied $n = 0$ Landau level, a similar scenario seen for the case of $\sigma_H = 0$. The correlator for the ground state,

$$\Gamma = \frac{1}{2\pi\ell_c^2}\big(u_m \mathbb{1}_2 - v_m\beta\big)\big(P_1 - \frac{1}{2}\,\mathbb{1}_4\big) \tag{6.74}$$

Here P_1 is the projection operator constructed from the $SU(4)$ components of occupied $n = 0$ Landau level. The correlator for the hole and particle,

$$\begin{aligned}\Gamma^h &= \frac{1}{2}(\mathbb{1}_2 - \beta)P_h \\ \Gamma^p &= \frac{1}{2}(\mathbb{1}_2 - \beta)P_p\end{aligned} \tag{6.75}$$

Here P_h and P_p are the projections operator constructed from the $SU(4)$ components of hole and particle states of excitations. We use these coincident correlator to compute the contributions from the symmetry breaking terms in rest of this section.

At the end of this section once again we discuss variation of the gaps with the tilted magnetic field and compare the results with that seen in the quantum Hall experiments in tilted magnetic fields.

Valley-spin polarized ground state

For the valley-spin polarized state, the $SU(4)$ components of $n = 0$ Landau level is,

$$|1\rangle = |+\rangle|\uparrow\rangle \tag{6.76}$$

The $SU(4)$ components of hole wave function

$$|h\rangle = |+\rangle|\uparrow\rangle \tag{6.77}$$

The $SU(4)$ components of particle wave function are constructed by choosing a linear combination of three unoccupied sub-levels of $n = 0$ Landau level,

$$|p\rangle = \cos(\frac{\theta_p}{2})|+\rangle|\uparrow\rangle + \mathrm{e}^{\mathrm{i}\,\varphi_p}\sin(\frac{\theta_p}{2})|\gamma_p|\downarrow\rangle\Big) \tag{6.78}$$

The details of computation for each symmetry breaking term is shown in section **??**

Gap contribution from nearest neighbour term,

$$\Delta_V = -2\kappa_V v_m \sin^2(\frac{\theta_p}{2})\cos^2(\frac{\gamma_p}{2}) + 2\kappa_V v_m \tag{6.79}$$

From it dependence on the particle state angle variable we can infer that this term prefers only a spin flip with no change in valley quantum number.

Hubbard term contribution is also depends on the angle parameters of particle state,

$$\Delta_U = 2\kappa_U v_m \sin^2(\frac{\theta_p}{2})\cos^2(\frac{\gamma_p}{2}) - \kappa_U(v_m - u_m)\sin^2(\frac{\theta_p}{2}) \tag{6.80}$$

This term prefers a flip in valley quantum number and spin in the eigenstate of σ^z operator.

The Zeeman term contribution,

$$\Delta_Z = \kappa_Z \sin^2(\frac{\theta_p}{2}) \tag{6.81}$$

prefers the angle variables for particle state exactly similar to that of Hubbard term.

The minimization of total gap from symmetry breaking terms was preformed numerically and we find three possible excitations for valley-spin polarized state.

$$(i).\, \theta_p = \pi, \gamma_p = 0 \qquad |+\rangle|\downarrow\rangle \qquad \Delta = -2\kappa_V v_m + \kappa_U(v_m + u_m) + \kappa_Z \tag{6.82}$$

$$(ii).\, \theta_p = 0 \qquad |-\rangle|\uparrow\rangle \qquad \Delta = 0 \tag{6.83}$$

$$(iii).\, \gamma_p = \pi, \theta_p = \pi \qquad |-\rangle|\downarrow\rangle \qquad \Delta = -\kappa_U(v_m - u_m) + \kappa_Z \tag{6.84}$$

The region in U-V phase space where these excitations are possible is shown in Fig.6.4. The dependence of these excitation gap is shown in Fig.6.5. The excitation $|-\rangle|\uparrow\rangle$ has no variation with B_T whereas both the other excitations have linear and increasing dependence on B_T.

Ferrimagnetic ground state

The ferrimagnetic ground state is doubly degenerate, here choose on of them. The $SU(4)$ components of occupied $n = 0$ Landau level,

$$|1\rangle = \cos(\frac{\gamma_0}{2})|+\rangle|\uparrow\rangle + \mathrm{e}^{\mathrm{i}\,\Omega_0} \sin(\frac{\gamma_0}{2})|-\rangle|\downarrow\rangle \tag{6.85}$$

Here γ_0 is obtained from the mean field energy minimization

$$\cos(\gamma_0) = \frac{1}{2}\frac{u_m}{v_m^2 - u_m^2}\frac{\kappa_Z}{\kappa_U - \kappa_V}$$

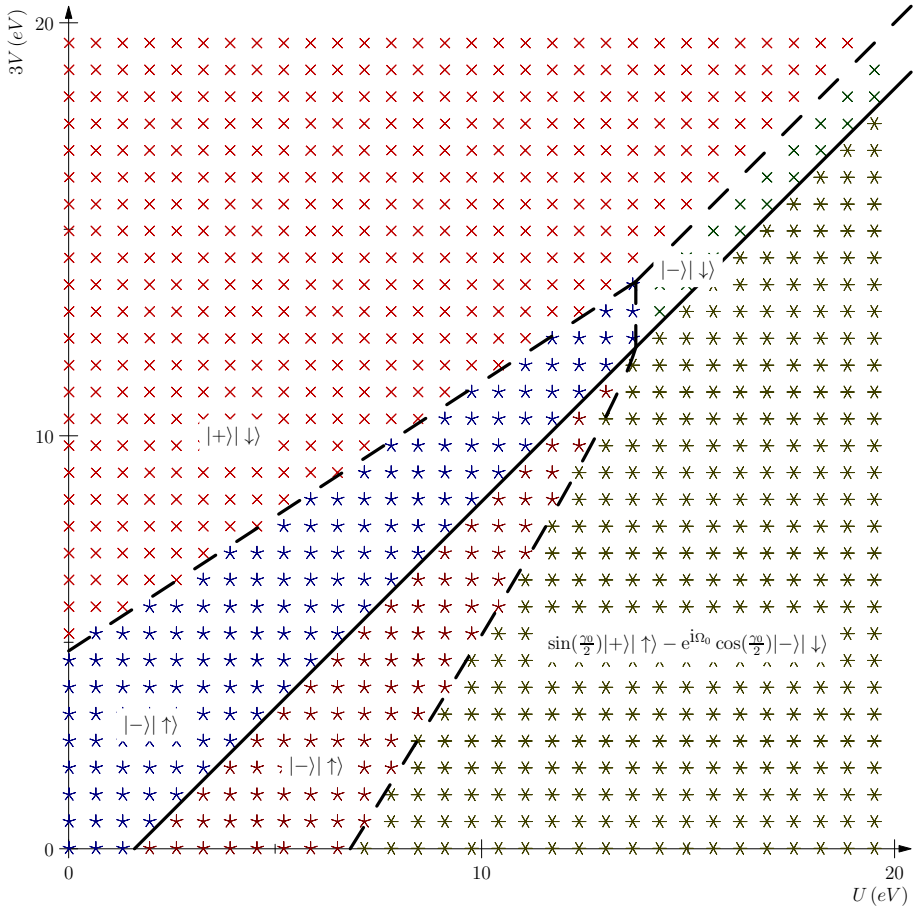

Figure 6.4: The figure shows the variation of particle-hole excitations for both the phases for Hall conductivity at $\sigma_H = 1$ i.e valley-spin polarized state and ferrimagnetic state. These two phases are separated by the dashed line and ground state chosen for the excitation calculation is mentioned on the top and right side. Each shaded region is labeled with the excitation preferred

The $SU(4)$ components of hole wave function

$$|h\rangle = \cos(\frac{\gamma_0}{2})|+\rangle|\uparrow\rangle + \mathrm{e}^{\mathrm{i}\,\Omega_0}\sin(\frac{\gamma_0}{2})|-\rangle|\downarrow\rangle \tag{6.86}$$

The $SU(4)$ components of particle wave function is obtained by taking a suitable linear combination of unoccupied levels,

$$\begin{aligned}|p\rangle = \cos(\frac{\theta_p}{2})\Big(\sin(\frac{\gamma_0}{2})|+\rangle|\uparrow\rangle - \mathrm{e}^{\mathrm{i}\,\Omega_0}\cos(\frac{\gamma_0}{2})|-\rangle|\downarrow\rangle\Big) \\ + \mathrm{e}^{\mathrm{i}\,\phi_p}\sin(\frac{\theta_p}{2})\Big(\cos(\frac{\gamma_p}{2})|+\rangle|\downarrow\rangle + \mathrm{e}^{\mathrm{i}\,\Omega_p}\sin(\frac{\gamma_p}{2})|-\rangle|\uparrow\rangle\Big)\end{aligned} \tag{6.87}$$

Contributions to gap from nearest neighbour interaction

$$\begin{aligned}\Delta_V = -\frac{1}{2}\kappa_V\Bigg(\sin^2(\frac{\theta_p}{2})\Big(2v_m(\cos(\gamma_p)+\cos(\gamma_0))\cos(\gamma_0) + (v_m+u_m)\sin^2(\gamma_0)\Big) \\ - 2(v_m-u_m)\cos^2(\gamma_0) - 2(v_m+u_m)\Bigg)\end{aligned} \tag{6.88}$$

and from the Hubbard term

$$\begin{aligned}\Delta_U = \frac{1}{2}\kappa_U\Bigg(\sin^2(\frac{\theta_p}{2})\Big(2v_m(\cos(\gamma_p)+\cos(\gamma_0))\cos(\gamma_0) + (v_m+u_m)\sin^2(\gamma_0) \\ + (v_m-u_m)(1-\cos(\gamma_0)\cos(\gamma_p))\Big) - 2(v_m-u_m)\cos^2(\gamma_0)\Bigg)\end{aligned} \tag{6.89}$$

The Zeeman term results in

$$\Delta_Z = \frac{1}{2}\Big(\kappa_Z\sin^2(\frac{\theta_p}{2})(\cos(\gamma_p)-\cos(\gamma_0)) + 2\kappa_Z\cos(\gamma_0)\Big) \tag{6.90}$$

The gap that depends on angle parameters that was minimized numerically,

$$\Delta = \sin^2(\frac{\theta_p}{2})\Big(2(\kappa_U-\kappa_V)v_m\cos^2(\frac{\gamma_p}{2}) - \kappa_U(v_m-u_m) + \kappa_Z\Big) \tag{6.91}$$

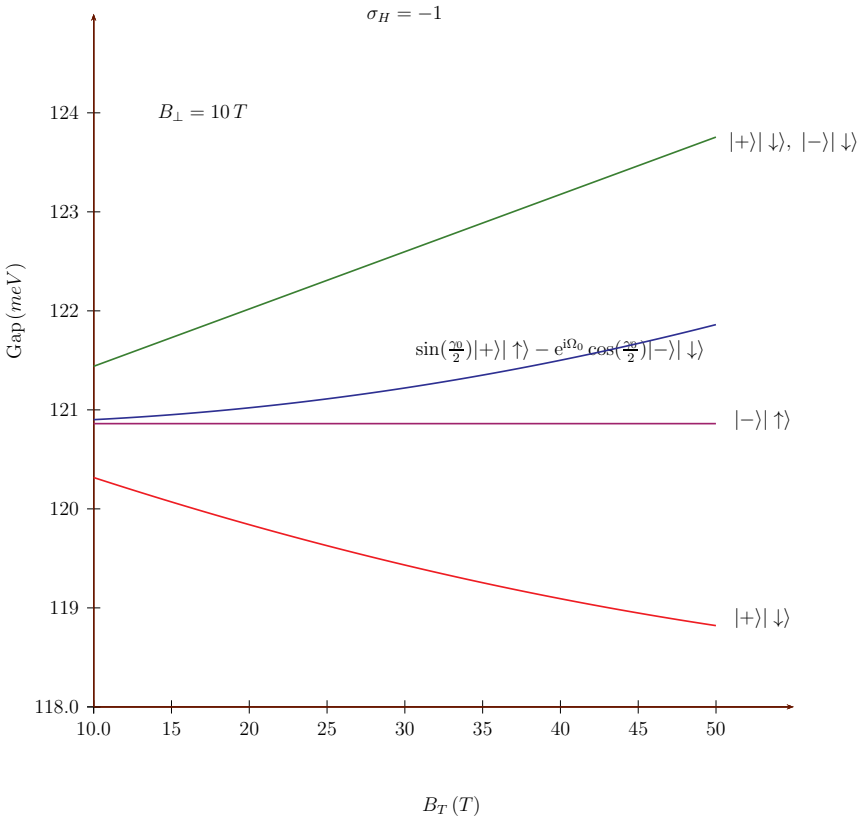

Figure 6.5: The figure shows the variation of particle-hole gap with respect to B_T for all the two phases for quantum Hall state at $\sigma_H = -1$. Top linear line and constant line are the gaps for the valley-spin polarized state. The two curves with quadratic variation with B_T are for the ferrimagnetic state. The nature of excitation is indicated with each curve.

1.

$$\theta_p = 0, \qquad |p\rangle = \sin(\frac{\gamma_0}{2})|+\rangle|\uparrow\rangle - e^{i\,\Omega_0}\cos(\frac{\gamma_0}{2})|-\rangle|\downarrow\rangle$$

$$\Delta = 0 \tag{6.92}$$

2.

$$\theta_p = \pi, \gamma_p = \pi, \qquad |p\rangle = |-\rangle|\uparrow\rangle$$

$$\Delta = \frac{1}{2}\Big((\kappa_U - \kappa_V)\Big(- 2v_m\cos(\gamma_0) + (v_m + u_m)(1 + \cos(\gamma_0))\Big)(1 - \cos(\gamma_0)) + \Big(\kappa_U(v_m - u_m) - \kappa_Z\Big)(1 + \cos(\gamma_0))\Big) \tag{6.93}$$

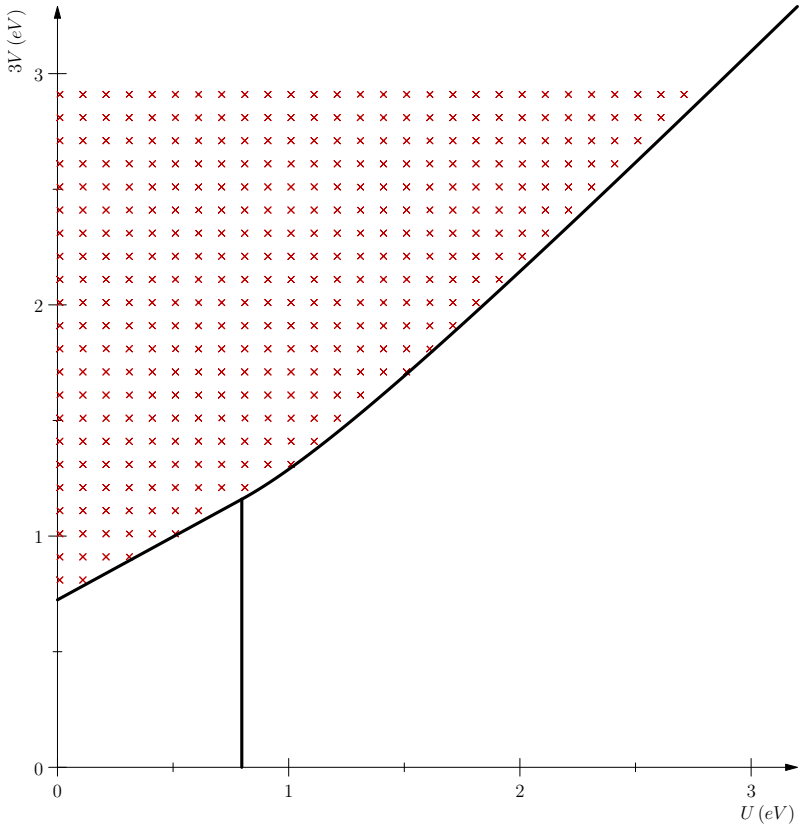

Figure 6.6: Delineated region in U-V phase diagram marked with region where the particle-hole gap decreases with increase in B_T for the ground state at $\sigma_H = 0$ within our interacting model hamiltonian. The region marked also corresponds to the charge ordered state ground state for $\sigma_H = 0$.

The tilted magnetic field dependence of the excitations in valley-spin polarized state can be divided into class. Either there is no variation or increases with B_T. The excitations for the ferrimagnetic state can also be classified into two categories, one has very small quadratic dependence that increases with B_T. The second one decreases with B_T.

6.4 Connection with experiments

In this section we compare the results obtained from our interacting model with that observed in experiments.

Young et. al. in reference [21] report that variation of activation gap with B_T. They had reported gaps for $\sigma_H = 0$ decreases with increasing B_T, which lead them to conclude

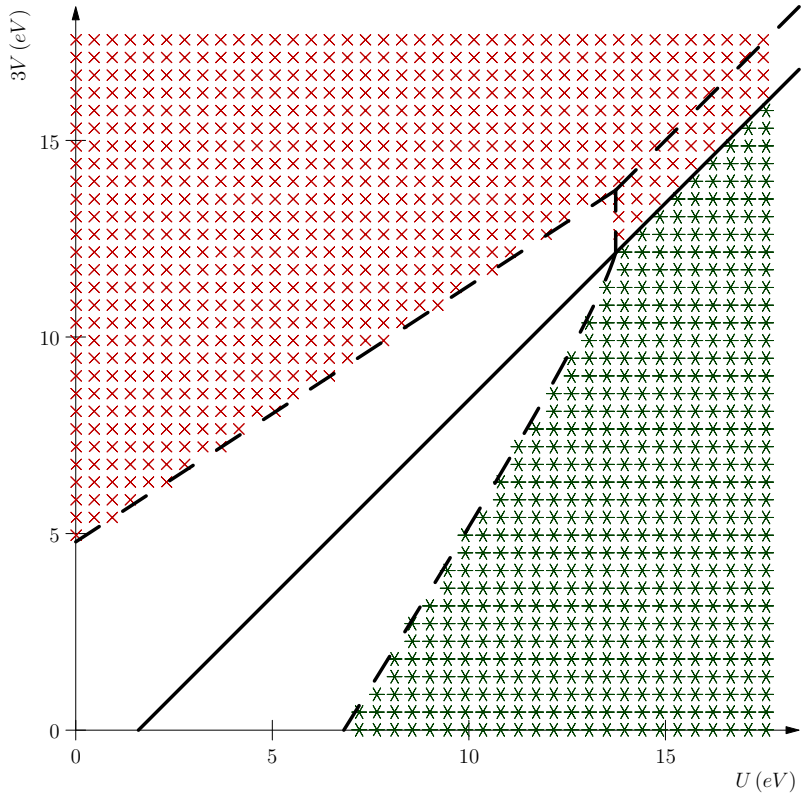

Figure 6.7: The region delineated here is for where particle-hole gaps increase with B_T for interacting continuum model at $\sigma_H = -1$ ground state. The region marked with red '$\times$' is also the region for the valley-spin polarized ground state for $\sigma_H = -1$. And region marked with green '$*$' is for ferrimagnet ordered ground state at Hall conductivity $\sigma_H = -1$.

that the ground state for $\sigma_H = 0$ is spin unpolarized state. The Fig.(6.6) shows the region in the U-V phase space where the particle-hole activation gaps decrease with B_T. This delineated region also corresponds to the charge ordered ground state for the Hall plateau at $\sigma_H = 0$, which is spin unpolarized ground state. Our conclusion coincides with the one drawn for $\sigma_H = 0$ with that of given in reference [21].

The activation gaps for the state at Hall conductivity $\sigma_H = -1$ showed a variation which was given a linear fit, which increases with B_T in reference [21]. It was also reported that effective g-factor for the Zeeman coupling was greated than two and concluded that excitation are caused by skyrmion-antiskyrmion from a valley-spin polarized ground state. In Fig.6.7, we show the region in U-V phase space that show increase in particle-hole gaps with B_T. The delineated region conrresponds to region with valley-spin polarized

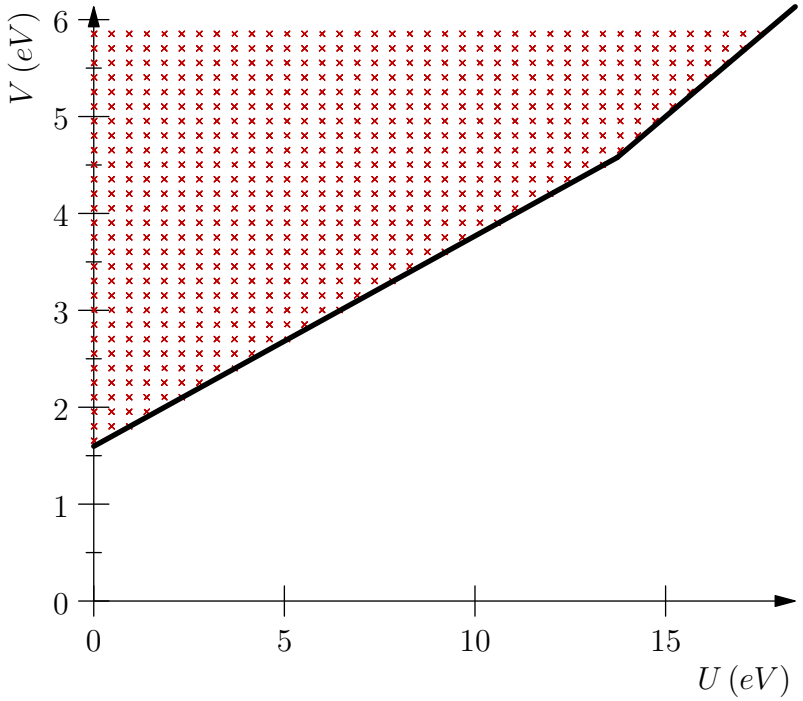

Figure 6.8: Region delineated here is the intersection of regions shown in Fig.6.6 and Fig.6.7. This shows the range of value for parameters U and V for our model that is consistent with excitations observed in quantum Hall experiments.

and ferrimagnetic ordered ground states for $\sigma_H = -1$ within our model computations.

Fig.6.8 shows the region in the U-V phase space that is consistent with the excitations observed in quantum Hall experiment [21]. This region was deduced by taking the intersection of delineated regions from the Fig.(6.6) and Fig.(6.7), which are regions consistent with experiment for excitation observed for Hall plateaus at $\sigma_H = 0$ and $\sigma_H = -1$ [21].

6.5 Summary

We summarize the results obtained in this chapter

1. We obtained phase diagram for the ground state for $\sigma_H = 0$ using the symmetry breaking terms of our model. The three possible phases in U-V parameter space shown in Fig.6.1.

2. Phase diagram was also obtained for $\sigma_H = -1$. The two possible ground states in the U-V parameter space is shown in Fig.6.2

3. The tilted magnetic field gaps for the ground states for Hall conductivity $\sigma_H = 0$ is shown in Fig.6.3 and the charge ordered state behavior is consistent with that seen in experiments. Fig.6.6 shows delineated region in U-V phase space that is consistent activation gaps seen in experiments for our interacting model.

4. The tilted magnetic field gaps for $\sigma_H = -1$ shown in Fig.6.5 has also regions that are consistent with the experiments. And the Fig.6.7 shows the region in U-V phase space.

5. Fig.6.8 shows the range for the values U and V parameters for our model can take that are consistent with current experiments.

Chapter 7

Summary

In the chapter we enumerate the findings of this thesis.

1. Exact analytical solutions for Dirac particle in cross electric and magnetic field were found using the trick of Lorentz boost.

2. Numerical computations for the cross electric and magnetic field subjected to graphene on lattice were shown to confirm the effects of Landau levels is not an artifact of continuum model.

3. The phenomenon of dielectric breakdown was discussed and predictions were made about difference of dielectric breakdown for $n = 0$ and $n \neq 0$ Landau levels. And this was verified in quantum Hall experiments by Singh and Deshmukh [18]

4. We have derived a systematic continuum approximation for the interacting lattice model for graphene. The lattice interaction terms yields a leading $SU(4)$ terms and sub-leading part. We justified replacing the sub-leading part with the terms resulting from the nearest neighbour interaction. We have presented the interacting continuum model that we adopt in this thesis in Eq.(3.26)

5. We showed that the Landau levels for massive Dirac particle provides the same

$SU(4)$ polarization for both partially occupied $n = 0$ Landau levels and filled Dirac sea.

6. We described the number of parameters needed for the variational ground states for the Hall conductivity $\sigma_H = 0$ and $\sigma_H = -1$.

7. We developed the two point correlator for a massive Dirac particle in magnetic field.

8. With the knowledge of two point correlator for a massive Dirac particle we constructed the two point correlator and coincident correlator for Dirac particle in graphene to be used for variational mean field computations.

9. We have showed that the Coulomb interaction breaks the $SU(4)$ symmetry spontaneously for the ground states for Hall conductivity at $\sigma_H = 0$ and $\sigma_H = -1$.

10. The order parameter for spontaneous symmetry breaking is the mass of the Dirac particle which is proportional to a dimensionless $\alpha = \kappa_C/\kappa_t$, which depends on dielectric constant.

11. The order parameter is proportional to magnetic field and tends to zero as magnetic field goes to zero which indicates spontaneous symmetry breaking of $SU(4)$ symmetry by Coulomb interaction in presence of magnetic field.

12. The particle-hole gaps from symmetric model showed a square root dependence on the applied magnetic field. Our symmetric model without disorder taken into account over estimates the gaps when compared with experimental values.

13. We obtained phase diagram for the ground state for $\sigma_H = 0$ using the symmetry breaking terms of our model. The three possible phases in U-V parameter space shown in Fig.6.1.

14. Phase diagram was also obtained for $\sigma_H = -1$. The two possible ground states in the U-V parameter space is shown in Fig.6.2

15. The tilted magnetic field gaps for the ground states for Hall conductivity $\sigma_H = 0$ is shown in Fig.6.3 and the charge ordered state behavior is consistent with that seen in experiments.

16. The tilted magnetic field gaps for $\sigma_H = -1$ shown in Fig.6.5 has also regions that are consistent with the experiments.

17. Fig.6.8 is our prediction for the range of values U and V can take for our model to explain the current quantum Hall experiments.

Appendices

Appendix A

Landau levels of massless and massive Dirac particles

A.1 Massless Dirac particle

Hamiltonian for massless Dirac particle in $(2+1)d$ in presence of magnetic field,

$$h = v_F \, \boldsymbol{\alpha} \cdot \boldsymbol{\pi} \tag{A.1}$$

$\boldsymbol{\pi}$ is the conjugate momenta in presence of magnetic field.

Eigenvalues for the hamiltonian

$$\epsilon_{n,l} = \text{sgn}(n)\sqrt{2|n|}\,\frac{\hbar v_F}{\ell_c} \tag{A.2}$$

The corresponding wave functions, for $n \neq 0$

$$\phi_{n,l}(\boldsymbol{r}) = \frac{1}{\sqrt{2}} \begin{pmatrix} \varphi_{|n|-1,l+1}(\boldsymbol{r}) \\ \text{i sgn}(n)\varphi_{|n|,l}(\boldsymbol{r}) \end{pmatrix} \tag{A.3}$$

For $n = 0$,

$$\phi_{0,l}(\boldsymbol{r}) = \begin{pmatrix} 0 \\ \\ \varphi_{0,l}(\boldsymbol{r}) \end{pmatrix} \tag{A.4}$$

ℓ_c is the magnetic length, $\varphi_{n,l}(\boldsymbol{r})$ are wave functions of non-relativistic electron gas in magnetic field.

$$\varphi_{n,l}(\boldsymbol{r}) = \frac{(-1)^n}{\sqrt{2\pi\ell_c^2}} \sqrt{\frac{n!}{(n+l)!}}\, \mathrm{e}^{-\mathrm{i}\, l\theta}\, \xi^{\frac{l}{2}} \mathrm{e}^{-\frac{\xi}{2}} L_n^l(\xi) \tag{A.5}$$

Here $\xi = r^2/2\ell_c^2$

A.2 Massive Dirac particle

$$h = v_F\, \boldsymbol{\alpha} \cdot \boldsymbol{\pi} + \beta\, m \tag{A.6}$$

Eigenvalues

$$\epsilon_{n,l} = \mathrm{sgn}(n) \sqrt{2|n| \left(\frac{\hbar v_F}{\ell_c}\right)^2 + m^2} \tag{A.7}$$

Corresponding wave functions for $n \neq 0$

$$\phi_{n,l}(\boldsymbol{r}) = \frac{1}{\sqrt{2\,\epsilon_{n,l}(\epsilon_{n,l} + m)}} \begin{pmatrix} (\epsilon_{n,l} + m)\varphi_{|n|-1,l+1}(\boldsymbol{r}) \\ \mathrm{i}\ \sqrt{2|n|}\frac{\hbar v_F}{\ell_c}\varphi_{|n|,l}(\boldsymbol{r}) \end{pmatrix} \tag{A.8}$$

For $n = 0$,

$$\phi_{0,l}(\boldsymbol{r}) = \begin{pmatrix} 0 \\ \\ \varphi_{0,l}(\boldsymbol{r}) \end{pmatrix} \tag{A.9}$$

$\varphi_{n,l}(\boldsymbol{r})$ is given by Eq.A.5.

Appendix B

Solution for cross electric and magnetic field

$$h = v_F\, \boldsymbol{\alpha} \cdot \boldsymbol{\pi} + e\, E\, x\, \mathbb{1}_2 \tag{B.1}$$

Time dependent Schrodinger equation

$$\mathrm{i}\,\hbar \frac{\partial}{\partial t}\Psi(\boldsymbol{x}, t) = (v_F \boldsymbol{\alpha} \cdot \boldsymbol{\pi} + e\, E\, x \mathbb{1}_2)\Psi(\boldsymbol{x}, t) \tag{B.2}$$

$$x^0 = v_F\, t, \qquad x^1 = x, \qquad x^2 = y \tag{B.3}$$

$$p^0 = \frac{\mathrm{i}\,\hbar}{v_F}\frac{\partial}{\partial t}, \qquad p^1 = -\mathrm{i}\,\hbar \frac{\partial}{\partial x}, \qquad p^2 = -\mathrm{i}\,\hbar \frac{\partial}{\partial y} \tag{B.4}$$

$$\Big((p_0 - \frac{eE}{v_F}x)\mathbb{1} - \alpha_x p_x - \alpha_y(p_y + eB\,x)\Big)\Psi(\boldsymbol{x}, t) = 0 \tag{B.5}$$

$$\begin{pmatrix} p_0 \\ p_y \end{pmatrix} = \begin{pmatrix} \cosh(\theta) & -\sinh(\theta) \\ -\sinh(\theta) & \cosh(\theta) \end{pmatrix} \begin{pmatrix} \tilde{p}_0 \\ \tilde{p}_y \end{pmatrix} \tag{B.6}$$

$$\Big(\mathrm{e}^{\theta\alpha_y}\tilde{p}_0 - \alpha_x \tilde{p}_x - \mathrm{e}^{\theta\alpha_y}\tilde{p}_y - eB\big(1 + \alpha_y \frac{E}{v_F B}\big)\tilde{x}\Big)\Psi(\boldsymbol{x}, t) = 0 \tag{B.7}$$

Choose $\beta = \frac{E}{v_F B} = \tanh(\theta)$

$$\left(\mathrm{e}^{\theta\alpha_y}\tilde{p}_0 - \alpha_x\tilde{p}_x - \mathrm{e}^{\theta\alpha_y}\left(\tilde{p}_y + e\frac{B}{\cosh(\theta)}\tilde{x}\right)\right)\Psi(\boldsymbol{x},t) = 0 \tag{B.8}$$

Making use of the identity

$$\mathrm{e}^{\alpha_y\frac{\theta}{2}}\alpha_x\mathrm{e}^{\alpha_y\frac{\theta}{2}} = \alpha_x \tag{B.9}$$

and

$$\tilde{\Psi}(\tilde{\boldsymbol{x}},\tilde{t}) = \mathrm{e}^{\frac{\theta}{2}\alpha_y}\Psi(\boldsymbol{x},t) \tag{B.10}$$

$$\left(\tilde{p}_0 - \alpha_x\tilde{p}_x - (\tilde{p}_y + e\tilde{B}\tilde{x})\right)\tilde{\Psi}(\tilde{\boldsymbol{x}},\tilde{t}) = 0 \tag{B.11}$$

$$\tilde{B} = B\sqrt{1-\beta^2} \tag{B.12}$$

Eigenvalues

$$\tilde{\epsilon}_{n,\tilde{k}_y} = \mathrm{sgn}(n)\sqrt{2|n|}\frac{\hbar v_F}{\tilde{\ell}_c} \tag{B.13}$$

here

$$\tilde{\ell}_c = \ell_c(1-\beta^2)^{-\frac{1}{4}}$$

Eigenvectors for the time-independent Landau level problem,

$$\phi_{n,\tilde{k}_y}(\tilde{\boldsymbol{x}}) = \frac{1}{\sqrt{2}}\begin{pmatrix} \varphi_{|n|-1,\tilde{k}_y}(\tilde{\boldsymbol{x}}) \\ \mathrm{i}\ \mathrm{sgn}(n)\varphi_{|n|,\tilde{k}_y}(\tilde{\boldsymbol{x}}) \end{pmatrix} \tag{B.14}$$

Here $\varphi_{n,\tilde{k}_y}(\tilde{\boldsymbol{x}})$ is eigen functions non-relativistic Landau level problem in Landau gauge.

$$\varphi_{n,\tilde{k}_y}(\tilde{\boldsymbol{x}}) = A_n\mathrm{e}^{\mathrm{i}\,\tilde{k}_y\tilde{y}}\mathrm{e}^{-\frac{\tilde{\xi}^2}{2}}H_n(\tilde{\xi}) \tag{B.15}$$

Here $H_n(x)$ is hermite polynomial and proportionality constant, A_n is fixed by normalization and depends on n.

$$\tilde{\xi} = \frac{\tilde{x} + \tilde{k}_y\tilde{\ell}_c^2}{\tilde{\ell}_c} \tag{B.16}$$

Apply inverse Lorentz transformation on *three-vector*, we have following results,

$$\begin{aligned}\epsilon_{n,k_y} &= \frac{\tilde{\epsilon}_{n,\tilde{k}_y}}{\cosh(\theta)} - \hbar v_F k_y \tanh(\theta) \\ &= \mathrm{sgn}(n)\sqrt{2|n|}\frac{\hbar v_F}{\ell_c}(1-\beta^2)^{\frac{3}{4}} - \hbar v_F k_y \beta\end{aligned} \tag{B.17}$$

$$\begin{aligned}\tilde{k}_y &= \frac{k_y}{\cosh(\theta)} + \frac{\tilde{\epsilon}_{n,\tilde{k}_y}}{\hbar v_F}\tanh(\theta) \\ &= k_y(1-\beta^2)^{\frac{1}{2}} + \mathrm{sgn}(n)\sqrt{2|n|}\frac{1}{\ell_c}\beta(1-\beta^2)^{\frac{1}{4}}\end{aligned} \tag{B.18}$$

We use invariance of scalar product of two 3-vectors under Lorentz transformation

$$\tilde{\epsilon}_{n,\tilde{k}_y}\tilde{t} - \tilde{k}_y\,\tilde{y} = \epsilon_{n,k_y}t - k_y\,y \tag{B.19}$$

and

$$\frac{\tilde{x} + \tilde{k}_y\tilde{\ell}_c^2}{\tilde{\ell}_c} \to \xi = \frac{(1-\beta^2)^{\frac{1}{4}}}{\ell_c}\Big(x + k_y\,\ell_c^2 + \mathrm{sgn}(n)\sqrt{2|n|}\ell_c\frac{\beta}{(1-\beta^2)^{\frac{1}{4}}}\Big) \tag{B.20}$$

the eigen functions for the cross magnetic and electric field

$$\phi_{n,k_y}(\boldsymbol{x}) = \frac{\mathrm{e}^{-\frac{\theta}{2}\alpha_y}}{\sqrt{2\cosh(\theta)}}\begin{pmatrix}\varphi_{|n|-1,k_y}(\boldsymbol{x}) \\ \mathrm{i}\,\mathrm{sgn}(n)\varphi_{|n|,k_y}(\boldsymbol{x})\end{pmatrix} \tag{B.21}$$

Here $\varphi_{n,k_y}(\boldsymbol{x})$ is eigen functions non-relativistic Landau level problem in Landau gauge.

Appendix C

Continuum approximation: Interactions

$$\mathcal{H}_C = \frac{1}{2}\sum_{\boldsymbol{n},\boldsymbol{m}}\sum_{r,s}(\hat{n}_{\boldsymbol{n},r} - \frac{1}{2}\langle\hat{n}\rangle)V_C(|\boldsymbol{n}_r - \boldsymbol{m}_s|)(\hat{n}_{\boldsymbol{m},s} - \frac{1}{2}\langle\hat{n}\rangle) \tag{C.1}$$

The summation has a constraint that when $\boldsymbol{n} = \boldsymbol{m}$ then $r \neq s$

$$\hat{n}_{\boldsymbol{n},r,\sigma} = c^{\dagger}_{\boldsymbol{n},r,\sigma}c_{\boldsymbol{n},r,\sigma} \tag{C.2}$$

$$\hat{n}_{\boldsymbol{n},r} = \sum_{\sigma=\uparrow,\downarrow}\hat{n}_{\boldsymbol{n},r,\sigma} \tag{C.3}$$

$$\hat{n}_{\boldsymbol{n}} = \sum_{r=1,2}\hat{n}_{\boldsymbol{n},r} \tag{C.4}$$

$$\hat{n} = \sum_{\boldsymbol{n}}\sum_{r=1,2}\hat{n}_{\boldsymbol{n},r} \tag{C.5}$$

Applying projection operator Eq.(3.3), applied on the number operators,

$$\begin{aligned} c^{\dagger}_{\boldsymbol{n},1,\sigma}c_{\boldsymbol{n},1,\sigma} \approx{}& \psi^{\dagger}_{1,+,\sigma}(\boldsymbol{n})\psi_{1,+,\sigma}(\boldsymbol{n}) + \psi^{\dagger}_{2,-,\sigma}(\boldsymbol{n})\psi_{2,-,\sigma}(\boldsymbol{n}) \\ &+ \mathrm{e}^{-\mathrm{i}\,(\boldsymbol{K}_+ - \boldsymbol{K}_-)\cdot\boldsymbol{n}}\psi^{\dagger}_{1,+,\sigma}(\boldsymbol{n})\psi_{2,-,\sigma}(\boldsymbol{n}) \\ &+ \mathrm{e}^{\mathrm{i}\,(\boldsymbol{K}_+ - \boldsymbol{K}_-)\cdot\boldsymbol{n}}\psi^{\dagger}_{2,-,\sigma}(\boldsymbol{n})\psi_{1,+,\sigma}(\boldsymbol{n}) \end{aligned} \tag{C.6}$$

$$
\begin{aligned}
c^{\dagger}_{\boldsymbol{n},2,\sigma}c_{\boldsymbol{n},2,\sigma} \approx \psi^{\dagger}_{2,+,\sigma}(\boldsymbol{n})\psi_{2,+,\sigma}(\boldsymbol{n}) + \psi^{\dagger}_{1,-,\sigma}(\boldsymbol{n})\psi_{1,-,\sigma}(\boldsymbol{n}) \\
- \mathrm{e}^{-\mathrm{i}\,(\boldsymbol{K}_{+}-\boldsymbol{K}_{-})\cdot\boldsymbol{n}}\psi^{\dagger}_{2,+,\sigma}(\boldsymbol{n})\psi_{1,-,\sigma}(\boldsymbol{n}) \\
- \mathrm{e}^{\mathrm{i}\,(\boldsymbol{K}_{+}-\boldsymbol{K}_{-})\cdot\boldsymbol{n}}\psi^{\dagger}_{1,-,\sigma}(\boldsymbol{n})\psi_{2,+,\sigma}(\boldsymbol{n})
\end{aligned} \tag{C.7}
$$

Making the substitutions

$$
\begin{aligned}
\psi^{\dagger}_{1,+,\sigma}\psi_{1,+,\sigma} &= \Psi^{\dagger}(\boldsymbol{n})\Big(\frac{1+\beta}{2}\Big)\Big(\frac{1+\tau^{z}}{2}\Big)\Psi(\boldsymbol{n}) \\
\psi^{\dagger}_{1,-,\sigma}\psi_{1,-,\sigma} &= \Psi^{\dagger}(\boldsymbol{n})\Big(\frac{1+\beta}{2}\Big)\Big(\frac{1-\tau^{z}}{2}\Big)\Psi(\boldsymbol{n}) \\
\psi^{\dagger}_{2,+,\sigma}\psi_{2,+,\sigma} &= \Psi^{\dagger}(\boldsymbol{n})\Big(\frac{1-\beta}{2}\Big)\Big(\frac{1+\tau^{z}}{2}\Big)\Psi(\boldsymbol{n}) \\
\psi^{\dagger}_{2,-,\sigma}\psi_{2,-,\sigma} &= \Psi^{\dagger}(\boldsymbol{n})\Big(\frac{1-\beta}{2}\Big)\Big(\frac{1-\tau^{z}}{2}\Big)\Psi(\boldsymbol{n}) \\
\psi^{\dagger}_{1,+,\sigma}\psi_{2,-,\sigma} &= \Psi^{\dagger}(\boldsymbol{n})\Big(\frac{\alpha^{x}+\mathrm{i}\,\alpha^{y}}{2}\Big)\Big(\frac{\tau^{x}+\mathrm{i}\,\tau^{y}}{2}\Big)\Psi(\boldsymbol{n}) \\
\psi^{\dagger}_{2,-,\sigma}\psi_{1,+,\sigma} &= \Psi^{\dagger}(\boldsymbol{n})\Big(\frac{\alpha^{x}-\mathrm{i}\,\alpha^{y}}{2}\Big)\Big(\frac{\tau^{x}-\mathrm{i}\,\tau^{y}}{2}\Big)\Psi(\boldsymbol{n}) \\
\psi^{\dagger}_{2,+,\sigma}\psi_{1,-,\sigma} &= \Psi^{\dagger}(\boldsymbol{n})\Big(\frac{\alpha^{x}-\mathrm{i}\,\alpha^{y}}{2}\Big)\Big(\frac{\tau^{x}+\mathrm{i}\,\tau^{y}}{2}\Big)\Psi(\boldsymbol{n}) \\
\psi^{\dagger}_{1,-,\sigma}\psi_{2,+,\sigma} &= \Psi^{\dagger}(\boldsymbol{n})\Big(\frac{\alpha^{x}+\mathrm{i}\,\alpha^{y}}{2}\Big)\Big(\frac{\tau^{x}-\mathrm{i}\,\tau^{y}}{2}\Big)\Psi(\boldsymbol{n})
\end{aligned} \tag{C.8}
$$

The number operators can be approximated in terms of slow and fast varying modes as,

$$
\begin{aligned}
\hat{n}_{\boldsymbol{n},1,\sigma} \approx \frac{1}{2}\Psi^{\dagger}(\boldsymbol{n})\Psi(\boldsymbol{n}) + \frac{1}{2}\Psi^{\dagger}(\boldsymbol{n})\beta\tau^{z}\Psi(\boldsymbol{n}) \\
+ \frac{1}{4}\mathrm{e}^{-\mathrm{i}\,\phi(\boldsymbol{n})}\Big(\big(\Psi^{\dagger}(\boldsymbol{n})\alpha^{x}\tau^{x}\Psi(\boldsymbol{n}) - \Psi^{\dagger}(\boldsymbol{n})\alpha^{y}\tau^{y}\Psi(\boldsymbol{n})\big) \\
+ \mathrm{i}\,\big(\Psi^{\dagger}(\boldsymbol{n})\alpha^{x}\tau^{y}\Psi(\boldsymbol{n}) + \Psi^{\dagger}(\boldsymbol{n})\alpha^{y}\tau^{x}\Psi(\boldsymbol{n})\big)\Big) \\
+ \frac{1}{4}\mathrm{e}^{\mathrm{i}\,\phi(\boldsymbol{n})}\Big(\big(\Psi^{\dagger}(\boldsymbol{n})\alpha^{x}\tau^{x}\Psi(\boldsymbol{n}) - \Psi^{\dagger}(\boldsymbol{n})\alpha^{y}\tau^{y}\Psi(\boldsymbol{n})\big) \\
- \mathrm{i}\,\big(\Psi^{\dagger}(\boldsymbol{n})\alpha^{x}\tau^{y}\Psi(\boldsymbol{n}) + \Psi^{\dagger}(\boldsymbol{n})\alpha^{y}\tau^{x}\Psi(\boldsymbol{n})\big)\Big)
\end{aligned} \tag{C.9}
$$

$$\begin{aligned}\hat{n}_{\boldsymbol{n},2,\sigma} \approx \frac{1}{2}\Psi^\dagger(\boldsymbol{n})\Psi(\boldsymbol{n}) - \frac{1}{2}\Psi^\dagger(\boldsymbol{n})\beta\tau^z\Psi(\boldsymbol{n}) \\ - \frac{1}{4}\mathrm{e}^{-\mathrm{i}\,\phi(\boldsymbol{n})}\Big(\big(\Psi^\dagger(\boldsymbol{n})\alpha^x\tau^x\Psi(\boldsymbol{n}) + \Psi^\dagger(\boldsymbol{n})\alpha^y\tau^y\Psi(\boldsymbol{n})\big) \\ + \mathrm{i}\,\big(\Psi^\dagger(\boldsymbol{n})\alpha^x\tau^y\Psi(\boldsymbol{n}) - \Psi^\dagger(\boldsymbol{n})\alpha^y\tau^x\Psi(\boldsymbol{n})\big)\Big) \\ - \frac{1}{4}\mathrm{e}^{\mathrm{i}\,\phi(\boldsymbol{n})}\Big(\big(\Psi^\dagger(\boldsymbol{n})\alpha^x\tau^x\Psi(\boldsymbol{n}) + \Psi^\dagger(\boldsymbol{n})\alpha^y\tau^y\Psi(\boldsymbol{n})\big) \\ - \mathrm{i}\,\big(\Psi^\dagger(\boldsymbol{n})\alpha^x\tau^y\Psi(\boldsymbol{n}) - \Psi^\dagger(\boldsymbol{n})\alpha^y\tau^x\Psi(\boldsymbol{n})\big)\Big) \quad \text{(C.10)}\end{aligned}$$

Here $\mathrm{e}^{\pm\mathrm{i}\,\phi(\boldsymbol{n})}$ are the fast varying modes.

Consider the four fermion terms,

$$\begin{aligned}\mathcal{H}_I = \frac{1}{2}\sum_{\substack{\boldsymbol{n},\boldsymbol{m}\\ \boldsymbol{n}\neq\boldsymbol{m}}}\Big(V(r)\hat{n}_{\boldsymbol{n},1,\sigma}\hat{n}_{\boldsymbol{m},1,\tilde{\sigma}} + V(r)\hat{n}_{\boldsymbol{n},2,\sigma}\hat{n}_{\boldsymbol{m},2,\tilde{\sigma}}\Big) \\ + \frac{1}{2}\sum_{\substack{\boldsymbol{n},\boldsymbol{m}\\ \boldsymbol{n}\neq\boldsymbol{m}}}\Big(V(d_1)\hat{n}_{\boldsymbol{n},1,\sigma}\hat{n}_{\boldsymbol{m},2,\tilde{\sigma}} + V(d_2)\hat{n}_{\boldsymbol{n},2,\sigma}\hat{n}_{\boldsymbol{m},1,\tilde{\sigma}}\Big) \\ + \frac{1}{2}V(\tilde{a})\sum_{\boldsymbol{n}}\Big(\hat{n}_{\boldsymbol{n},1,\sigma}\hat{n}_{\boldsymbol{n},2,\tilde{\sigma}} + \hat{n}_{\boldsymbol{n},2,\sigma}\hat{n}_{\boldsymbol{n},1,\tilde{\sigma}}\Big) \quad \text{(C.11)}\end{aligned}$$

From the Figure 3.1

$$r = |\boldsymbol{n}_s - \boldsymbol{m}_s| \quad \text{(C.12)}$$

$$\begin{aligned}d_1 = \sqrt{r^2 - 2r\tilde{a}\cos\theta + \tilde{a}^2} \\ d_2 = \sqrt{r^2 + 2r\tilde{a}\cos\theta + \tilde{a}^2}\end{aligned} \quad \text{(C.13)}$$

Here $\tilde{a} = a/\sqrt{3}$, a is the lattice constant.

$$V(r) = \frac{1}{4\pi\epsilon}\frac{e^2}{r} \quad \text{(C.14)}$$

For $r >> \tilde{a}$,

$$\begin{aligned}V(d_1) = V(r)\Big(1 + \frac{\tilde{a}}{r}\cos\theta + \frac{1}{2}\frac{\tilde{a}^2}{r^2}(3\cos^2\theta - 1) + \dots\Big) \\ V(d_2) = V(r)\Big(1 - \frac{\tilde{a}}{r}\cos\theta + \frac{1}{2}\frac{\tilde{a}^2}{r^2}(3\cos^2\theta - 1) + \dots\Big)\end{aligned} \quad \text{(C.15)}$$

After long wavelength approximation,

$$|\boldsymbol{n}_s - \boldsymbol{m}_s| \to |\boldsymbol{x} - \boldsymbol{y}| = r \tag{C.16}$$

$$\sum_{\boldsymbol{n}} \to \frac{1}{a^2} \int_{\boldsymbol{x}} \tag{C.17}$$

$$\psi_{\alpha,\tau,\sigma}(\boldsymbol{n}) \to a\, \Psi_{\alpha,\tau,\sigma}(\boldsymbol{x}) \tag{C.18}$$

$$\langle \hat{n} \rangle = \frac{1}{N} \sum_{\boldsymbol{n}} \hat{n}_{\boldsymbol{n}} \to \frac{1}{\mathsf{V}} a^2 \int_{\boldsymbol{x}} \langle \Psi^\dagger(\boldsymbol{x}) \Psi(\boldsymbol{x}) \rangle = a^2 \bar{\rho} \tag{C.19}$$

$$\bar{\rho} = \frac{1}{\mathsf{V}} \int_{\boldsymbol{x}} \langle \Psi^\dagger(\boldsymbol{x}) \Psi(\boldsymbol{x}) \rangle \tag{C.20}$$

$$\begin{aligned}
\hat{n}_{\boldsymbol{n},1,\sigma} \hat{n}_{\boldsymbol{m},1,\tilde{\sigma}} &\to \frac{a^2}{4} \Big(\Psi^\dagger(\boldsymbol{x}) \Psi(\boldsymbol{x}) + \Psi^\dagger(\boldsymbol{x}) \beta \tau^z \Psi(\boldsymbol{x}) \Big) \Big(\Psi^\dagger(\boldsymbol{y}) \Psi(\boldsymbol{y}) + \Psi^\dagger(\boldsymbol{y}) \beta \tau^z \Psi(\boldsymbol{y}) \Big) \\
\hat{n}_{\boldsymbol{n},2,\sigma} \hat{n}_{\boldsymbol{m},2,\tilde{\sigma}} &\to \frac{a^2}{4} \Big(\Psi^\dagger(\boldsymbol{x}) \Psi(\boldsymbol{x}) - \Psi^\dagger(\boldsymbol{x}) \beta \tau^z \Psi(\boldsymbol{x}) \Big) \Big(\Psi^\dagger(\boldsymbol{y}) \Psi(\boldsymbol{y}) - \Psi^\dagger(\boldsymbol{y}) \beta \tau^z \Psi(\boldsymbol{y}) \Big) \\
\hat{n}_{\boldsymbol{n},1,\sigma} \hat{n}_{\boldsymbol{m},2,\tilde{\sigma}} &\to \frac{a^2}{4} \Big(\Psi^\dagger(\boldsymbol{x}) \Psi(\boldsymbol{x}) + \Psi^\dagger(\boldsymbol{x}) \beta \tau^z \Psi(\boldsymbol{x}) \Big) \Big(\Psi^\dagger(\boldsymbol{y}) \Psi(\boldsymbol{y}) - \Psi^\dagger(\boldsymbol{y}) \beta \tau^z \Psi(\boldsymbol{y}) \Big)
\end{aligned} \tag{C.21}$$

Separating the interaction term in the leading order of contribution at large separations,

$$\begin{aligned}
\mathcal{H}_I = \frac{1}{2} \int_{\substack{\boldsymbol{x},\boldsymbol{y} \\ \boldsymbol{x} \neq \boldsymbol{y}}} & V(r) \Psi^\dagger(\boldsymbol{x}) \Psi(\boldsymbol{x}) \Psi^\dagger(\boldsymbol{y}) \Psi(\boldsymbol{y}) \\
& + \frac{1}{2} \int_{\substack{\boldsymbol{x},\boldsymbol{y} \\ \boldsymbol{x} \neq \boldsymbol{y}}} V(r) \Big(\frac{1}{4} \frac{\tilde{a}^2}{r^2} (3 \cos^2 \theta - 1) + \dots \Big) \\
& \Big(\Psi^\dagger(\boldsymbol{x}) \Psi(\boldsymbol{x}) \Psi^\dagger(\boldsymbol{y}) \Psi(\boldsymbol{y}) - \Psi^\dagger(\boldsymbol{x})\, \beta \tau^z\, \Psi(\boldsymbol{x})\; \Psi^\dagger(\boldsymbol{y})\, \beta \tau^z\, \Psi(\boldsymbol{y}) \Big) \\
& + \text{Contact interaction term along one nearest bond}
\end{aligned} \tag{C.22}$$

Appendix D

Continuum approximation: Nearest neighbour terms

The nearest neighbour interaction on honeycomb lattice,

$$\mathcal{H}_V = V \sum_{\boldsymbol{n},\sigma,\tilde{\sigma}} c^{\dagger}_{\boldsymbol{n},1,\sigma} c_{\boldsymbol{n},1,\sigma} \big(c^{\dagger}_{\boldsymbol{n},2,\tilde{\sigma}} c_{\boldsymbol{n},2,\tilde{\sigma}} + c^{\dagger}_{\boldsymbol{n}+\boldsymbol{e}_2,2,\tilde{\sigma}} c_{\boldsymbol{n}+\boldsymbol{e}_2,2,\tilde{\sigma}} + c^{\dagger}_{\boldsymbol{n}+\boldsymbol{e}_1+\boldsymbol{e}_2,2,\tilde{\sigma}} c_{\boldsymbol{n}-\boldsymbol{e}_1+\boldsymbol{e}_2,2,\tilde{\sigma}} \big) \tag{D.1}$$

Rewriting the nearest neighbour interaction term and subtracting the background charge due to positive ions,

$$\mathcal{H}_V = V \sum_{\boldsymbol{n}} \left(\sum_{i=1}^{3} (\hat{n}_{\boldsymbol{n},1} - \frac{1}{2}\langle \hat{n} \rangle)(\hat{n}_{\boldsymbol{n}+\boldsymbol{b}_i,2} - \frac{1}{2}\langle \hat{n} \rangle) \right) \tag{D.2}$$

Here the summation over index $i = 1, 2, 3$ is for the three nearest neighbour for each carbon site.

Now consider the four fermion terms,

$$\mathcal{H}_V = V \sum_{\boldsymbol{n}} \hat{n}_{\boldsymbol{n},1} \Big(\sum_{i=1}^{3} \hat{n}_{\boldsymbol{n}+\boldsymbol{b}_i,2} \Big) \tag{D.3}$$

Using Eq.(C.10) and retaining the leading terms and dropping the derivatives of fermion operator terms and fast varying modes, we can approximate

$$\sum_{i=1}^{3} \hat{n}_{\boldsymbol{n}+\boldsymbol{b}_i,2} \approx \frac{3}{4}\Psi^\dagger(\boldsymbol{n})\Psi(\boldsymbol{n}) - \frac{3}{4}\Psi^\dagger(\boldsymbol{n})\beta\tau^z\Psi(\boldsymbol{n}) \tag{D.4}$$

Here we make use of the fact, $(1 + \mathrm{e}^{\mathrm{i}\,\frac{2\pi}{3}} + \mathrm{e}^{\mathrm{i}\,\frac{4\pi}{3}}) = 0$

Now using Eq.(C.9) and taking the continuum approximation as described in previous chapter.

$$\mathcal{H}_V = \frac{3}{4}Va^2 \int_{\boldsymbol{x}} \Big(\big(\Psi^\dagger(\boldsymbol{x})\Psi(\boldsymbol{x})\big)^2 - \big(\Psi^\dagger(\boldsymbol{x})\beta\tau^z\Psi(\boldsymbol{x})\big)^2 \Big) \tag{D.5}$$

The net continuum limit for the nearest neighbour interaction when the background charge is deducted,

$$\mathcal{H}_V = \frac{3}{4}Va^2 \int_{\boldsymbol{x}} \Big(\big(\Psi^\dagger(\boldsymbol{x})\Psi(\boldsymbol{x})\big)^2 - \big(\Psi^\dagger(\boldsymbol{x})\beta\tau^z\Psi(\boldsymbol{x})\big)^2 - 2\,\bar{\rho}\,\Psi^\dagger(\boldsymbol{x})\Psi(\boldsymbol{x}) + \bar{\rho}^2 \Big) \tag{D.6}$$

Appendix E

Continuum approximation: Hubbard terms

The Hubbard interaction,

$$\mathcal{H}_U = U \sum_{\boldsymbol{n}} \sum_{r} \hat{n}_{\boldsymbol{n},r,\uparrow} \hat{n}_{\boldsymbol{n},r,\downarrow} \tag{E.1}$$

We rewrite the Hubbard term in manifestly $SU(2)$ spin rotation invariant form,

$$\mathcal{H}_U = U \sum_{\boldsymbol{n},r} \Big(-\frac{2}{3} S^a_{\boldsymbol{n},r} S^a_{\boldsymbol{n},r} + \frac{1}{2} \hat{n}_{\boldsymbol{n},r} \Big) \tag{E.2}$$

$$= \frac{U}{2} \sum_{\boldsymbol{n}} \sum_{r} (\hat{n}^2_{\boldsymbol{n},r} - \hat{n}_{\boldsymbol{n},r}) \tag{E.3}$$

Rewriting the above equation after subtracting the background charge,

$$\mathcal{H}_U = \frac{U}{2} \sum_{\boldsymbol{n}} \Big((\hat{n}_{\boldsymbol{n},1})^2 + (\hat{n}_{\boldsymbol{n},2})^2 - \langle \hat{n} \rangle \hat{n}_{\boldsymbol{n}} + \frac{1}{2} \langle \hat{n} \rangle^2 - \hat{n}_{\boldsymbol{n}} + \langle \hat{n} \rangle \Big) \tag{E.4}$$

Consider the four fermion terms and gathering slow varying modes for density-density operators for each sub-lattice index

$$\hat{n}_{\boldsymbol{n},1,\sigma}\hat{n}_{\boldsymbol{n},1,\sigma} \approx \frac{1}{4}\Big(\Psi^\dagger(\boldsymbol{n})\Psi(\boldsymbol{n}) + \Psi^\dagger(\boldsymbol{n})\beta\tau^z\Psi(\boldsymbol{n})\Big)^2 + \frac{1}{16}\Big(\big(\Psi^\dagger(\boldsymbol{n})\alpha^x\tau^x\Psi(\boldsymbol{n}) - \Psi^\dagger(\boldsymbol{n})\alpha^y\tau^y\Psi(\boldsymbol{n})\big)^2 + \big(\Psi^\dagger(\boldsymbol{n})\alpha^x\tau^y\Psi(\boldsymbol{n}) + \Psi^\dagger(\boldsymbol{n})\alpha^y\tau^x\Psi(\boldsymbol{n})\big)^2\Big) \quad \text{(E.5)}$$

$$\hat{n}_{\boldsymbol{n},2,\sigma}\hat{n}_{\boldsymbol{n},2,\sigma} \approx \frac{1}{4}\Big(\Psi^\dagger(\boldsymbol{n})\Psi(\boldsymbol{n}) - \Psi^\dagger(\boldsymbol{n})\beta\tau^z\Psi(\boldsymbol{n})\Big)^2 + \frac{1}{16}\Big(\big(\Psi^\dagger(\boldsymbol{n})\alpha^x\tau^x\Psi(\boldsymbol{n}) + \Psi^\dagger(\boldsymbol{n})\alpha^y\tau^y\Psi(\boldsymbol{n})\big)^2 + \big(\Psi^\dagger(\boldsymbol{n})\alpha^x\tau^y\Psi(\boldsymbol{n}) - \Psi^\dagger(\boldsymbol{n})\alpha^y\tau^x\Psi(\boldsymbol{n})\big)^2\Big) \quad \text{(E.6)}$$

Taking the continuum approximation,

$$\mathcal{H}_U = \frac{U}{2}a^2\int_{\boldsymbol{x}}\frac{1}{2}\Big(\big(\Psi^\dagger(\boldsymbol{x})\Psi(\boldsymbol{x})\big)^2 + \big(\Psi^\dagger(\boldsymbol{x})\beta\tau^z\Psi(\boldsymbol{x})\big)^2 + \frac{1}{2}\sum_{j,k=x,y}\big(\Psi^\dagger(\boldsymbol{x})\alpha^j\tau^k\Psi(\boldsymbol{x})\big)^2\Big) \quad \text{(E.7)}$$

Rewriting the Hubbard term after removing the background charge,

$$\mathcal{H}_U = \frac{1}{4}Ua^2\int_{\boldsymbol{x}}\Big(\big(\Psi^\dagger(\boldsymbol{x})\Psi(\boldsymbol{x})\big)^2 + \big(\Psi^\dagger(\boldsymbol{x})\beta\tau^z\Psi(\boldsymbol{x})\big)^2 + \frac{1}{2}\sum_{j,k=x,y}\big(\Psi^\dagger(\boldsymbol{x})\alpha^j\tau^k\Psi(\boldsymbol{x})\big)^2 - 2\,\bar{\rho}\,\Psi^\dagger(\boldsymbol{x})\Psi(\boldsymbol{x}) + \bar{\rho}^2\Big) - \frac{U}{2}\int_{\boldsymbol{x}}\big(\Psi^\dagger(\boldsymbol{x})\Psi(\boldsymbol{x}) - \bar{\rho}\big) \quad \text{(E.8)}$$

Appendix F

Propagator for non-relativistic electron in magnetic field

In general to compute the propagator, we need to evaluate

$$K(x,t;x_0,t_0) = \int \mathcal{D}[q(t)]\ \mathrm{e}^{\frac{\mathrm{i}}{\hbar}\int_{t_0}^{t} dt\ L(q,\dot{q},t)} \tag{F.1}$$

with boundary condition $q(t) = x$ and $q(t_0) = x_0$

Lagrangian for charged particle in electromagnetic field

$$L = \frac{1}{2}m\dot{\boldsymbol{r}}^2 - q\Phi(\boldsymbol{r}) + q\boldsymbol{A}(\boldsymbol{r})\cdot\dot{\boldsymbol{r}} \tag{F.2}$$

For electron in a constant magnetic field along z-axis and working with symmetric gauge for vector potential

$$q = -e, \qquad \boldsymbol{A}(\boldsymbol{r}) = \frac{B}{2}(-y,x,0), \qquad \Phi(\boldsymbol{r}) = 0$$

Lagrangian for electron in magnetic field,

$$L = \frac{m}{2}\left(\dot{x}^2 + \dot{y}^2 - \omega_c(-y\dot{x} + x\dot{y})\right) \tag{F.3}$$

Here $\omega_c = eB/m$ is the cyclotron frequency.

The propagator is by evaluating contributions from the classical part which gives the spatial part of the propagator and the fluctuations around the classical motion which contributes to the normalization. The action $S = \int \mathrm{d}t\ L$ has contributions motions, classical and fluctuations.

$$\boldsymbol{r} = \boldsymbol{r}_{cl} + \boldsymbol{\eta}$$

with boundary conditions,

$$(x_{cl}(0), y_{cl}(0) = (x_0, y_0) \quad \text{and} \quad (x_{cl}(T), y_{cl}(T) = (x, y)$$

$$(\eta_x(0), \eta_y(0)) = 0 = (\eta_x(T), \eta_y(T))$$

This results $S = S_{cl} + S^{'}$

$$S^{'} = \int_0^T \mathrm{d}t\ \frac{m}{2}\left(\dot{\eta_x}^2 + \dot{\eta_y}^2 - \omega_c(-\eta_y\dot{\eta_x} + \eta_x\dot{\eta_y})\right) \tag{F.4}$$

the cross terms vanish after integration by parts and applying classical equations of motions

$$\begin{aligned} \ddot{x}_{cl} + \omega_c\dot{y}_{cl} &= 0 \\ \ddot{y}_{cl} - \omega_c\dot{x}_{cl} &= 0 \end{aligned} \tag{F.5}$$

The propagator

$$K(\boldsymbol{r}, T; \boldsymbol{r}_0, 0) = \mathrm{e}^{\frac{\mathrm{i}}{\hbar}S_{cl}} \int \mathcal{D}[\boldsymbol{\eta}(t)]\ \mathrm{e}^{\frac{\mathrm{i}}{\hbar}S^{'}} \tag{F.6}$$

The solutions to classical equation of motion,

$$\begin{aligned} x_{cl} &= \bar{x} + c\sin(\omega_c t + \phi) \\ y_{cl} &= \bar{y} - c\cos(\omega_c t + \phi) \end{aligned} \tag{F.7}$$

The constants are fixed by the boundary conditions,

$$x_0 = \bar{x} + c\sin(\phi) \qquad y_0 = \bar{y} - c\cos(\phi) \tag{F.8}$$

$$x = \bar{x} + c\sin(\omega_c T + \phi) \qquad y = \bar{y} - c\cos(\omega_c T + \phi) \tag{F.9}$$

$$\begin{aligned} x - x_0 &= 2c\cos(\frac{\omega_c T}{2} + \phi)\sin(\frac{\omega_c T}{2}) \\ y - y_0 &= 2c\sin(\frac{\omega_c T}{2} + \phi)\sin(\frac{\omega_c T}{2}) \\ \\ c &= \frac{1}{2}\frac{|\boldsymbol{r} - \boldsymbol{r}_0|}{\sin(\frac{\omega_c T}{2})} \\ \tan(\frac{\omega_c T}{2} + \phi) &= \frac{y - y_0}{x - x_0} \\ \int_0^T \mathrm{d}t\ \frac{m}{2}(\dot{x}^2 + \dot{y}^2) &= \frac{m}{2}c^2\omega_c^2 T \end{aligned} \tag{F.10}$$

$$\int_0^T \mathrm{d}t\ \frac{m}{2}(-\omega_c)(-y\dot{x} + x\dot{y})$$

$$= \frac{m}{2}c\,\omega_c\left(\bar{y}\sin(\omega_c t + \phi) + \bar{x}\cos(\omega_c + \phi)\right)\Big|_0^T - \frac{m}{2}c^2\omega_c^2 T$$

$$\begin{aligned} S_{cl} &= \frac{m}{2}c\,\omega_c\big(\bar{y}(\sin(\omega_c T + \phi) - \sin(\phi)) + \bar{x}(\cos(\omega_c T + \phi) - \cos(\phi)) \\ &= \frac{m\omega_c}{2}(\bar{y}(x - x_0) - \bar{x}(y - y_0)) \end{aligned}$$

Here we made use of Eq.(F.10)

$$\bar{x} = \frac{1}{2}\left((x+x_0) - (y-y_0)\cot(\frac{\omega_c T}{2})\right)$$
$$\bar{y} = \frac{1}{2}\left((y+y_0) + (y-y_0)\cot(\frac{\omega_c T}{2})\right)$$

$$S_{cl} = \frac{m\omega_c}{2}\left(\frac{1}{2}|\boldsymbol{r}-\boldsymbol{r}_0|^2\cot(\frac{\omega_c T}{2}) + (xy_0 - yx_0)\right) \tag{F.11}$$

$$\mathrm{e}^{\frac{\mathrm{i}}{\hbar}S_{cl}} = \mathrm{e}^{\mathrm{i}\frac{|\boldsymbol{r}-\boldsymbol{r}_0|^2}{4\ell_c^2}\cot(\frac{\omega_c T}{2})+\mathrm{i}\frac{1}{2\ell_c^2}(xy_0-yx_0)} \tag{F.12}$$

$$Z = \mathrm{Tr}[\mathrm{e}^{-\beta H}] = \sum_{n,l}\mathrm{e}^{-\beta(n+\frac{1}{2})\hbar\omega_c} = \int \mathrm{d}\boldsymbol{q}\langle\boldsymbol{q}|\mathrm{e}^{-\beta H}|\boldsymbol{q}\rangle$$
$$= \frac{1}{2\sinh(\frac{\beta\hbar\omega_c}{2})} = \int \mathrm{d}\boldsymbol{q}\; K(\boldsymbol{q}, -\mathrm{i}\,\hbar\beta; \boldsymbol{q}, 0)$$

The evaluation of fluctuation part with the boundary condition

$$\int \mathcal{D}[\boldsymbol{\eta}(t)]\;\mathrm{e}^{\frac{\mathrm{i}}{\hbar}S'} = \frac{1}{\mathrm{A}}\sum_{n,l}\mathrm{e}^{\beta(n+\frac{1}{2})\hbar\omega_c} = \frac{1}{2\pi\ell_c^2}\frac{1}{2\sinh(\mathrm{i}\,\frac{\omega_c t}{2})} \tag{F.13}$$

here $\beta = \mathrm{i}\,t/\hbar$ and using relation $\sinh(\mathrm{i}\,\theta) = \mathrm{i}\,\sin\theta$, the propagator for the non-relativistic electron in magnetic field,

$$K(\boldsymbol{r}, t; \boldsymbol{r}_0, 0) = \frac{1}{2\pi\ell_c^2}\frac{1}{2\mathrm{i}\,\sin(\frac{\omega_c t}{2})}e^{\mathrm{i}\frac{|\boldsymbol{r}-\boldsymbol{r}_0|^2}{4\ell_c^2}\cot(\frac{\omega_c t}{2})}e^{\mathrm{i}\frac{1}{2\ell_c^2}(xy_0-yx_0)} \tag{F.14}$$

Appendix G

Integral for Coulomb gap calculation

The integral that we want to consider,

$$\mathcal{I} = \frac{1}{(2\pi)^2} \iint_{z_1,z_2} \frac{1}{|z_1 - z_2|} \frac{1}{l!} \left(\frac{\bar{z}_1 z_2}{2}\right)^l \mathrm{e}^{-\frac{1}{2}\bar{z}_1 z_2} \mathrm{e}^{-\frac{1}{4}(1+\alpha)|z_1 - z_2|^2} \tag{G.1}$$

Here z_1 and z_2 are complex variables, l takes non-negative integer values and $\alpha \geq 1$ is real number. Consider the integral,

$$\mathcal{I}(\lambda) = \frac{1}{(2\pi)^2} \frac{(-1)^l}{l!} \iint_{z_1,z_2} \frac{1}{|z_1 - z_2|} \left(\frac{\bar{z}_1 z_2}{2}\right)^l \mathrm{e}^{-\frac{\lambda}{2}\bar{z}_1 z_2} \mathrm{e}^{-\frac{1}{4}(1+\alpha)|z_1 - z_2|^2} \tag{G.2}$$

Assuming we can solve the above integral, then the integral, $\mathcal{I}$ in Eq.(G.1) can be obtained by repeated differentiation with respect to λ.

$$\mathcal{I} = \frac{\mathrm{d}^l}{\mathrm{d}\lambda^l} \mathcal{I}(\lambda) \bigg|_{\lambda=1} \tag{G.3}$$

Make a change of variables in Eq.(G.2),

$$z_1 = Z + \frac{z}{2} \tag{G.4}$$

$$z_2 = Z - \frac{z}{2} \tag{G.5}$$

$$\bar{z}_1 z_2 = (\bar{Z} + \frac{\bar{z}}{2})(Z - \frac{z}{2}) = |Z|^2 - \frac{1}{4}|z|^2 + \frac{1}{2}(Z\bar{z} - \bar{Z}z) \tag{G.6}$$

Now substitute, $Z = X - \mathrm{i}\,Y$

$$\begin{aligned}\bar{z}_1 z_2 = X^2 + Y^2 - \frac{1}{4}|z|^2 + \frac{1}{2}\Big((X + \mathrm{i}\,Y)\bar{z} - (X - \mathrm{i}\,Y)z\Big) \\ = X^2 + Y^2 - \frac{1}{4}|z|^2 + X\frac{z - \bar{z}}{2} + Y\frac{\mathrm{i}\,(z + \bar{z})}{2}\end{aligned} \tag{G.7}$$

Completing the squares for the variable X and Y

$$\begin{aligned}\bar{z}_1 z_2 = (X + \frac{z - \bar{z}}{4})^2 + (Y + \frac{i(z + \bar{z})}{4})^2 - \frac{1}{4}|z|^2 - (\frac{z - \bar{z}}{4})^2 - (\frac{i(z + \bar{z})}{4})^2 \\ = \left(X + \frac{z - \bar{z}}{4}\right)^2 + \left(Y + \frac{i(z + \bar{z})}{4}\right)^2\end{aligned} \tag{G.8}$$

$$\begin{aligned}\mathcal{I}(\lambda) = \frac{1}{(2\pi)^2}\frac{(-1)^l}{l!}\int_z \frac{1}{|z|}\, e^{-\frac{1}{4}(1+\alpha)|z|^2} \int_{-\infty}^{+\infty} \mathrm{d}X\, \mathrm{e}^{-\lambda\frac{1}{2}(X + \frac{z-\bar{z}}{4})^2} \\ \int_{-\infty}^{+\infty} \mathrm{d}Y\, \mathrm{e}^{-\lambda\frac{1}{2}(Y + \frac{i(z+\bar{z})}{4})^2}\end{aligned} \tag{G.9}$$

The integration for X and Y and simple shifted gaussian integrals and converting back the relative complex variable to real quantity,

$$\mathcal{I}(\lambda) = \frac{1}{(2\pi)^2}\frac{(-1)^l}{l!}\left(\sqrt{\frac{2\pi}{\lambda}}\right)^2 \int_0^{\infty} 2\pi \mathrm{d}r\, e^{-\frac{1}{4}(1+\alpha)r^2} \tag{G.10}$$

Thus,

$$\mathcal{I}(\lambda) = \frac{(-1)^l}{l!}\frac{1}{\lambda}\sqrt{\frac{\pi}{2\alpha}} \tag{G.11}$$

Using the Eq.(G.3)

$$\mathcal{I} = \sqrt{\frac{\pi}{(1+\alpha)}} \tag{G.12}$$

Appendix H

Contact terms

Redefine the contact correlator to suppress $1/2\pi\ell_c^2$ factor, $\Gamma = \frac{1}{2\pi\ell_c^2}\tilde{\Gamma}$ Here we are using the fact that mass matrix takes the form

$$M = m\big(2\sum_{j\in\text{occ}} P_j - \mathbb{1}_4\big) \tag{H.1}$$

$$\tilde{\Gamma} = \big(u_m\,\mathbb{1}_2 - v_m\,\beta\big)\otimes\Big(\sum_{j\in\text{occ}} P_j - \frac{1}{2}\,\mathbb{1}_4\Big) \tag{H.2}$$

Here $j \in$ occ is summation occupied $SU(4)$ states of $n = 0$ Landau level. We make use of completeness relation to arrive at,

$$\sum_{j\in\text{unocc}} P_j = \mathbb{1}_4 - \sum_{j\in\text{occ}} P_j \tag{H.3}$$

$\tilde{\Gamma}\,\tilde{\Gamma}$ terms

$$\text{Tr}[\tilde{\Gamma}\tilde{\Gamma}] = 2(v_m^2 + u_m^2) \tag{H.4}$$

using the fact that $\text{Tr}[P_iP_j] = \delta_{i,j}$

$\beta\tau^z\,\tilde{\Gamma}$ **terms**

$$\beta\tau^z\tilde{\Gamma} = -\big(v_m\,\mathbb{1}_2 - u_m\,\beta\big)\otimes\Big(\sum_{j\in\text{occ}}\tau^z P_j - \frac{1}{2}\,\tau^z\Big) \tag{H.5}$$

$$\text{Tr}[\beta\tau^z\tilde{\Gamma}] = -2v_m\sum_{j\text{occ}}\text{Tr}[\tau^z P_j] \tag{H.6}$$

$$\text{Tr}[\beta\tau^z\tilde{\Gamma}\beta\tau^z\tilde{\Gamma}] = 2\big(v_m^2+u_m^2\big)\sum_{i,j\in\text{occ}}\text{Tr}[\tau^z P_i\tau^z P_j] + 2\big(v_m^2+u_m^2\big)(1-\sum_{j\in\text{occ}}1) \tag{H.7}$$

$$\begin{aligned}(\text{Tr}[\beta\tau^z\tilde{\Gamma}])^2 - \text{Tr}[\beta\tau^z\tilde{\Gamma}\beta\tau^z\tilde{\Gamma}] \\ = \sum_{i,j\in\text{occ}}\Big(4v_m^2\text{Tr}[\tau^z P_i]\text{Tr}[\tau^z P_j] - 2\big(v_m^2+u_m^2\big)\text{Tr}[\tau^z P_i\tau^z P_j]\Big) \\ - 2\big(v_m^2+u_m^2\big)(1-\sum_{j\in\text{occ}}1)\end{aligned} \tag{H.8}$$

$\alpha^a\tau^b\,\tilde{\Gamma}$ **terms**

$$\alpha^a\tau^b\tilde{\Gamma} = \big(u_m\,\alpha^a - v_m\,\alpha^a\beta\big)\otimes\Big(\sum_{j\in\text{occ}}\tau^b P_j - \frac{1}{2}\,\tau^b\Big) \tag{H.9}$$

$$\text{Tr}[\alpha^a\tau^b\tilde{\Gamma}] = 0 \tag{H.10}$$

$$\text{Tr}[\alpha^a\tau^b\tilde{\Gamma}\alpha^a\tau^b\tilde{\Gamma}] = 4\big(u_m^2-v_m^2\big)\Big(\sum_{i,j\in\text{occ}}\text{Tr}[\tau^b P_i\tau^b P_j] + (1-\sum_{j\in\text{occ}}P_j)\Big) \tag{H.11}$$

$$\begin{aligned}\frac{1}{2}\sum_{a,b=x,y}\Big(\big(\text{Tr}[\alpha^a\tau^b\tilde{\Gamma}]\big)^2 - \text{Tr}[\alpha^a\tau^b\tilde{\Gamma}\alpha^a\tau^b\tilde{\Gamma}] \\ = 2(v_m^2-u_m^2)\sum_{i,j\in\text{occ}}\big(\text{Tr}[\tau^x P_i\tau^x P_j] + \text{Tr}[\tau^y P_i\tau^y P_j]\big) \\ + 4(v_m^2-u_m^2)\big(1-\sum_{j\in\text{occ}}P_j\big)\end{aligned} \tag{H.12}$$

$\sigma^z\tilde{\Gamma}$ **term**

$$\text{Tr}[\sigma^z\,\tilde{\Gamma}] = u_m\sum_{i\in\text{occ}}\text{Tr}[\sigma^z\,P_i] \tag{H.13}$$

Appendix I

Ground state energy for $\sigma_H = 0$

$$M = \{m, m, -m, -m\} \tag{I.1}$$

$$|1\rangle = \cos(\frac{\gamma_1}{2})|+\rangle|\boldsymbol{n}_1\rangle + \mathrm{e}^{\mathrm{i}\,\Omega_1}\sin(\frac{\gamma_1}{2})|-\rangle|-\boldsymbol{n}_2\rangle \tag{I.2}$$

$$|2\rangle = \cos(\frac{\gamma_2}{2})|+\rangle|-\boldsymbol{n}_1\rangle + \mathrm{e}^{\mathrm{i}\,\Omega_2}\sin(\frac{\gamma_2}{2})|-\rangle|\boldsymbol{n}_2\rangle \tag{I.3}$$

$$\begin{aligned}\langle 1|\sigma^z|1\rangle &= \frac{1}{2}(\cos(\theta_1) - \cos(\theta_2)) + \frac{1}{2}\cos(\gamma_1)(\cos(\theta_1) + \cos(\theta_2)) \\ \langle 2|\sigma^z|2\rangle &= -\frac{1}{2}(\cos(\theta_1) - \cos(\theta_2)) - \frac{1}{2}\cos(\gamma_2)(\cos(\theta_1) + \cos(\theta_2))\end{aligned} \tag{I.4}$$

$$\mathrm{Tr}[\sigma^z\,\tilde{\Gamma}] = u_m\big(\cos(\gamma_1) - \cos(\gamma_2)\big)\big(\cos(\theta_1) + \cos(\theta_2)\big) \tag{I.5}$$

$$\mathrm{Tr}[\tilde{\Gamma}\tilde{\Gamma}] = 2(v_m^2 + u_m^2) \tag{I.6}$$

$$\langle 1|\tau^z|1\rangle = \cos(\gamma_1) \tag{I.7}$$

$$\langle 2|\tau^z|2\rangle = \cos(\gamma_2) \tag{I.8}$$

$$\langle 2|\tau^z|1\rangle = 0 \tag{I.9}$$

$$(\mathrm{Tr}[\beta\,\tau^z\,\tilde{\Gamma}])^2 - \mathrm{Tr}[\beta\,\tau^z\,\tilde{\Gamma}\,\beta\,\tau^z\,\tilde{\Gamma}] = 8v_m^2\cos(\gamma_1)\cos(\gamma_2) + 2(v_m-u_m)^2\big(\cos^2(\gamma_1)+\cos^2(\gamma_2)\big) - 2v_m^2 - 2u_m^2 \quad \text{(I.10)}$$

$$|\langle 1|\tau^x|1\rangle|^2 + |\langle 1|\tau^y|1\rangle|^2 = (1-\cos^2(\gamma_1))|\langle \boldsymbol{n}_1| - \boldsymbol{n}_2\rangle|^2 \quad \text{(I.11)}$$

$$|\langle 2|\tau^x|2\rangle|^2 + |\langle 2|\tau^y|2\rangle|^2 = (1-\cos^2(\gamma_2))|\langle \boldsymbol{n}_1| - \boldsymbol{n}_2\rangle|^2 \quad \text{(I.12)}$$

$$|\langle 2|\tau^x|1\rangle|^2 + |\langle 2|\tau^y|1\rangle|^2 = (1-\cos(\gamma_1)\cos(\gamma_2))|\langle \boldsymbol{n}_1|\boldsymbol{n}_2\rangle|^2 \quad \text{(I.13)}$$

$$\frac{1}{2}\sum_{a,b=x,y}\Big(\big(\mathrm{Tr}[\alpha^a\,\tau^b\,\tilde{\Gamma}]\big)^2 - \mathrm{Tr}[\alpha^a\tau^b\tilde{\Gamma}\alpha^a\tau^b\tilde{\Gamma}\Big) = -2(v_m^2-u_m^2)\big(\cos^2(\gamma_1)+\cos^2(\gamma_2)\big) + 2(v_m^2-u_m^2)\big(\cos(\gamma_1)-\cos(\gamma_2)\big)^2|\langle \boldsymbol{n}_1| - \boldsymbol{n}_2\rangle|^2 \quad \text{(I.14)}$$

$$\langle \mathcal{H}_V\rangle = -\frac{\mathrm{V}}{2\pi\ell_c^2}\kappa_V\Big(8v_m^2\cos(\gamma_1)\cos(\gamma_2) + 2\big(v_m^2-u_m^2\big)\big(\cos^2(\gamma_1)+\cos^2(\gamma_2)\big)\Big) \quad \text{(I.15)}$$

$$\langle \mathcal{H}_U\rangle = \frac{\mathrm{V}}{2\pi\ell_c^2}\kappa_U\Big(8v_m^2\cos(\gamma_1)\cos(\gamma_2) + 2\big(v_m^2-u_m^2\big)\big(\cos(\gamma_1)-\cos(\gamma_2)\big)^2|\langle \boldsymbol{n}_1|\boldsymbol{n}_2\rangle|^2 - 4\big(v_m^2+u_m^2\big)\Big) \quad \text{(I.16)}$$

$$\langle \mathcal{H}_Z\rangle = -\frac{\mathrm{V}}{2\pi\ell_c^2}\kappa_Z u_m\big(\cos(\gamma_1)-\cos(\gamma_2)\big)\big(\cos(\theta_1)+\cos(\theta_2)\big) \quad \text{(I.17)}$$

I.1 Minimization

Collecting the angle dependent terms

$$\mathcal{E} = 2\big(v_m^2 - u_m^2\big)\Bigg(- \frac{4v_m^2}{v_m^2 - u_m^2}(\kappa_V - \kappa_U)\cos(\gamma_1)\cos(\gamma_2) - \kappa_V\big(\cos^2(\gamma_1) + \cos^2(\gamma_2)\big)$$
$$+ \frac{1}{2}\kappa_U\big(\cos(\gamma_1) - \cos(\gamma_2)\big)^2\big(1 + \cos(\theta_1)\cos(\theta_2) + \cos(\varphi_1 - \varphi_2)\sin(\theta_1)\sin(\theta_2)\big)$$
$$- \kappa_Z\frac{u_m}{2(v_m^2 - u_m^2)}\big(\cos(\gamma_1) - \cos(\gamma_2)\big)\big(\cos(\theta_1) - \cos(\theta_2)\big) \quad \text{(I.18)}$$

Derivative w.r.t $\varphi_1 - \varphi_2$:

$$\big(\cos(\gamma_1) - \cos(\gamma_2)\big)^2\sin(\varphi_1 - \varphi_2)\sin(\theta_1)\sin(\theta_2) = 0$$

Energy minimizes for $\varphi_1 - \varphi_2 = \pi$

The minimum value for the rest of angle parameters that minimizes the mean field energy was obtained numerically. We used downhill simplex routine “amoeba” provided in Numerical Recipes in C.

Appendix J

Ground state energy $\sigma_H = -1$

$$M = \{m, -m, -m, -m\} \tag{J.1}$$

$$|1\rangle = \cos(\frac{\gamma_1}{2})|+\rangle|\boldsymbol{n}_1\rangle + \mathrm{e}^{\mathrm{i}\,\Omega_1}\sin(\frac{\gamma_1}{2})|-\rangle|-\boldsymbol{n}_2\rangle \tag{J.2}$$

$$\langle 1|\sigma^z|1\rangle = \frac{1}{2}(\cos(\theta_1) + \cos(\theta_2)) + \frac{1}{2}\cos(\gamma_1)(\cos(\theta_1) - \cos(\theta_2)) \tag{J.3}$$

$$\mathrm{Tr}[\sigma\,\tilde{\Gamma}] = u_m\Big(\big(\cos(\theta_1) + \cos(\theta_2)\big) + \cos(\gamma_1)\big(\cos(\theta_1) - \cos(\theta_2)\big)\Big) \tag{J.4}$$

$$\mathrm{Tr}[\tilde{\Gamma}\tilde{\Gamma}] = 2(v_m^2 + u_m^2) \tag{J.5}$$

$$\langle 1|\tau^z|1\rangle = \cos(\gamma_1) \tag{J.6}$$

$$(\mathrm{Tr}[\beta\,\tau^z\,\tilde{\Gamma}])^2 - \mathrm{Tr}[\beta\,\tau^z\,\tilde{\Gamma}\,\beta\,\tau^z\,\tilde{\Gamma}] = 2\big(v_m^2 - u_m^2\big)\cos^2(\gamma_1) \tag{J.7}$$

$$|\langle 1|\tau^x|1\rangle|^2 + |\langle 1|\tau^y|1\rangle|^2 = (1 - \cos^2(\gamma_1))|\langle \boldsymbol{n}_1| - \boldsymbol{n}_2\rangle|^2 \tag{J.8}$$

$$\frac{1}{2}\sum_{a,b=x,y}\Big(\big(\mathrm{Tr}[\alpha^a\,\tau^b\,\tilde{\Gamma}]\big)^2 - \mathrm{Tr}[\alpha^a\tau^b\tilde{\Gamma}\alpha^a\tau^b\tilde{\Gamma}}\Big)$$
$$= -2\big(v_m^2 - u_m^2\big)\sin^2(\gamma_1)|\langle \boldsymbol{n}_1| - \boldsymbol{n}_2\rangle|^2 \tag{J.9}$$

$$\langle \mathcal{H}_V \rangle = -\frac{\mathrm{V}}{2\pi\ell_c^2}\kappa_V \Big(2\big(v_m^2 - u_m^2\big)\cos^2(\gamma_1) + 2(v_m^2 + u_m^2) \Big) \tag{J.10}$$

$$\langle \mathcal{H}_U \rangle = \frac{\mathrm{V}}{2\pi\ell_c^2}\kappa_U \Big(-2\big(v_m^2 - u_m^2\big)\sin^2(\gamma_1)|\langle \boldsymbol{n}_1|\boldsymbol{n}_2\rangle|^2 - 4u_m^2 \Big) \tag{J.11}$$

$$\langle \mathcal{H}_Z \rangle = -\frac{\mathrm{V}}{2\pi\ell_c^2}\kappa_Z \Big(u_m \Big(\big(\cos(\theta_1) - \cos(\theta_2)\big) + \cos(\gamma_1)\big(\cos(\theta_1) + \cos(\theta_2)\big) \Big) \Big) \tag{J.12}$$

J.1 Minimization

Collect the angle parameter dependent terms for symmetry breaking terms

$$\begin{aligned} \mathcal{E} = -2\big(v_m^2 - u_m^2\big) \Big(& \kappa_V \cos^2(\gamma_1) \\ & + \frac{1}{2}\kappa_U \sin^2(\gamma_1) \Big(1 + \cos(\theta_1)\cos(\theta_2) + \cos(\varphi_1 - \varphi_2)\sin(\theta_1)\sin(\theta_2) \Big) \\ & + \kappa_Z \frac{u_m}{2(v_m^2 - u_m^2)} \Big(\big(\cos(\theta_1) + \cos(\theta_2)\big) + \cos(\gamma_1)\big(\cos(\theta_1) - \cos(\theta_2)\big) \Big) \Big) \end{aligned} \tag{J.13}$$

Derivative w.r.t $\varphi_1 - \varphi_2$:

$$\sin(\varphi_1 - \varphi_2)\sin(\theta_1)\sin(\theta_2) = 0 \tag{J.14}$$

The energy minimizes when $\varphi_1 - \varphi_2 = 0$ because the coefficient is always positive for the range of θ_1 and θ_2

The minimum value for the rest angle parameters that minimizes the mean field energy was obtained numerically. We used downhill simplex routine “amoeba” provided in Numerical Recipes in C.

Appendix K

Excitations : $\sigma_H = 0$

K.1 General expression for excitations

$$\Delta_{\mathbb{G}} = \big(\text{Tr}[\mathbb{G}\Gamma^{(p)}] - \text{Tr}[\mathbb{G}\Gamma^{(h)}]\big)\text{Tr}[\mathbb{G}\Gamma] - \text{Tr}[\mathbb{G}\Gamma^{(p)}\mathbb{G}\Gamma] + \text{Tr}[\mathbb{G}\Gamma^{(h)}\mathbb{G}\Gamma] \tag{K.1}$$

$$\mathbb{G} = \mathbb{1}_2\mathbb{1}_4, \beta\tau^z, \alpha^j\tau^k$$

$$\Gamma = G_m(2(P_1 + P_2) - \mathbb{1}_4), \qquad \Gamma^{(\mathtt{x})} = GP_{\mathtt{x}} \tag{K.2}$$

$P_{\mathtt{x}}$ is projection for particle or hole.

$$\text{Tr}[\alpha\tau\Gamma^{(\mathtt{x})}] = \text{Tr}[\alpha G]\text{Tr}[\tau P_{\mathtt{x}}] \tag{K.3}$$

$$\text{Tr}[\alpha\tau\Gamma] = \text{Tr}[\alpha G_m]\Big(2\text{Tr}[\tau P_1] + 2\text{Tr}[\tau P_2] - \text{Tr}[\tau]\Big) \tag{K.4}$$

$$\text{Tr}[\alpha\tau\Gamma^{(\mathtt{x})}\alpha\tau\Gamma] = \text{Tr}[\alpha G\alpha G_m]\Big(2\text{Tr}[\tau P_{\mathtt{x}}\tau P_1] + 2\text{Tr}[\tau P_{\mathtt{x}}\tau P_2]) - \text{Tr}[P_{\mathtt{x}}]\Big) \tag{K.5}$$

For a general $\alpha\tau$ term,

$$\begin{aligned}\Delta_{\alpha\tau} = {} & \text{Tr}[\alpha G]\text{Tr}[\alpha G_m]\Big(\text{Tr}[\tau P_p] - \text{Tr}[\tau P_h]\Big)\Big(2\text{Tr}[\tau P_1] + 2\text{Tr}[\tau P_2] - \text{Tr}[\tau]\Big) \\ & - 2\text{Tr}[\alpha G\alpha G_m]\Big(\text{Tr}[\tau P_p\tau P_1] + \text{Tr}[\tau P_p\tau P_2] - \text{Tr}[\tau P_h\tau P_1] - \text{Tr}[\tau P_h\tau P_2]\Big)\end{aligned} \tag{K.6}$$

$$\Delta_{\sigma^z} = \text{Tr}[\sigma^z \Gamma^{(p)}] - \text{Tr}[\sigma^z \Gamma^{(h)}] = \text{Tr}[\sigma^z P_p] - \text{Tr}[\sigma^z P_h] \tag{K.7}$$

$$G_m = \frac{1}{2\pi\ell_c^2}\tilde{G}_m$$

$$\tilde{G}_m = \frac{1}{2}(u_m \mathbb{1}_2 - v_m \beta) \qquad G = \frac{1}{2}(\mathbb{1}_2 - \beta) \tag{K.8}$$

$$\text{Tr}[\tilde{G}_m] = u_m \qquad \text{Tr}[G] = 1 \tag{K.9}$$

$$\text{Tr}[\beta\tilde{G}_m] = -v_m \qquad \text{Tr}[\beta G] = -1 \tag{K.10}$$

$$\text{Tr}[\alpha^j\tilde{G}_m] = 0 \qquad \text{Tr}[\alpha^j G] = 0 \tag{K.11}$$

$$\text{Tr}[G\tilde{G}_m] = \frac{1}{2}(u_m + v_m) \tag{K.12}$$

$$\text{Tr}[\beta G \beta \tilde{G}_m] = \frac{1}{2}(u_m + v_m) \tag{K.13}$$

$$\text{Tr}[\alpha^j G \alpha^j \tilde{G}_m] = \frac{1}{2}(u_m - v_m) \tag{K.14}$$

$$\Delta_{\mathbb{1}} = 2\text{Tr}[GG_m] = v_m + u_m \tag{K.15}$$

$$\begin{aligned}\Delta_{\beta\tau^z} = {} & 2v_m\Big(\text{Tr}[\tau^z P_p] - \text{Tr}[\tau^z P_h]\Big)\Big(\text{Tr}[\tau^z P_1] + \text{Tr}[\tau^z P_2]\Big) \\ & - (v_m + u_m)\Big(\text{Tr}[\tau^z P_p \tau^z P_1] + \text{Tr}[\tau^z P_p \tau^z P_2] - \text{Tr}[\tau^z P_h \tau^z P_1] - \text{Tr}[\tau^z P_h \tau^z P_2]\Big)\end{aligned} \tag{K.16}$$

$$\Delta_{\alpha^j\tau^k} = (v_m - u_m)\Big(\text{Tr}[\tau^k P_p \tau^k P_1] + \text{Tr}[\tau^k P_p \tau^k P_2] - \text{Tr}[\tau^k P_h \tau^k P_1] - \text{Tr}[\tau^k P_h \tau^k P_2]\Big) \tag{K.17}$$

$$\Delta_{\sigma^z} = \text{Tr}[\sigma^z P_p] - \text{Tr}[\sigma^z P_h] \tag{K.18}$$

K.2 Charge ordered state

Ground state $SU(4)$ components,

$$|1\rangle = |+\rangle|\boldsymbol{n}\rangle \qquad |2\rangle = |+\rangle|-\boldsymbol{n}\rangle \tag{K.19}$$

Particle and hole $SU(4)$ components,

$$|p\rangle = |-\rangle|\boldsymbol{n}_p\rangle \qquad |h\rangle = |+\rangle|\boldsymbol{n}_h\rangle \tag{K.20}$$

Here,

$$|\boldsymbol{n}_p\rangle = \cos(\frac{\theta_p}{2})|+\rangle + \mathrm{e}^{\mathrm{i}\,\phi_p}\sin(\frac{\theta_p}{2})|-\rangle$$
$$|\boldsymbol{n}_h\rangle = \cos(\frac{\theta_h}{2})|+\rangle + \mathrm{e}^{\mathrm{i}\,\phi_h}\sin(\frac{\theta_h}{2})|-\rangle$$

$$\mathrm{Tr}[\tau^z P_p] - \mathrm{Tr}[\tau^z P_h] = -2 \tag{K.21}$$

$$\mathrm{Tr}[\tau^z P_1] + \mathrm{Tr}[\tau^z P_2] = 2 \tag{K.22}$$

$$\mathrm{Tr}[\tau^z P_p \tau^z P_1] = 0 \qquad \mathrm{Tr}[\tau^z P_p \tau^z P_2] = 0 \tag{K.23}$$

$$\mathrm{Tr}[\tau^z P_h \tau^z P_1] = |\langle\boldsymbol{n}|\boldsymbol{n}_h\rangle|^2 \qquad \mathrm{Tr}[\tau^z P_h \tau^z P_2] = |\langle-\boldsymbol{n}|\boldsymbol{n}_h\rangle|^2 \tag{K.24}$$

$$\mathrm{Tr}[\tau^k P_p \tau^k P_1] = |\langle\boldsymbol{n}|\boldsymbol{n}_p\rangle|^2 \qquad \mathrm{Tr}[\tau^k P_p \tau^k P_2] = |\langle-\boldsymbol{n}|\boldsymbol{n}_p\rangle|^2 \tag{K.25}$$

$$\mathrm{Tr}[\tau^k P_h \tau^k P_1] = 0 \qquad \mathrm{Tr}[\tau^k P_h \tau^k P_2] = 0 \tag{K.26}$$

$$\mathrm{Tr}[\sigma^z P_p] - \mathrm{Tr}[\sigma^z P_h] = \cos(\theta_p) - \cos(\theta_h) \tag{K.27}$$

$$\Delta_{\mathbb{1}_4} = (v_m + u_m) \tag{K.28}$$

$$\Delta_{\beta\tau^z} = -8v_m + (v_m + u_m) \tag{K.29}$$

$$\Delta_{\alpha^j\tau^k} = v_m - u_m \tag{K.30}$$

$$\Delta_{\sigma^z} = \cos(\theta_p) - \cos(\theta_h) \tag{K.31}$$

Gaps contribution from the symmetry breaking terms,

$$\Delta_V = -4\kappa_V v_m \tag{K.32}$$

$$\Delta_U = 2\kappa_U v_m \tag{K.33}$$

$$\Delta_Z = -\frac{1}{2}\kappa_Z(\cos(\theta_p) - \cos(\theta_h)) \tag{K.34}$$

Minimum for $\theta_p = 0$ and $\theta_h = \pi$, hence

$$|p\rangle = |-\rangle|\uparrow\rangle, \qquad |h\rangle = |+\rangle|\downarrow\rangle \tag{K.35}$$

K.3 Ferromagnetic state

Ground state $SU(4)$ components,

$$|1\rangle = |+\rangle|\uparrow\rangle \qquad\qquad |2\rangle = |-\rangle|\uparrow\rangle \tag{K.36}$$

Particle and hole $SU(4)$ components,

$$|p\rangle = |\gamma_p\rangle|\downarrow\rangle \qquad\qquad |h\rangle = |\gamma_h|\uparrow\rangle \tag{K.37}$$

Here,

$$|\gamma_p\rangle = \cos(\frac{\gamma_p}{2})|+\rangle + \mathrm{e}^{\mathrm{i}\,\Omega_p}\sin(\frac{\gamma_p}{2})|-\rangle$$

$$|\gamma_h\rangle = \cos(\frac{\gamma_h}{2})|+\rangle + \mathrm{e}^{\mathrm{i}\,\Omega_h}\sin(\frac{\gamma_h}{2})|-\rangle$$

$$\mathrm{Tr}[\tau^z P_p] - \mathrm{Tr}[\tau^z P_h] = \cos(\gamma_p) - \cos(\gamma_h) \tag{K.38}$$

$$\mathrm{Tr}[\tau^z P_1] + \mathrm{Tr}[\tau^z P_2] = 0 \tag{K.39}$$

$$\mathrm{Tr}[\tau^z P_p \tau^z P_1] = 0 \qquad \mathrm{Tr}[\tau^z P_p \tau^z P_2] = 0 \tag{K.40}$$

$$\mathrm{Tr}[\tau^z P_h \tau^z P_1] = \cos^2(\frac{\gamma_h}{2}) \qquad \mathrm{Tr}[\tau^z P_h \tau^z P_2] = \sin^2(\frac{\gamma_h}{2}) \tag{K.41}$$

$$\mathrm{Tr}[\tau^k P_p \tau^k P_1] = 0 \qquad \mathrm{Tr}[\tau^k P_p \tau^k P_2] = 0 \tag{K.42}$$

$$\mathrm{Tr}[\tau^k P_h \tau^k P_1] = \sin^2(\frac{\gamma_h}{2}) \qquad \mathrm{Tr}[\tau^k P_h \tau^k P_2] = \cos^2(\frac{\gamma_h}{2}) \tag{K.43}$$

$$\mathrm{Tr}[\sigma^z P_p] - \mathrm{Tr}[\sigma^z P_h] = -2 \tag{K.44}$$

$$\Delta_{\mathbb{1}_4} = (v_m + u_m) \tag{K.45}$$

$$\Delta_{\beta\tau^z} = (v_m + u_m) \tag{K.46}$$

$$\Delta_{\alpha^j\tau^k} = -(v_m - u_m) \tag{K.47}$$

$$\Delta_{\sigma^z} = -2 \tag{K.48}$$

Contributions from the symmetry breaking terms,

$$\Delta_V = 0 \tag{K.49}$$

$$\Delta_U = 2\kappa_U v_m \tag{K.50}$$

$$\Delta_Z = \kappa_Z \tag{K.51}$$

Gap contributions are independent of angle parameters.

K.4 Canted state

$SU(4)$ components of the ground state,

$$|1\rangle = |+\rangle|\boldsymbol{n}_1\rangle \qquad\qquad |2\rangle = |-\rangle|\boldsymbol{n}_2\rangle \tag{K.52}$$

$$\theta_1 - \theta_2 = 0, \qquad \phi_1 - \phi_2 = \pi, \qquad \cos(\frac{\theta_1+\theta_2}{2}) = \frac{1}{4}\frac{u_m}{v_m^2-u_m^2}\frac{\tilde{Z}}{U}$$

Particle and hole $SU(4)$ components,

$$|p\rangle = \cos(\frac{\theta_p}{2})|+\rangle|-\boldsymbol{n}_1\rangle + \mathrm{e}^{\mathrm{i}\,\phi_p}\sin(\frac{\theta_p}{2})|-\rangle|-\boldsymbol{n}_2\rangle \tag{K.53}$$

$$|h\rangle = \cos(\frac{\theta_h}{2})|+\rangle|\boldsymbol{n}_1\rangle + \mathrm{e}^{\mathrm{i}\,\phi_h}\sin(\frac{\theta_h}{2})|-\rangle|\boldsymbol{n}_2\rangle \tag{K.54}$$

$$\tag{K.55}$$

Here,

$$|\boldsymbol{n}_1\rangle = \cos(\frac{\theta_1}{2})|+\rangle + \mathrm{e}^{\mathrm{i}\,\phi_1}\sin(\frac{\theta_1}{2})|-\rangle$$

$$|\boldsymbol{n}_2\rangle = \cos(\frac{\theta_2}{2})|+\rangle + \mathrm{e}^{\mathrm{i}\,\phi_2}\sin(\frac{\theta_2}{2})|-\rangle$$

$$\mathrm{Tr}[\tau^z P_p] - \mathrm{Tr}[\tau^z P_h] = \cos(\theta_p) - \cos(\theta_h) \tag{K.56}$$

$$\mathrm{Tr}[\tau^z P_1] + \mathrm{Tr}[\tau^z P_2] = 2 \tag{K.57}$$

$$\mathrm{Tr}[\tau^z P_p \tau^z P_1] = 0 \qquad \mathrm{Tr}[\tau^z P_p \tau^z P_2] = 0 \tag{K.58}$$

$$\mathrm{Tr}[\tau^z P_h \tau^z P_1] = \cos^2(\frac{\theta_h}{2}) \qquad \mathrm{Tr}[\tau^z P_h \tau^z P_2] = \sin^2(\frac{\theta_h}{2}) \tag{K.59}$$

$$\mathrm{Tr}[\tau^k P_p \tau^k P_1] = \sin^2(\frac{\theta_p}{2})|\langle \boldsymbol{n}_1| - \boldsymbol{n}_2\rangle|^2 \quad \mathrm{Tr}[\tau^k P_p \tau^k P_2] = \cos^2(\frac{\theta_p}{2})|\langle -\boldsymbol{n}_1|\boldsymbol{n}_2\rangle|^2 \tag{K.60}$$

$$\mathrm{Tr}[\tau^k P_h \tau^k P_1] = \sin^2(\frac{\theta_h}{2})|\langle \boldsymbol{n}_1|\boldsymbol{n}_2\rangle|^2 \qquad \mathrm{Tr}[\tau^k P_h \tau^k P_2] = \cos^2(\frac{\theta_h}{2})|\langle \boldsymbol{n}_1|\boldsymbol{n}_2\rangle|^2 \tag{K.61}$$

$$\tag{K.62}$$

$$\mathrm{Tr}[\sigma^z P_p] - \mathrm{Tr}[\sigma^z P_h] = -2\cos(\frac{\theta_1+\theta_2}{2}) \tag{K.63}$$

$$\Delta_{\mathbb{1}_4} = (v_m + u_m) \tag{K.64}$$

$$\Delta_{\beta\tau^z} = (v_m + u_m) \tag{K.65}$$

$$\Delta_{\alpha^j\tau^k} = (v_m - u_m) - 2(v_m - u_m)\cos^2(\frac{\theta_1+\theta_2}{2}) \tag{K.66}$$

$$\Delta_{\sigma^z} = -2\cos(\frac{\theta_1+\theta_2}{2}) \tag{K.67}$$

Contributions from the symmetry breaking terms,

$$\Delta_V = 0 \tag{K.68}$$

$$\Delta_U = 2\kappa_U\Big(v_m - (v_m - u_m)\cos^2(\frac{\theta_1+\theta_2}{2})\Big) \tag{K.69}$$

$$\Delta_Z = \kappa_Z\cos(\frac{\theta_1+\theta_2}{2}) \tag{K.70}$$

Gap contributions turn out to be independent of angle parameters.

Appendix L

Excitations : $\sigma_H = -1$

L.1 General expression for excitations

$$\Delta_{\mathbb{G}} = \big(\text{Tr}[\mathbb{G}\Gamma^{(p)}] - \text{Tr}[\mathbb{G}\Gamma^{(h)}]\big)\text{Tr}[\mathbb{G}\Gamma] - \text{Tr}[\mathbb{G}\Gamma^{(p)}\mathbb{G}\Gamma] + \text{Tr}[\mathbb{G}\Gamma^{(h)}\mathbb{G}\Gamma] \tag{L.1}$$

$$\mathbb{G} = \mathbb{1}_2\mathbb{1}_4, \beta\tau^z, \alpha^j\tau^k$$

$$\Gamma = G_m(2P_1 - \mathbb{1}_4), \qquad \Gamma^{(\mathrm{x})} = GP_{\mathrm{x}} \tag{L.2}$$

Here P_{x} is projection for particle or hole state.

$$\text{Tr}[\alpha\tau\Gamma^{(\mathrm{x})}] = \text{Tr}[\alpha G]\text{Tr}[\tau P_{\mathrm{x}}] \tag{L.3}$$

$$\text{Tr}[\alpha\tau\Gamma] = \text{Tr}[\alpha G_m]\Big(2\text{Tr}[\tau P_1] - \text{Tr}[\tau]\Big) \tag{L.4}$$

$$\text{Tr}[\alpha\tau\Gamma^{(\mathrm{x})}\alpha\tau\Gamma] = \text{Tr}[\alpha G\alpha G_m]\Big(2\text{Tr}[\tau P_{\mathrm{x}}\tau P_1] - \text{Tr}[P_{\mathrm{x}}]\Big) \tag{L.5}$$

$$\begin{aligned}\Delta_{\alpha\tau} = \text{Tr}[\alpha G]\text{Tr}[\alpha G_m]\Big(\text{Tr}[\tau P_p] - \text{Tr}[\tau P_h]\Big)\Big(2\text{Tr}[\tau P_1] - \text{Tr}[\tau]\Big) \\ - 2\text{Tr}[\alpha G\alpha G_m]\Big(\text{Tr}[\tau P_p\tau P_1] - \text{Tr}[\tau P_h\tau P_1]\Big)\end{aligned} \tag{L.6}$$

$$\Delta_{\sigma^z} = \text{Tr}[\sigma^z\Gamma^{(p)}] - \text{Tr}[\sigma^z\Gamma^{(h)}] = \text{Tr}[\sigma^z P_p] - \text{Tr}[\sigma^z P_h] \tag{L.7}$$

$$G_m = \frac{1}{2\pi\ell_c^2}\tilde{G}_m$$

$$\tilde{G}_m = \frac{1}{2}(u_m \mathbb{1}_2 - v_m\beta) \qquad G = \frac{1}{2}(\mathbb{1}_2 - \beta) \tag{L.8}$$

$$\mathrm{Tr}[\tilde{G}_m] = u_m \qquad \mathrm{Tr}[G] = 1 \tag{L.9}$$

$$\mathrm{Tr}[\beta\tilde{G}_m] = -v_m \qquad \mathrm{Tr}[\beta G] = -1 \tag{L.10}$$

$$\mathrm{Tr}[\alpha^j\tilde{G}_m] = 0 \qquad \mathrm{Tr}[\alpha^j G] = 0 \tag{L.11}$$

$$\mathrm{Tr}[G\tilde{G}_m] = \frac{1}{2}(u_m + v_m) \tag{L.12}$$

$$\mathrm{Tr}[\beta G\beta\tilde{G}_m] = \frac{1}{2}(u_m + v_m) \tag{L.13}$$

$$\mathrm{Tr}[\alpha^j G\alpha^j\tilde{G}_m] = \frac{1}{2}(u_m - v_m) \tag{L.14}$$

$$\Delta_{\mathbb{1}} = 2\mathrm{Tr}[GG_m] = v_m + u_m \tag{L.15}$$

$$\Delta_{\beta\tau^z} = 2v_m\Big(\mathrm{Tr}[\tau^z P_p] - \mathrm{Tr}[\tau^z P_h]\Big)\mathrm{Tr}[\tau^z P_1] - (v_m + u_m)\Big(\mathrm{Tr}[\tau^z P_p\tau^z P_1] - \mathrm{Tr}[\tau^z P_h\tau^z P_1]\Big) \tag{L.16}$$

$$\Delta_{\alpha^j\tau^k} = (v_m - u_m)\Big(\mathrm{Tr}[\tau^k P_p\tau^k P_1] - \mathrm{Tr}[\tau^k P_h\tau^k P_1]\Big) \tag{L.17}$$

$$\Delta_{\sigma^z} = \mathrm{Tr}[\sigma^z P_p] - \mathrm{Tr}[\sigma^z P_h] \tag{L.18}$$

L.2 Valley and spin polarized state

$SU(4)$ components of ground state, hole and particle state

$$\begin{aligned} |1\rangle = |h\rangle &= |+\rangle|\uparrow\rangle \\ |p\rangle &= \cos(\frac{\theta_p}{2})|-\rangle|\uparrow\rangle + \mathrm{e}^{\mathrm{i}\,\phi_p}\sin(\frac{\theta_p}{2})|\gamma_p\rangle|\downarrow\rangle \end{aligned} \tag{L.19}$$

Here,

$$|\gamma_p\rangle = \cos(\frac{\gamma_p}{2})|+\rangle + \mathrm{e}^{\mathrm{i}\,\Omega_p}\sin(\frac{\gamma_p}{2})|-\rangle$$

$$\mathrm{Tr}[\tau^z P_p] - \mathrm{Tr}[\tau^z P_h] = -\cos^2(\frac{\theta_p}{2}) + \sin^2(\frac{\theta_p}{2})\cos(\gamma_p) - 1 \tag{L.20}$$

$$\mathrm{Tr}[\tau^z P_1] = 1 \tag{L.21}$$

$$\mathrm{Tr}[\tau^z P_p \tau^z P_1] = 0 \qquad \mathrm{Tr}[\tau^z P_h \tau^z P_1] = 1 \tag{L.22}$$

$$\mathrm{Tr}[\tau^k P_p \tau^k P_1] = \cos^2(\frac{\theta_p}{2}) \qquad \mathrm{Tr}[\tau^k P_h \tau^k P_1] = 0 \tag{L.23}$$

$$\mathrm{Tr}[\sigma^z P_p] - \mathrm{Tr}[\sigma^z P_h] = \cos(\theta_p) - 1 \tag{L.24}$$

$$\Delta_{\mathbb{1}_4} = (v_m + u_m) \tag{L.25}$$

$$\Delta_{\beta\tau^z} = 2v_m\Big(-\cos^2(\frac{\theta_p}{2}) + \sin^2(\frac{\theta_p}{2})\cos(\gamma_p) - 1\Big) + (v_m + u_m) \tag{L.26}$$

$$= 2v_m \sin^2(\frac{\theta_p}{2})(1 + \cos(\gamma_p)) - 3v_m + u_m \tag{L.27}$$

$$\Delta_{\alpha^j\tau^k} = (v_m - u_m)\cos^2(\frac{\theta_p}{2}) \tag{L.28}$$

$$= -(v_m - u_m)\sin^2(\frac{\theta_p}{2}) + (v_m - u_m) \tag{L.29}$$

$$\Delta_{\sigma^z} = \cos(\theta_p) - 1 = -2\sin^2(\frac{\theta_p}{2}) \tag{L.30}$$

Contributions from symmetry breaking terms,

$$\Delta_V = -4\kappa_V v_m \sin^2(\frac{\theta_p}{2})\cos^2(\frac{\gamma_p}{2}) + 4\kappa_V v_m \tag{L.31}$$

$$\Delta_U = 4\kappa_U v_m \sin^2(\frac{\theta_p}{2})\cos^2(\frac{\gamma_p}{2}) - 2\kappa_U(v_m - u_m)\sin^2(\frac{\theta_p}{2}) \tag{L.32}$$

$$\Delta_Z = 2\kappa_Z \sin^2(\frac{\theta_p}{2}) \tag{L.33}$$

The gap that depends on angle parameters that need to be minimized,

$$\Delta = \sin^2(\frac{\theta_p}{2})\Big(2(\kappa_U - \kappa_V)v_m \cos^2(\frac{\gamma_p}{2}) - \kappa_U(v_m - u_m) + \kappa_Z\Big) \tag{L.34}$$

Minimization(numerically) results

- $\theta_p = 0$ i.e $|p\rangle = |-\rangle|\uparrow\rangle$ and the gap is $\Delta = 0$
- $\theta_p = \pi$ and $\gamma_p = 0$ i.e. $|p\rangle = |+\rangle|\downarrow\rangle$ for $\kappa_V > \kappa_U$

  and the gap is $\Delta = -2\kappa_V v_m + \kappa_U(v_m + u_m) + \kappa_Z$
- $\theta_p = \pi$ and $\gamma_p = \pi$ i.e. $|p\rangle = |-\rangle|\downarrow\rangle$ for $\kappa_V < \kappa_U$

  and the gap is $\Delta = -\kappa_U(v_m - u_m) + \kappa_Z$

Equations of lines:

$$\begin{aligned}
\kappa_V &= \frac{1}{2}\Big(1 + \frac{u_m}{v_m}\Big)\kappa_U + \frac{1}{2v_m}\kappa_Z \\
\kappa_U &= \frac{1}{v_m - u_m}\kappa_Z \\
\kappa_V &= \kappa_U
\end{aligned} \tag{L.35}$$

In the figure the line are given by equation

$$\begin{aligned}
3V &= \frac{1}{2}\Big(1 + \frac{u_m}{v_m}\Big)U + \frac{1}{2v_m}\tilde{Z} \\
U &= \frac{1}{v_m - u_m}\tilde{Z} \\
3V &= U
\end{aligned} \tag{L.36}$$

L.3 Canted valley - Ferrimagnet

Ground state, hole and particle state $SU(4)$ components,

$$\begin{aligned}|1\rangle = |h\rangle &= \cos(\frac{\gamma_0}{2})|+\rangle|\uparrow\rangle + \mathrm{e}^{\mathrm{i}\,\Omega_0}\sin(\frac{\gamma_0}{2})|-\rangle|\downarrow\rangle \\ |p\rangle &= \cos(\frac{\theta_p}{2})\Big(\sin(\frac{\gamma_0}{2})|+\rangle|\uparrow\rangle - \mathrm{e}^{\mathrm{i}\,\Omega_0}\cos(\frac{\gamma_0}{2})|-\rangle|\downarrow\rangle\Big) \\ &\quad + \mathrm{e}^{\mathrm{i}\,\phi_p}\sin(\frac{\theta_p}{2})\Big(\cos(\frac{\gamma_p}{2})|+\rangle|\downarrow\rangle + \mathrm{e}^{\mathrm{i}\,\Omega_p}\sin(\frac{\gamma_p}{2})|-\rangle|\uparrow\rangle\Big)\end{aligned} \tag{L.37}$$

$$\mathrm{Tr}[\tau^z P_p] - \mathrm{Tr}[\tau^z P_h] = -\cos^2(\frac{\theta_p}{2})\cos(\gamma_0) + \sin^2(\frac{\theta_p}{2})\cos(\gamma_p) - \cos(\gamma_0) \tag{L.38}$$

$$= \sin^2(\frac{\theta_p}{2})(\cos(\gamma_p) + \cos(\gamma_0)) - 2\cos(\gamma_0) \tag{L.39}$$

$$\mathrm{Tr}[\tau^z P_1] = \cos(\gamma_0) \tag{L.40}$$

$$\mathrm{Tr}[\tau^z P_p \tau^z P_1] = \cos^2(\frac{\theta_p}{2})\sin^2(\gamma_0) \qquad \mathrm{Tr}[\tau^z P_h \tau^z P_1] = \cos^2(\gamma_0) \tag{L.41}$$

$$\sum_{k=x,y}\mathrm{Tr}[\tau^k P_p \tau^k P_1] = \sin^2(\frac{\theta_p}{2})(1 - \cos(\gamma_0)\cos(\gamma_p)) \quad \sum_{k=x,y}\mathrm{Tr}[\tau^k P_h \tau^k P_1] = 0 \tag{L.42}$$

$$\mathrm{Tr}[\sigma^z P_p] - \mathrm{Tr}[\sigma^z P_h] = -\cos^2(\frac{\theta_p}{2})\cos(\gamma_0) - \sin^2(\frac{\theta_p}{2})\cos(\gamma_p) - \cos(\gamma_0) \tag{L.43}$$

$$= -\sin^2(\frac{\theta_p}{2})(\cos(\gamma_p) - \cos(\gamma_0)) - 2\cos(\gamma_0) \tag{L.44}$$

$$\Delta_{\mathbb{1}_4} = v_m + u_m \tag{L.45}$$

$$\Delta_{\beta\tau^z} = 2v_m\Big(\sin^2(\frac{\theta_p}{2})(\cos(\gamma_p)+\cos(\gamma_0)) - 2\cos(\gamma_0)\Big)\cos(\gamma_0) + (v_m+u_m)\Big(\sin^2(\frac{\theta_p}{2})\sin^2(\gamma_0) + \cos(2\gamma_0)\Big)$$
$$= \sin^2(\frac{\theta_p}{2})\Big(2v_m(\cos(\gamma_p)+\cos(\gamma_0))\cos(\gamma_0) + (v_m+u_m)\sin^2(\gamma_0)\Big) - 2(v_m-u_m)\cos^2(\gamma_0) - (v_m+u_m) \quad \text{(L.46)}$$

$$\sum_{j,k=x,y}\Delta_{\alpha^i\tau^k} = 2(v_m-u_m)\sin^2(\frac{\theta_p}{2})(1-\cos(\gamma_0)\cos(\gamma_p)) \quad \text{(L.47)}$$

$$\Delta_{\sigma^z} = -\big(\sin^2(\frac{\theta_p}{2})(\cos(\gamma_p)-\cos(\gamma_0)) + 2\cos(\gamma_0)\big) \quad \text{(L.48)}$$

The contributions from the $SU(4)$ symmetry breaking terms,

$$\Delta_V = -\kappa_V\Big(\sin^2(\frac{\theta_p}{2})\Big(2v_m(\cos(\gamma_p)+\cos(\gamma_0))\cos(\gamma_0) + (v_m+u_m)\sin^2(\gamma_0)\Big) - 2(v_m-u_m)\cos^2(\gamma_0) - 2(v_m+u_m)\Big) \quad \text{(L.49)}$$

$$\Delta_U = \kappa_U\Big(\sin^2(\frac{\theta_p}{2})\Big(2v_m(\cos(\gamma_p)+\cos(\gamma_0))\cos(\gamma_0) + (v_m+u_m)\sin^2(\gamma_0) + (v_m-u_m)(1-\cos(\gamma_0)\cos(\gamma_p))\Big) - 2(v_m-u_m)\cos^2(\gamma_0)\Big) \quad \text{(L.50)}$$

$$\Delta_Z = \kappa_Z\sin^2(\frac{\theta_p}{2})(\cos(\gamma_p)-\cos(\gamma_0)) + 2\kappa_Z\cos(\gamma_0) \quad \text{(L.51)}$$

Gap that depends on the angle parameters,

$$\Delta = \frac{1}{2}\sin^2(\frac{\theta_p}{2})\Big((\kappa_U-\kappa_V)\Big(2v_m(\cos(\gamma_p)+\cos(\gamma_0))\cos(\gamma_0)+(v_m+u_m)(1-\cos^2(\gamma_0))\Big) + \kappa_U(v_m-u_m)(1-\cos(\gamma_0)\cos(\gamma_p)) + \kappa_Z(\cos(\gamma_p)-\cos(\gamma_0))\Big) \quad \text{(L.52)}$$

Minimization done numerically and the results are

- $\theta_p = 0$, i.e. $|p\rangle = \sin(\frac{\gamma_0}{2})|+\rangle|\uparrow\rangle - \mathrm{e}^{\mathrm{i}\,\Omega_0}\cos(\frac{\gamma_0}{2})|-\rangle|\downarrow\rangle$, the gap $\Delta = 0$
- $\theta_p = \pi$ and $\gamma_p = \pi$ $|p\rangle = |-\rangle|\uparrow\rangle$ and the gap
  $\Delta = \frac{1}{2}\Big((\kappa_U - \kappa_V)\Big(-2v_m\cos(\gamma_0) + (v_m + u_m)(1+\cos(\gamma_0))\Big)(1-\cos(\gamma_0))$
  $+\Big(\kappa_U(v_m - u_m) - \kappa_Z\Big)(1+\cos(\gamma_0))\Big)$

Bibliography

[1] Dmitry A. Abanin, Benjamin E. Feldman, Amir Yacoby, and Bertrand I. Halperin. Fractional and integer quantum hall effects in the zeroth landau level in graphene. *Phys. Rev. B*, 88:115407, Sep 2013.

[2] Dmitry A. Abanin, Kostya S. Novoselov, Uli Zeitler, Patrick A. Lee, A. K. Geim, and L. S. Levitov. Dissipative quantum hall effect in graphene near the dirac point. *Physical Review Letters*, 98:196806, 2007.

[3] Jason Alicea and Matthew P. A. Fisher. Graphene integer quantum hall effect in the ferromagnetic and paramagnetic regimes. *Phys. Rev. B*, 74:075422, Aug 2006.

[4] K. I. Bolotin, K. J. Sikes, J. Hone, H. L. Stormer, and P. Kim. Temperature-dependent transport in suspended graphene. *Phys. Rev. Lett.*, 101:096802, Aug 2008.

[5] Joseph G. Checkelsky, Lu Li, and N. P. Ong. Zero-energy state in graphene in a high magnetic field. *Phys. Rev. Lett.*, 100(20):206801, May 2008.

[6] Joseph G. Checkelsky, Lu Li, and N. P. Ong. Divergent resistance at the dirac point in graphene: Evidence for a transition in a high magnetic field. *Phys. Rev. B*, 79(11):115434, Mar 2009.

[7] Jean-Noël Fuchs and Pascal Lederer. Spontaneous parity breaking of graphene in the quantum hall regime. *Phys. Rev. Lett.*, 98:016803, Jan 2007.

[8] M. L. Glasser. Summation over feynman histories: Charged particle in a uniform magnetic field. *Phys. Rev.*, 133:B831–B834, Feb 1964.

[9] M. O. Goerbig, R. Moessner, and B. Douçot. Electron interactions in graphene in a strong magnetic field. *Phys. Rev. B*, 74:161407, Oct 2006.

[10] V. P. Gusynin and S. G. Sharapov. Unconventional integer quantum hall effect in graphene. *Phys. Rev. Lett.*, 95:146801, Sep 2005.

[11] Igor F. Herbut. Theory of integer quantum hall effect in graphene. *Phys. Rev. B*, 75:165411, Apr 2007.

[12] Z. Jiang, Y. Zhang, H. L. Stormer, and P. Kim. Quantum hall states near the charge-neutral dirac point in graphene. *Phys. Rev. Lett.*, 99(10):106802, Sep 2007.

[13] Maxim Kharitonov. Phase diagram for the $\nu = 0$ quantum hall state in monolayer graphene. *Phys. Rev. B*, 85:155439, Apr 2012.

[14] Kentaro Nomura and Allan H. MacDonald. Quantum hall ferromagnetism in graphene. *Phys. Rev. Lett.*, 96:256602, Jun 2006.

[15] K. S. Novoselov, D. Jiang, F. Schedin, T. J. Booth, V. V. Khotkevich, S. V. Morozov, and A. K. Geim. Two-dimensional atomic crystals. *Proceedings of the National Academy of Sciences of the United States of America*, 102(30):10451–10453, 2005.

[16] K.S. Novoselov, A.K. Geim, S.V. Morozov, D. Jiang, M. I. Katsnelson, I. V. Grigorieva, S. V. Dubonos, and A.A. Firsov. Two-dimensional gas of massless dirac fermions in graphene. *Nature*, 438:197, 2005.

[17] Dean C R., Young A F., Meric I., Lee C., Wang L., Sorgenfrei S., Watanabe K., Taniguchi T., Kim P., Shepard K L., and Hone J. Boron nitride substrates for high-quality graphene electronics. *Nat Nano*, 5(10):722–726, Oct 2010.

[18] Vibhor Singh and Mandar M. Deshmukh. Nonequilibrium breakdown of quantum hall state in graphene. *Phys. Rev. B*, 80:081404, Aug 2009.

[19] Csaba Tőke, Paul E. Lammert, Vincent H. Crespi, and Jainendra K. Jain. Fractional quantum hall effect in graphene. *Phys. Rev. B*, 74:235417, Dec 2006.

[20] Kun Yang, S. Das Sarma, and A. H. MacDonald. Collective modes and skyrmion excitations in graphene $su(4)$ quantum hall ferromagnets. *Phys. Rev. B*, 74:075423, Aug 2006.

[21] A. F. Young, C. R. Dean, L. Wang, H. Ren, P. Cadden-Zimansky, K. Watanabe, T. Taniguchi, J. Hone, K. L. Shepard, and P. Kim. Spin and valley quantum hall ferromagnetism in graphene. *Nat Phys*, 8(7):550–556, Jul 2012.

[22] Y. Zhang, Z. Jiang, J. P. Small, M. S. Purewal, Y.-W. Tan, M. Fazlollahi, J. D. Chudow, J. A. Jaszczak, H. L. Stormer, and P. Kim. Landau-level splitting in graphene in high magnetic fields. *Phys. Rev. Lett.*, 96(13):136806, Apr 2006.

[23] Yuanbo Zhang, Yan-Wen Tan, Horst L. Stormer, and Philip Kim. Experimental observation of the quantum hall effect and berry's phase in graphene. *Nature*, 438:201, 2005.